

UNIVERSITE CATHOLIQUE DE LOUVAIN
FACULTE DES SCIENCES
ECOLE DE STATISTIQUE, BIOSTATISTIQUE
ET SCIENCES ACTUARIELLES



TEMPORAL ANALYSIS OF THE EVOLUTION OF EXTREME VALUES USING CLIMATOLOGICAL DATA

Promoteur : Johan SEGERS Mémoire présenté en vue de l'obtention du
[] Lecteurs : Anna KIRILIOUK Master en statistiques, orientation générale
Michel CRUCIFIX par : **Antoine PISSEORT**

Juin 2017

Abstract

This thesis aims to analyse extreme temperatures from Uccle and assess their nonstationarity. trend in the location parameter of the temperatures assessing the climate warming. After having proven it by hand of splines's derivatives that a correction for simultaneous intervals led to non-significant changes , we will do it by hand of the Extreme Value Theory (EVT) that there is indeed an upward trend in the location parameter of the temperatures assessing the climate warming. First of all, we will do introductory analysis of the trend... and we will discover that.. The analysis will focus on yearly maxima and hence we will go through with EVT by defining and presenting the usual methods such as GEV.

Regarding the computations, we took advantage of a high-level language (c++) to make our analysis efficient and also made use of parallel computing to decrease computation time for time consuming...

Keywords • Extreme Value Theory • block-maxima model • peaks-over-threshold method • trend analysis • Bayesian inference • Generalized Additive Models with splines smoothing • Neural Networks • nonstationary models • Markov Chain Monte Carlo • Hamiltonian Monte Carlo • Parallel computing • R package • Shiny application

Acknowledgements

I would first like to thank my thesis supervisor Johan Segers for all his help and his guidance during this whole year. The repeated appointments we have had

I also would like to thank the "Institut Royal de Météorologie" (IRM) of Belgium for his help and his guidance but also for his provided quality datasets.

A bit less usual, I would like to thank the open source community such as R or LaTeX can benefit. For me and for a number of student, it has been a nonnegligable source of ideas and the most efficient source of learning.

Finally, I want to thank my family and my friends, but also Bernadette for her support and all the time I have spent writing in her room for my thesis but also during my whole academic studies.

Contents

Introduction	xⁱ
I Theoretical Framework : Extreme Value Theory	3
1 Method of Block Maxima	4
1.1 Preliminaries	5
1.2 Extremal Types Theorem : Extreme Value distributions	7
1.2.1 Generalized Extreme Value Distribution	7
1.3 Applications : Examples of Convergence to GEV	10
1.4 Maximum Domain of Attraction	13
1.4.1 Domain of attraction for the 3 types of GEV	14
1.4.2 Closeness under tail equivalence property	16
1.4.3 Domain of attraction of the GEV	17
1.5 Return Levels and Return Periods	17
1.6 Inference	18
1.6.1 Likelihood-based Methods	19
1.6.2 Other Estimator : Probability-Weighted-Moments	20
1.7 Model Diagnostics : Goodness-of-Fit	20
1.7.1 Return Level Plot	21
2 Peaks-Over-Threshold Method	23
2.1 Preliminaries	24
2.2 Characterization of the Generalized Pareto Distribution	24
2.2.1 Outline proof of the GPD and justification from GEV	25
2.2.2 Dependence of the scale parameter	26
2.2.3 Three different types of GPD : Comparison with GEV	26
2.3 Return Levels	27
2.4 Inference : Parameter Estimation	28
2.5 Inference : Threshold Selection	28

2.5.1	Standard Threshold Selection Methods	28
2.5.2	Varying Threshold : Mixture Models	30
3	Relaxing The Independence Assumption	32
3.1	Stationary Extremes	33
3.1.1	The extremal index	34
Clusters of exceedances	34	
New parameters	34	
Return levels	35	
3.1.2	Modelling in Block Maxima	35
3.2	Non-Stationary Extremes	35
3.2.1	Block-Maxima	36
3.3	Return Levels : New Definitions	38
3.4	Neural Networks for Nonstationary Series : GEV-CDN	39
3.4.1	Generalized Maximum Likelihood	40
3.4.2	Architecture of the GEV-CDN Network	41
3.4.3	Prevent Overfitting : Bagging	42
3.4.4	Confidence Intervals : Bootstrapping Methods	42
4	Bayesian Extreme Value Theory	44
4.1	Prior Elicitation	45
4.1.1	Non-informative Priors	46
4.1.2	Informative Priors	47
4.2	Bayesian Computation : Markov Chains	47
4.2.1	Algorithms	47
4.2.2	Hamiltonian Monte Carlo	48
4.2.3	Computational efficiency comparison	48
4.3	Convergence Diagnostics	48
4.3.1	Proposal Distribution	49
4.3.2	The problem of auto and cross-correlations in the chains	50
4.4	Posterior Predictive	50
4.5	Bayesian Predictive Accuracy for Model Validation	51
4.5.1	Cross-validation for predictive accuracy	51
4.6	Bayesian Inference ?	52
4.6.1	Bayesian Credible Intervals	52
4.6.2	Distribution of Quantiles : Return Levels	53
4.7	Bayesian Model Averaging	53

4.8 Bayesian Neural Networks	53
II Experimental Framework : Extreme Value Analysis of Maximum Temperatures	54
5 Introduction to the Analysis	55
Repository for the code : R Package	56
Visualization Tool : Shiny Application	56
5.1 Presentation of the Analysis : Temperatures from Uccle	57
5.2 First Analysis : Annual Maxima	57
5.2.1 Descriptive Analysis	57
5.2.2 First visualization with simple models	58
5.2.3 Deeper Trend Analysis : Splines derivatives in GAM	58
Pointwise vs Simultaneous intervals	59
Methodology	59
Final Results	61
5.3 Comments and Structure of the Analysis	62
6 Analysis in Block Maxima	63
Block-length	64
R packages for EVT	64
6.1 Inference of the Stationary Model	64
6.1.1 Return Levels	65
6.1.2 Diagnostics	66
6.1.3 Stationary Analysis	67
POT	68
6.2 Parametric Nonstationary Analysis	68
6.2.1 Comparing Different Models	68
6.2.2 Selected Model, Diagnostics and Inference	69
6.3 Improvements with Neural Networks	71
6.3.1 Models and Results	71
6.3.2 Bagging	73
6.3.3 Inference : Confidence intervals by Bootstrap	74
6.4 Comments and Comparisons with POT	74
7 Bayesian Analysis in Block Maxima	76
Note on the available R package : evdbayes	77

7.1	From Our Functions (R package)	77
7.2	From HMC algorithm using STAN language	77
7.3	Ratio of Uniform : <code>revdbayes</code> package	77
7.4	Comparisons	77
7.4.1	STAN	77
7.5	Comparison with frequentists results	78
Conclusion		78
Appendix		79
A Statistical tools for Extreme Value Theory		II
A.1	Tails of the distributions	II
A.2	Convergence concepts	III
A.3	Varying functions	IV
A.4	Diagnostic Plots : Quantile and Probability Plots	IV
A.5	Estimators Based on Extreme Order Statistics for EVI	V
B Bayesian Methods		VII
B.1	Algorithms	VII
B.1.1	Metropolis–Hastings Algorithm	VII
B.1.2	Gibbs Sampler	VIII
B.1.3	Hamiltonian Monte Carlo	IX
C Other Figures and Tables		XII
D Github Repository Structure		XVIII

List of Figures

1.1	GEV distribution with the normal as benchmark (dotted lines) and a zoom on the parts of interest to better visualize the behaviour in the tails. In green, we retrieve the Gumbel distribution ($\xi = 0$). In red, we retrieve the Weibull-type ($\xi < 0$) while in blue, we get the Fréchet-type ($\xi > 0$). The endpoints for the Weibull and the Fréchet are denoted by the red and blue filled circles respectively.	10
2.1	Kernel density estimates for the whole series (grey) and for the series of excess over the threshold of $u = 30^\circ c$ (red). More information on the data will be given in Part II.	24
3.1	General framework of the fully-connected nonstationary GEV-CDN based on Cannon [2010]. The input layer will still the time itself in our application, i.e. $x_i(t) = t$, $\forall i = 1, \dots, I$ but it can be other covariates. The hidden layer represent additional complexity incorporated in the model and the output layer represent the three GEV parameters. (1) and (2) represent the functional relationships (3.17)-(3.18) between layers.	41
5.1	Yearly maxima together with three first models that represent the trend. Note that shaded grey area around the linear regression fit represent its 95% pointwise confidence interval on the fitted values (i.e., $\pm 1.96 \times \sigma_{pred}(\text{year})$) while blue dotted lines are prediction intervals taking also into account the prediction uncertainty.	58
5.2	Draws from the posterior distribution of the model. Notice the large uncertainty associated to the posterior draws (grey lines). The coverages are calculated for $M = 10^4$ simulations.	60
5.3	Plots of the first derivative $f'_{(20)}(\text{year})$ of the estimated splines on the retained GAM model. Grey area represents 95% confidence bands. Sections of the spline where the confidence interval does not include zero are indicated by thicker lines.	61
6.1	Quantile (left) and probability (right) plots for the stationary GEV model fitted by MLE.	66
6.2	(Left) Return level plot with red lines representing normal confidence intervals, and blue points the individual profile likelihood intervals for return levels. Horizontal dotted line represent the right endpoint of the fitted model in green and the maximum of the series in black. (Right) kernel density in black compared with the density of the fitted model in green, with dotted lines representing the endpoints of the empirical distribution, and green doted lines still represent the same right endpoint of the fitted EV-Weibull.	67

6.3	(left) Residual probability plot and (right) residual quantile plot on the Gumbel scale for the nonstationary GEV model allowing for a linear trend in the location parameter fitted by MLE.	70
6.4	Return levels (in blue) of the nonstationary GEV model allowing linear trend on $\mu(t)$. Dotted red line represent horizon after $n = 116$ years and black lines represent the series [1980 – 2016].	70
6.5	(Left) observations with quantiles from Model 2 estimated in Table 6.5. (Right) observations with same quantiles coming from the nonstationary and nonlinear bootstrap aggregated model with $M = 1000$ resamples. Note that in a stationary context, the 50%, 90% and 95% quantiles represent return levels with return periods of 2, 10 and 20 years respectively.	73
6.6	Residual bootstrap 95% intervals computed with the GEV-CDN model allow a linear nonstationary location parameter only (left), and for the nonlinear nonstationary model in location and scale parameters only with 2 hidden layers (right).	75
C.1	GEV distribution for different values of the three parameters	XII
C.2	Violin-plot and density plot for each seasons. (Right) vertical dotted lines represent the mean of each distribution.	XIII
C.3	ACF and PACF for the residuals of the fitted GAM model with assumed independent errors	XIII
C.4	Diagnostics of the chosen GAM model with Whinte Noise process on the errors, based on the residuals.	XIV
C.5	Series of annual maxima together with the fitted GAM model (in green) with MA(1) model on the residuals . Thicker lines indicate that the increase is significant for <u>pointwise</u> confidence interval. Shaded area represent a "95%" interval for the predicted values which looks quite narrow.	XIV
C.6	Profile likelihood intervals for the stationary GEV parameters. The two horizontal dotted lines represent the 95% (above) and 99% (below) confidence intervals by taking the intersection with the horizontal axis.	XV
C.7	95% Profile likelihood intervals for return levels with return periods of 2, 10 and 100. We kept the same x -scales for the three plots but not the y -scales. We used the <code>ismev</code> package but we modified the function to allow for more flexibility because the default y -scale in produced ugly visualizations for high return levels. Green lines represent the intervals from Table 6.3 computed with another package from E.Gilleland, <code>extRemes</code>	XV
C.8	ACF and PACF for the series of annual maxima.	XV
C.9	Plot of all daily TX that exceeded $30^\circ c$ in the period [1901,2016] in Uccle. Red lines highlights two periods of heavy heat waves during summers 1911 and 1976.	XVI
C.10	This graph gathers the two plots of Figure 6.5 which could yield to a better visualization.	XVI
C.11	Left plots show the parametric bootstrap 95% intervals computed with the GEV-CDN model allow a linear nonstationary location parameter only, and Right plots show these interval for the nonlinear nonstationary model in location and scale parameters with 2 hidden layes.	XVII

List of Tables

1.1	Two cases for the <i>density distribution</i> of the GEV	9
5.1	Proportion of the M posterior simulations which are covered by the confidence intervals	61
6.1	MLE's of the three GEV parameters assuming a independent (stationary) context.	64
6.2	Stationary GEV parameters estimated by PWM.	65
6.3	The m -year return level estimates and 95% intervals. Last line computes the length's differences between the normal and the profile likelihood intervals.	66
6.4	Comparisons of nested GEV models with nonstationary parameters. Significant p-values at level 5% are shown in bold.	69
6.5	MLE's of the nonstationary GEV parameters of Model 3 with a linear trend on $\mu(t) = \beta_0 + \beta_1 \cdot t$	69
6.6	Comparisons of nonstationary GEV-CDN models fitted by GML. Linear models have the identity activation function and the nonlinear models have the logistic sigmoid activation function.	72
6.7	Estimation by GML of the nonstationary parameters from the GEV-CDN Model 2 allowing a linear trend on the location $\mu(t) = \beta_0 + \beta_1 \cdot t$	72
C.1	Models' comparisons for the residuals of the GAM model based on AIC and BIC criterion.	XIII
C.2	Estimation of the bootstrap aggregated GEV-CDN model with 2 hidden layers for $\sigma(t)$ and $\mu(t)$, and $M = 500$ resamples. In red are denoted rough estimates of the nonstationary parameters as if the model were parametric for both parameters $\sigma(t) = \exp(\alpha_0 + \alpha_1 \cdot t)$ and $\mu(t) = \beta_0 + \beta_1 \cdot t$. But this is actually not reliable since there are 2 hidden layers, and only the shape parameter can be reliably estimated.	XVI

List of Abbreviations

For convenience, we place a list of all the abbreviations we will use in the text. However, these will always be defined in their first occurrence in the text.

DA	Domain of Attraction
df	(cumulative) distribution function
EVI	Extreme Value Index (ξ)
EVT	Extreme Value Theory
GEV	Generalized Extreme Value
GML	Generalized Maximum Likelihood
GPD	Generalized Pareto Distribution
MCMC	Marko Chain Monte Carlo
MH	Metropolis-Hastings (algorithm)
ML	Maximum Likelihood
MLE	Maximum Likelihood Estimator
NN	Neural Network
TN	Temperature miNimum
TX	Temperature maXimum

Introduction

Unlike its counterparts (see for example credit risk analysis, financial applications,...), the Extreme Value Theory (EVT) applied on broad environmental area such as meteorological data, has strong impacts on the people lives

An important question is still whether climate changes caused by anthropogenic activities will change the intensity and frequency of extreme events [Milly et al. \[2008\]](#).

The problem facing climate change evidence is the lack of past data to compare with her

For such an analysis, the number of parameters to take into account is considerable (and tend to infinity)

To make a parallel with Chaos Theory and the well-known butterfly effect which have strong applications in weather models

We anticipate that climate change to affect the extreme weather

[extremes in climate change p.347]

It has been proven that winter is becoming warmer in context of RC. (see naveau,...)

?

"The first myth about climate extremes, which has been purported by researchers in climatology or hydrology, among them prominent names, is that "extremes are defined as rare events" or similar. This myth is debunked by a simple bimodal PDF (Fig. 6.12a). The events sitting in the tails of that distribution are not rare" [\[Mudelsee, 2014, pp.257\]](#)

Until now, studies on climate extremes in Europe have usually had a strong national signature , or have had to make use of either a dataset with daily series from a very sparse network of meteorological stations (e.g. eight stations in Moberg et al. (2000)) or standardized data analysis performed by different researchers in different countries along the lines of agreed methodologies (e.g. Brazdil et al., 1996; Heino et al., 1999) [Klein Tank and Wijngaard \[2002\]](#)

Extrapolation !!!! See p154 [statistical analysis of extreme book]

Voir effet de l'ilot de chaleur -> urbanisation sur les tempés !

-> artificial warming on cities stations which were not(less) urbanized 100 years ago.

[In this thesis, efforts have been made to use power of (hyper)references into the text. While this not (yet ...) usable in printed versions, the reader may feel more comfortable in a numeric version to more easily handle the vast amount of sections, equations, references, etc... and the links that are made

between them.]

We can summarize the research question of this thesis as the following :

-

In this part, we will make use of general methods to assess if there is indeed a trend in the maximum temperatures

There are two main approaches in EVT, the block-maxima and the peaks-over-threshold approach (see [Section 2](#)) yielding to different extreme value distribution. The former aims at while the latter models the (...)

In [Chapter 1](#) we will present the method of block-maxima and derive the Generalized Extreme Value (GEV) distributions. In [Chapter 2](#) we will . In [Chapter 3](#) In Chapter 4 we will ..

Finally, we notice that this thesis will concentrate on the block-maxima (GEV) methods (see [Chapter 1](#)), i.e. to data relating to maxima over a period of 1 year. For example here in the introduction, or for the Bayesian analysis in [Chapter 5](#).

Part I

Theoretical Framework : Extreme Value Theory

CHAPTER 1

METHOD OF BLOCK MAXIMA

Contents

1.1	Preliminaries	5
1.2	Extremal Types Theorem : Extreme Value distributions	7
1.2.1	Generalized Extreme Value Distribution	7
1.3	Applications : Examples of Convergence to GEV	10
1.4	Maximum Domain of Attraction	13
1.4.1	Domain of attraction for the 3 types of GEV	14
1.4.2	Closeness under tail equivalence property	16
1.4.3	Domain of attraction of the GEV	17
1.5	Return Levels and Return Periods	17
1.6	Inference	18
1.6.1	Likelihood-based Methods	19
1.6.2	Other Estimator : Probability-Weighted-Moments	20
1.7	Model Diagnostics : Goodness-of-Fit	20
1.7.1	Return Level Plot	21

This chapter introduce the basics of EVT by considering the *block-maxima* approach. After defining useful concepts in [Section 1.1](#) to introduce the emergence of this theory, we will get into the leading theorem of EVT in [Section 1.2](#). [Section 1.3](#) will present some mathematical applications and [Section 1.4](#) conditions of this theorem in order to visualize the implications of the extremal theorem and the characterizations of the underlying distributions. [Section 1.5](#) will introduce key concepts of inference in EVT which will be presented in a general (and frequentist) way in [Section 1.6](#). Finally, [Section 1.7](#) provides some tools to assess the accuracy of the fitted model.

This chapter is mostly based on [Coles \[2001, chap.3\]](#), [Beirlant et al. \[2006, chap.2\]](#) and [Reiss and Thomas \[2007, chap.1-4\]](#), and other relevant articles.

1.1 Preliminaries

In the following, a sequence of independent and identically distributed (iid) random variables are assumed and written in the form $\{X_n\}_{n \in \mathbb{N}}$. The X_i 's share a common cumulative distribution function (df) F . The iid assumption will be relaxed in [Chapter 3](#).

Statistical Tools

Let $X_{(i)}$ denote the i -th ascending order statistic,

$$X_{(1)} \leq X_{(2)} \leq \dots \leq X_{(n)}, \quad (1.1)$$

assuming n observations. One order statistic is of particular interest, the *maximum* $X_{(n)}$

$$X_{(n)} := \max_{1 \leq i \leq n} X_i, \quad (1.2)$$

while the *minimum* $X_{(1)}$ can be defined it with respect to the maximum operator

$$X_{(1)} := \min_{1 \leq i \leq n} X_i = -\max_{1 \leq i \leq n} (-X_i). \quad (1.3)$$

This text will focus on maxima but it is important to keep in mind that the analysis made in the following can be extended to minima through relation (1.3).

Furthermore, we can retrieve the distribution of $X_{(n)}$. By definition,

$$\begin{aligned} \Pr\{X_{(n)} \leq x\} &= \Pr\{X_1 \leq x, \dots, X_n \leq x\} \\ &\stackrel{(\perp)}{=} \Pr\{X_1 \leq x\} \dots \Pr\{X_n \leq x\} \\ &= F^n(x), \end{aligned} \quad (1.4)$$

where the independence (\perp) follows directly from the iid assumption of the sequence $\{X_i\}$.

First Definitions and Theorems : Motivations

Definition 1.1 (Distributions of same type). *We say that two dfs G and G^* are of the **same type** if, for constants $a > 0$ and b we have*

$$G^*(az + b) = G(z), \quad \forall z. \quad (1.5)$$

△

This means that the distributions only differ in location and scale. This concept will be useful later in the text to derive the three different families of extreme value distributions which come from other distributions that are of the *same type*.

Principles of stability : Amongst the principles about EVT that will be covered during this text, EVT will be highly influenced by the principles of *stability*. It states that a model should remain valid and consistent whatever choices are made on the structure of this model. For example, if we propose a

model for the annual maximum temperatures and another for the 5-year maximum temperatures, the two models should be mutually consistent since the 5-year maximum will be the maximum of 5 annual maxima. Similarly, in a Peaks-Over-Threshold setting (presented in [Chapter 2](#)), a model for exceedances over a high threshold should remain valid for exceedances of higher thresholds.

Definition 1.2 (Max-stability). From [Leadbetter et al. \[1983\]](#) or [Resnick \[1987\]](#), we say that a distribution G is **max-stable** if, for each $n \in \mathbb{N}$ we have

$$G^n(a_n z + b_n) = G(z), \quad n = 1, 2, \dots, \quad (1.6)$$

for appropriate normalizing constants $a_n > 0$ and b_n . \triangle

In other words, taking powers of G results only in a change of location and scale. This concept will be closely connected with the fundamental limit law for extreme values that we will present in the [next Section](#). However, the power of max-stable processes is often used in a multivariate setting, whereas we will focus on univariate sequences. Refer for example to [Ribatet et al. \[2015\]](#) for an introduction on max-stable processes.

A fundamental concept of EVT is the concept of **degenerate** dfs. We recall that the df of a random variable is said to be *degenerate* if it assigns all probability to a single point. We illustrate this by the construction of the well-known *Central Limit Theorem* (CLT) that we will state below and which concerns the sample mean $\bar{X}_n = n^{-1} \sum_{i=1}^n X_i$. We know from the Weak Law of Large Numbers that \bar{X}_n will converge *almost surely* to the true mean μ (see¹ [Theorem A.1](#)). and thus in distribution, that is to a non-random single point, i.e. to a *degenerate* distribution

$$\Pr\{\bar{X}_n \leq x\} = \begin{cases} 0, & x < \mu; \\ 1, & x \geq \mu. \end{cases}$$

This is not useful, in particular for inferential purposes.

For this reason, CLT aims at finding a non-degenerate limiting distribution for \bar{X}_n , after allowing for normalization by sequences of constants. We will state it in its most basic form :

Theorem 0 (Central Limit Theorem). Let $\{X_i\}$ be a sequence of n iid random variables with $E(X_i^2) < \infty$. Then, as $n \rightarrow \infty$,

$$\sqrt{n}(\bar{X}_n - \mu) \xrightarrow{d} N(0, \sigma^2),$$

where $\mu = E(X_i)$ and $\sigma^2 = V(X) > 0$.

Then, by making a proper choice of some normalizing constants, μ and \sqrt{n} (as location and scale parameters respectively), we find the non-degenerate normal distribution in the limit for the empirical mean \bar{X}_n provided X_i has a nonzero variance and finite second moment.

With the same logic, we find for the distribution of maximum order statistics $X_{(n)}$

$$\lim_{n \rightarrow \infty} \Pr\{X_{(n)} \leq x\} = \lim_{n \rightarrow \infty} \Pr\{X_i \leq x\}^n = \begin{cases} 0, & F(x) < 1; \\ 1, & F(x) = 1, \end{cases} \quad (1.7)$$

¹[Appendix A.2](#) can be useful for a relevant short review of main concepts of convergence.

which is also a degenerate distribution.

Whereas the CLT dealt with the sample mean, EVT also aims to find a non-degenerate distribution in the limit of the maximum $X_{(n)}$ by means of normalization.

1.2 Extremal Types Theorem : Extreme Value distributions

Introduced by Fisher and Tippett [1928], later revised by Gnedenko [1943] and streamlined by de Haan [1970], the *extremal types theorem* is important for its applications in EVT. Let $\{X_i\}$ be a sequence of iid random variables with df F . It states the following :

Theorem 1.1 (Extremal Types). *If there exist sequences of normalizing constants $a_n > 0, b_n \in \mathbb{R}$ and a non-degenerate limiting distribution G such that*

$$\lim_{n \rightarrow \infty} \Pr\left\{a_n^{-1}(X_{(n)} - b_n) \leq z\right\} = F^n(a_n z + b_n) = G(z), \quad \forall z \in \mathbb{R}, \quad (1.8)$$

then G has the same type as one of the following distributions :

$$\boxed{\text{I}} : \quad G_1(z) = \exp\left\{-e^{-z}\right\}, \quad -\infty < z < \infty. \quad (1.9)$$

$$\boxed{\text{II}} : \quad G_{2,\alpha}(z) = \begin{cases} 0, & z \leq 0; \\ \exp\left\{-z^{-\alpha}\right\}, & z > 0. \end{cases} \quad (1.10)$$

$$\boxed{\text{III}} : \quad G_{3,\alpha}(z) = \begin{cases} \exp\left\{-(-z)^\alpha\right\}, & z < 0; \\ 1, & z \geq 0, \end{cases} \quad (1.11)$$

for some parameter $\alpha > 0$ in case II and III. □

These are termed the *standard extreme value distribution functions* and are differentiated by three types. Note that each real parameter α determines the type. Type **I** is commonly known as the *Gumbel* family while the type **II** and type **III** are known as the *Fréchet* and the *Weibull* families respectively. From the fact that G is of the *same type* as one of the three distribution, we can rescale these distributions by some normalizing parameters $a > 0$ (scale) and b (location), that is $G_{i,\alpha,a,b}(z) = G_{i,\alpha}\left(\frac{z-b}{a}\right)$ for $i = 2, 3$, and similarly for G_1 to obtain the *full EV distributions*.

This theorem considers an iid random sample, but it holds true even if the original scheme is no longer independent. We will present the stationary case in [Section 3.1](#). Furthermore, we will see in [Section 1.4](#) that F is in the *domain of attraction* of G .

1.2.1 Generalized Extreme Value Distribution

Von Mises [1936] showed that another representation is possible by taking the reparametrization $\xi = \alpha^{-1}$ of the extreme values dfs to obtain a continuous, unified model.

Hence, these three classes of extreme distributions can be expressed in the same functional form as

special cases of the single three-parameter *Generalized Extreme Value* (GEV) distribution

$$G(z) := G_{\xi, \mu, \sigma}(z) = \exp \left\{ - \left[1 + \xi \left(\frac{z - \mu}{\sigma} \right) \right]_+^{-\xi^{-1}} \right\}, \quad \xi \neq 0. \quad (1.12)$$

where $-\infty < \mu, \xi < \infty$ and $\sigma > 0$ with (μ, σ, ξ) being the three parameters of the model characterizing location, scale and shape respectively. We introduce the notation $y_+ = \max(y, 0)$ to denote that (1.12) is defined on $\{z : 1 + \xi \sigma^{-1}(z - \mu) > 0\}$. It ensures the term in the exponential function is negative, and the df converges to 1. It is important to note that this yields a vital condition for the GEV as it defines the endpoints from the three different characterizations of this distribution from the values of the shape parameter.

The GEV corresponds to the *Fréchet* family (1.10) whenever $\xi > 0$ and to the *Weibull* family (1.11) as $\xi < 0$. When $\xi = 0$, i.e. for the *Gumbel* family (1.9), the situation in (1.12) is not defined but is taken as the limit as $\xi \rightarrow 0$, leading to

$$G(z) := G_{\mu, \sigma}(z) = \exp \left\{ - \exp \left(\frac{z - \mu}{\sigma} \right) \right\}, \quad \xi = 0. \quad (1.13)$$

The shape parameter $\xi \in \mathbb{R}$ is called the *extreme value index* (EVI) and is at the center of the analysis in EVT. It determines, in some degree of accuracy, the type of the underlying distribution.

Following Coles [2001], we introduce an important theorem in Extreme Value Theory and that has many implications. This theorem states the following :

Theorem 1.2. *For any df F ,*

$$F \text{ is max-stable} \iff F \text{ is GEV}. \quad (1.14)$$

□

Hence, any df that is *max-stable* (see Definition 1.2) is also GEV (1.12)-(1.13), and vice-versa. To gain interesting insights of the implications of this theorem, we think it is useful to give an informal proof but only for the " \Leftarrow " as the converse requires a significant mathematical background. By using max-stability (Definition 1.2) and Theorem 1.2, this "proof" also gives intuition for Theorem 1.1.

Outline Proof of Extremal Types Theorem 1.1 (and Theorem 1.2) :

- If $a_n^{-1}(X_{(n)} - b_n)$ has the GEV as limit distribution for large n as defined in (1.8), then

$$\Pr \left\{ a_n^{-1}(X_{(n)} - b_n) \leq z \right\} \approx G(z).$$

Hence for any integer k , since nk is large, we have

$$\Pr \left\{ a_{nk}^{-1}(X_{(n)k} - b_{nk}) \leq z \right\} \approx G(z). \quad (1.15)$$

- Since $X_{(n)k}$ is the maximum of k variables having identical distribution as $X_{(n)}$,

$$\Pr \left\{ a_{nk}^{-1}(X_{(n)k} - b_{nk}) \leq z \right\} = \left[\Pr \left\{ a_{nk}^{-1}(X_{(n)} - b_{nk}) \leq z \right\} \right]^k, \quad (1.16)$$

giving two expressions for the distribution of $X_{(n)}$, by (1.15) and (1.16) :

$$\Pr\{X_{(n)} \leq z\} \approx G(a_n^{-1}(z - b_n)) \quad \text{and} \quad \Pr\{X_{(n)} \leq z\} \approx G^{1/k}(a_{nk}^{-1}(z - b_{nk})).$$

- It follows that G and $G^{1/k}$ are identical apart from location and scale coefficients. Hence, G is *max-stable* and therefore GEV. This gives intuition of the **extremal types** [Theorem 1.1](#).

□

In words, it means that taking power of G results only in a change of location and scale, and hence by recalling the expression of the distribution of $X_{(n)}$ (1.4), it is possible to find the non-degenerate GEV in the limit for $X_{(n)}$. More technical details can be found in [Leadbetter et al. \[1983\]](#).

Density

The density of the GEV distribution (1.12), $g(z) = \frac{dG(z)}{dz}$ (since we have absolute continuity) can be expressed in two forms, as depicted in Table 1.1.

Table 1.1: Two cases for the density distribution of the GEV

$\xi \neq 0$	$g(z) = \sigma^{-1} \left[1 + \xi \left(\frac{z-\mu}{\sigma} \right) \right]_+^{-\frac{1}{\xi}-1} \exp \left\{ - \left[1 + \xi \left(\frac{z-\mu}{\sigma} \right) \right]_+^{-\xi^{-1}} \right\};$
$\xi \rightarrow 0$	$g(z) = \sigma^{-1} \exp \left\{ - \left(\frac{z-\mu}{\sigma} \right) \right\} \exp \left\{ - \exp \left[- \left(\frac{z-\mu}{\sigma} \right) \right] \right\}.$

We can now try to visually represent these three families. The following Figure 1.1 depicts the GEV, defined with respect to the value of the shape parameter ξ .

It is important to point out that the location parameter μ does not represent the mean as in the classic statistical view rather it represents the “center” of the distribution; and the scale parameter σ is not the standard deviation but does govern the “size” of the deviations around μ . This can be visualized in Figure C.1 in [Appendix C](#) where we show the variation of the GEV distribution when we vary these parameters². We notice that the location parameter only implies a horizontal shift of the distribution, without changing its shape, and we see the influence of the scale parameter on the spread of the distribution around μ . For example if $\sigma \nearrow$, then the density will appear more flat.

In the following, we define the *left* and the *right endpoint* of a particular df F as respectively $*x$ and x_* , by :

$$*_x = \inf\{x \in \mathbb{R} : F(x) > 0\}, \quad \text{and} \quad x_* = \sup\{x \in \mathbb{R} : F(x) < 1\}. \quad (1.17)$$

Note that the Gumbel distribution is unbounded. The Fréchet distribution has a finite left endpoint in $*x = \mu - \sigma \cdot \xi^{-1}$ (blue circle in Figure 1.1), and its upper endpoint is $+\infty$ while the Weibull distribution has a finite right endpoint in $x_* = \mu - \sigma \cdot \xi^{-1}$ (red circle in Figure 1.1) and is unbounded in the left. This has serious impact on modeling. Since these endpoints are functions of the parameter values, will

²Moreover, a Shiny application has been built through the R package to visualize in the best way the influence of the parameters on this distribution. See intro of [Chapter 5](#) for an explanation on its use.

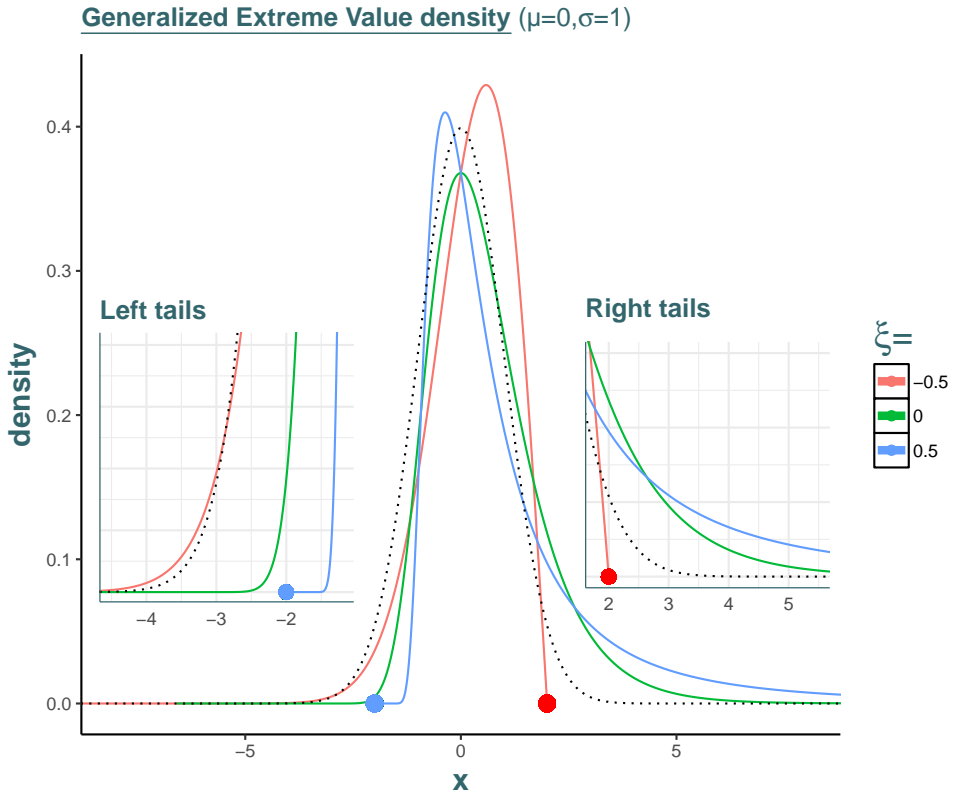


Figure 1.1: GEV distribution with the normal as benchmark (dotted lines) and a zoom on the parts of interest to better visualize the behaviour in the tails. In green, we retrieve the Gumbel distribution ($\xi = 0$). In red, we retrieve the Weibull-type ($\xi < 0$) while in blue, we get the Fréchet-type ($\xi > 0$). The endpoints for the Weibull and the Fréchet are denoted by the red and blue filled circles respectively.

see later in [Section 1.6.1](#) that it can make the likelihood computation unstable. We will particularly face this in the Bayesian [Chapter 4](#).

It can be useful to think not only about the specific form of data or the distribution they will fit and its characteristics, but also about how to retrieve these specific distributions in practice. That is why we detail some examples of how to construct such EV distributions for the three types in concrete cases, playing with the appropriate choice of sequences a_n and b_n to retrieve the pertaining distribution family.

1.3 Applications : Examples of Convergence to GEV

In real applications it is not easy to find the appropriate sequences, but it is useful to understand the concept of convergence to GEV by looking at some theoretical examples.

Convergence to Gumbel distribution

The **Type I** or **Gumbel** distribution G_1 can be retrieved by considering, for example, an iid exponentially distributed sequence $\{X_j\}$ of n random variables, that is $X_j \stackrel{iid}{\sim} Exp(\lambda)$ and taking the largest

of these values, $X_{(n)}$, as defined earlier. By definition, if the X_j have df F , then $F(x) = 1 - e^{-\lambda x}$ for $x > 0$. Hence, our goal is to find non-random sequences $\{b_n\}$, $\{a_n > 0\}$ such that

$$\lim_{n \rightarrow \infty} \Pr\left\{a_n^{-1}(X_{(n)} - b_n) \leq z\right\} = G_1(z). \quad (1.18)$$

Hence, we find that

$$\begin{aligned} \Pr\left\{a_n^{-1}(X_{(n)} - b_n) \leq z\right\} &= \Pr\{X_{(n)} \leq b_n + a_n z\} \\ &= \left[\Pr\{X_1 \leq b_n + a_n z\}\right]^n \\ &= \left[1 - \exp\{-\lambda(b_n + a_n z)\}\right]^n, \end{aligned}$$

from the iid assumption of the random variables and their exponential distribution. Hence, by choosing the sequences $a_n = \lambda^{-1}$ and $b_n = \lambda^{-1} \log n$ and reminding that

$$\left[1 - \exp\{-\lambda(b_n + a_n z)\}\right]^n = \left[1 - \frac{1}{n}e^{-z}\right]^n \xrightarrow{n \rightarrow \infty} \exp(-e^{-z}) := G_1(z),$$

we find the so-called standard *Gumbel* distribution in the limit. Note that the same can be retrieved with $X_j \stackrel{iid}{\sim} N(0, 1)$ and with sequences $a_n = -\Phi^{-1}(1/n)$ and $b_n = 1/a_n$.

Typically unbounded distributions, for example the Exponential and Normal, whose tails fall off exponentially or faster, will have the Gumbel limiting distribution for the maxima. They will have medians (and other quantiles) that grow as $n \rightarrow \infty$ at the rate of some power of $\log n$. This is a typical example of light-tailed distribution (i.e., whose tails decay exponentially, as defined in [Appendix A.1](#)).

Convergence to Fréchet distribution

The **Type II** or **Fréchet type** (or *Fréchet-Pareto*) distribution $G_2(x)$ has strong relations with the Pareto distribution and also the Generalized Pareto Distribution that will be presented in [Chapter 2](#). These are distributions which are typically heavy- or fat-tailed (see [Appendix A.1](#)).

Following [Beirlant et al. \[1996\]](#), when starting with a sequence $\{X_j\}$ of n iid random variables following a *basic* (or *generalized* with scale parameter set to 1) Pareto distribution with shape parameter $\alpha \in (0, \infty)$, $X_j \sim Pa(\alpha)$, we have

$$F(x) = 1 - x^{-\alpha}, \quad x \in [1, \infty). \quad (1.19)$$

Then, by setting $b_n = 0$, we can write

$$\begin{aligned} -n\bar{F}(a_n z + b_n) &= -n(a_n z + b_n)^{-\alpha} \\ &= \left[F^\leftarrow\left(1 - \frac{1}{n}\right)\right]^\alpha (a_n)^{-\alpha} (-z^{-\alpha}), \end{aligned}$$

where we define the quantity $F^\leftarrow(t) = \inf\{x \in \mathbb{R} : F(x) \geq t\}$ for $t < 0 < 1$ as the *generalized*

inverse³ of F . Hence, we see that by setting $a_n = n^{1/\alpha}$ and keeping $b_n = 0$, we have

$$\Pr\{a_n^{-1}X_{(n)} \leq z\} \rightarrow \exp(-z^{-\alpha}),$$

showing that for those particular values of the normalizing constants, we retrieve the Fréchet distribution in the limit of a basic Pareto distribution. The fact that b_n is set to zero can be understood intuitively for heavy-tailed distribution (see [Appendix A.1](#)) such as the Pareto distribution, a correction for location is not necessary to obtain a non-degenerate limiting distribution, see [Beirlant et al. \[1996, pp.51\]](#). More generally, we can state the following theorem :

Theorem 1.3 (Pareto-type distributions). *For the same choice of normalizing constants as above, i.e. $a_n = F^{\leftarrow}(1 - n^{-1})$ and $b_n = 0$ and for any $x \in \mathbb{R}$, if*

$$n[\bar{F}(a_n x)] = \frac{\bar{F}(a_n x)}{\bar{F}(a_n)} \rightarrow x^{-\alpha}, \quad n \rightarrow \infty, \tag{1.20}$$

then we say that " \bar{F} is of Pareto-type" or, more technically, " \bar{F} is regularly varying with index $-\alpha$ ". \square

This theorem helps to understand the shape of the tails of this kind of distributions. We define the concepts of *regularly varying functions*, and *slowly varying functions* in [Appendix A.3](#)

Convergence to EV Weibull distribution

The type **III** or **EV Weibull** family of distributions $G_3(x)$ arises in the limit of n iid uniform random variables $X_j \sim U[L, R]$ where L and $R > L$ are both in \mathbb{R} and denote respectively the Left and the Right endpoint of the domain of definition. We have by definition

$$F(x) = \frac{x - L}{R - L}, \quad x \in [L, R].$$

It is 0 for $x < L$ and 1 for $x > R$. We assume we are in the general case, i.e. $[L, R]$ can $\neq [0, 1]$. When choosing $a_n = R$ and $b_n = (R - L)/n$, we find the unit Reversed Weibull distribution $We(1, 1)$ in the limit

$$\begin{aligned} \Pr\{a_n^{-1}(X_{(n)} - b_n) \leq z\} &= \Pr\{X_{(n)} \leq b_n + a_n z\} \\ &= \left[1 - \frac{R - b_n - a_n z}{R - L}\right]^n, \quad L \leq b_n + a_n z \leq R \\ &= \left(1 + \frac{z}{n}\right)^n \rightarrow e^z, \quad z \leq 0 \quad \text{and} \quad n > |z|. \end{aligned}$$

The Weibull-type GEV with $\xi = -1$, is a typical example of the maximal behavior for bounded random variables with continuous distributions.

³We retrieve $x_t = F^{\leftarrow}(t)$, the t -quantile of F . Even if we will deal only with continuous and strictly increasing df, we prefer considering the *generalized inverse*, for sake of generalization.

Conditions and Comments

It stands to reason that the df F needs certain conditions for the limit to exist in [Theorem 1.1](#). There exists a *continuity condition* at the right endpoint x_* of F which rules out many important distributions. For example, it ensures that if F has a jump at its finite x_* (e.g. discrete distributions), then F cannot have a non-degenerate limit distribution as in (1.8). Examples are well documented in [Embrechts et al. \[1997, section 3.1\]](#) for the Poisson, Geometric and Negative Binomial distributions. We cannot find a nondegenerate distribution in the limit for these distributions even after normalization, which limit the scope for applications of the Extremal Types [Theorem 1.1](#).

It is not mandatory to find the normalizing sequences for inferential purposes. We can ignore the normalizing constants in practical applications and fit directly the GEV in our set of maxima. The parameters (μ, σ) will implicitly take the normalization into account, while the shape parameter ξ is not affected. More details on this are in [Chapter 3](#) with methods to estimate (μ, σ, ξ) in [Section 1.6](#).

1.4 Maximum Domain of Attraction

The preceding results can be summarized and obtained when considering *maximum domain of attraction* (MDA). The term "*maximum*" is typically used to make the difference with *sum-stable* distributions but as we only study maxima here, there is no possible confusion in our work. We will only write "*domain of attraction*" (DA) in the following for convenience.

Definition 1.3 (Domain of attraction). *We say that a distribution F is in the **domain of attraction** of an extreme value family G in (1.9)-(1.11), denoted by $F \in D(G)$, if there exist $a_n > 0$ and $b_n \in \mathbb{R}$ such that the distribution of $a_n^{-1}(X_{(n)} - b_n)$ converges in distribution to G , where $X_{(n)}$ is the maximum of an iid sequence $\{X_i\}$ with distribution F .* \triangle

Let ξ_k denote the EVI pertaining to some EV distribution G_k ($k = 1, 2, 3$). From [Theorem 1.1](#), the domains of attraction are well defined in the sense that $F \in D(G_i)$ and $F \in D(G_j)$ implies $\xi_i = \xi_j$.

At this point, we have all the necessary tools to the pertaining DA. But, before proceeding, it is necessary to point out that the characterization of the first DA (the Gumbel type) requires more technicalities going beyond the scope of this thesis. Although this class is important in theory, see e.g. [Pinheiro and Ferrari \[2015\]](#), it is less relevant for our purpose of modelling extremes in a practical case. It often requires other generalizations, for instance with additional parameters to surpass the issues of fitting empirical data. In the last subsection, we will present the unified framework, the domain of attraction pertaining to the GEV distributions, which is a summary for the three first domains of attraction presented.

In each of the characterization of the DA, we will present some of their most useful, necessary (and sometimes sufficient) conditions. We will derive their *von Mises conditions*, coming from [Von Mises \[1936\]](#) but revisited in [Falk and Marohn \[1993\]](#). These conditions are important in practice and intuitive because they make use of the *hazard function* of a df F , defined in the following, for sufficiently smooth distributions :

$$r(x) = \frac{f(x)}{\bar{F}(x)} = \frac{f(x)}{1 - F(x)}. \quad (1.21)$$

It involves the density function $f(x) = \frac{dF(x)}{dx}$ in the numerator and it can be thought as a measure of risk. It can be interpreted as the probability of "failure" in an infinitesimally small time period between x and $x + \delta x$ given that the subject has "survived" up until time x .

1.4.1 Domain of attraction for the 3 types of GEV

Domain of attraction for Gumbel distribution (G_1)

We derive here two ways of formulating necessary and sufficient condition for a df F to be in the Gumbel DA, namely $F \in D(G_1)$.

Theorem 1.4. *Following [Beirlant et al., 2006, pp.72], $F \in D(G_1)$ if and only if for some auxiliary function $b(\cdot)$, for every $v > 0$, the condition*

$$\frac{\bar{F}(x + b(x) \cdot v)}{\bar{F}(x)} \rightarrow e^{-v}, \quad (1.22)$$

as $x \rightarrow x_*$. Then,

$$\frac{b(x + v \cdot b(x))}{b(x)} \rightarrow 1.$$

□

More technical characterizations and conditions together with proofs can be found in Haan and Ferreira [2006, pp.20-33] based on the pioneering thesis of Haan [1970].

Let's now present his **von Mises criterion** as in [Beirlant et al., 2006, pp.73]:

Theorem 1.5 (von Mises). *If $r(x)$ (1.21) is ultimately positive in the neighbourhood of x_* , is differentiable there and satisfies*

$$\lim_{x \uparrow x_*} \frac{dr(x)}{dx} = 0, \quad (1.23)$$

then $F \in D(G_1)$.

□

The slope of the hazard function with respect to x is zero at the limit when x approaches the (infinite) right-endpoint. This ensures a condition on the lightness of the tails of F .

Examples of distributions in $D(G_1)$: distributions with tails that are exponentially decaying (light-tailed i.e. the exponential, Gamma, Weibull, logistic, ...) but also distributions that are moderately heavy-tailed such as the lognormal. To see this, consider a Taylor expansion :

$$\bar{G}_1(x) = 1 - \exp(-e^{-x}) \sim e^{-x}, \quad x \rightarrow \infty,$$

where " \sim " refers to the asymptotic equivalence function. Hence, we see the exponential decay of the tails for the Gumbel distribution.

Domain of attraction for Fréchet distribution (G_2)

Let's define $\alpha := \xi^{-1} > 0$ as the *index* of the Fréchet distribution in (1.10).

Definition 1.4 (Power law). *If we look at the tail of the distribution G_2 , a Taylor expansion tells us that*

$$\bar{G}_2(x) = 1 - \exp(-x^{-\alpha}) \sim x^{-\alpha}, \quad x \rightarrow \infty, \quad (1.24)$$

which means that G_2 tends to decrease as a power law. \triangle

Theorem 1.6. *We have $F \in G_2$ if and only if*

$$\bar{F}(x) = x^{-\alpha} L(x), \quad (1.25)$$

for some slowly varying function L (see [Appendix A.3](#) for the definition). \square

In this case and with $b_n = 0$,

$$F^n(a_n x) \xrightarrow{d} G_2(x), \quad x \in \mathbb{R},$$

with

$$a_n := F^{\leftarrow} \left(1 - \frac{1}{n} \right) = \left(\frac{1}{1-F} \right)^{\leftarrow}(n).$$

This theorem informs us that all dfs $F \in D(G_{2,\alpha})$ have an infinite right endpoint, that is $x_* = \sup\{x : F(x) < 1\} = \infty$. These distributions are all with regularly varying right-tail with index $-\alpha$ (see [Appendix A.3](#)), that is $F \in D(G_{2,\alpha}) \iff \bar{F} \in R_{-\alpha}$.

[Falk and Marohn \[1993\]](#) present the revisited **Von Mises condition** for this DA :

Theorem 1.7 (von Mises). *If F is absolutely continuous with density f and $x_* = \infty$ such that*

$$\lim_{x \uparrow \infty} x \cdot r(x) = \alpha > 0,$$

then $F \in D(G_{2,\alpha})$. \square

We illustrate this with the standard Pareto distribution, that is

$$F(x) = \left(1 - \left(\frac{x_m}{x} \right)^\alpha \right) 1_{x \geq x_m}, \quad \alpha > 0 \text{ and } x_m > 0.$$

By setting $K = x_m^\alpha$, we obtain $\bar{F}(x) = Kx^{-\alpha}$. Therefore, $a_n = (Kn)^{\alpha-1}$ and $b_n = 0$.

Examples of distributions in $D(G_2)$: distributions that are typically (very) fat-tailed (or heavy-tailed, see [Appendix A.1](#)) distributions, such that $E(X_+)^{\delta} = \infty$ for $\delta > \alpha$. This class of distributions is thus appropriate for phenomena with extremely large maxima, for example the rainfall process in some tropical zones. Common distributions include Pareto, Cauchy, Burr, etc. Another example is (1.24) showing that G_2 tends to decrease as a *power law*.

Domain of attraction for the EV Weibull distribution (G_3)

We start by recalling the relation between the Fréchet and the EV Weibull distributions

$$G_3(-x^{-1}) = G_2, \quad x > 0.$$

A certain symmetry occurs for these two types (e.g. Figure 1.1). Hence, this will be useful to characterize $D(G_3)$ using what we know about the Fréchet case.

Theorem 1.8. *We say that $F \in G_3$ as in (1.11) with index $\alpha = \xi^{-1} > 0$ if and only if there exists a finite right endpoint $x_* < \infty$ such that*

$$\bar{F}(x_* - x^{-1}) = x^{-\alpha} L(x), \quad (1.26)$$

where $L(\cdot)$ is a slowly varying function. \square

Hence for $F \in D(G_{3,\alpha})$, we have

$$a_n = x_* - F^\leftarrow(1 - n^{-1}), \quad b_n = x_*,$$

and hence

$$a_n^{-1} (X_{(n)} - b_n) \xrightarrow{d} G_3.$$

Finally, we present the **Von Mises condition** related to the G_3 DA.

Theorem 1.9 (von Mises). *For F having positive derivative on some $[x_0, x_*]$, with finite right endpoint $x_* < \infty$, then $F \in D(G_3)$ if*

$$\lim_{x \uparrow x_*} (x_* - x) \cdot r(x) = \alpha > 0. \quad (1.27)$$

\square

Similarly to the Fréchet case, there is still a probability mass from the hazard rate when x approaches its finite right endpoint, characterized by a non-null constant α which defines the left heavy tail and the right endpoint.

Examples of distributions in $D(G_3)$: dfs that are bounded to the right ($x_* < \infty$). Whereas the Fréchet type is preferable in an extreme analysis context as it allows for arbitrarily large values, most phenomena are typically bounded, hence we will use EV Weibull for the most attractive and flexible class for modelling extremes. For example, our case of modelling a process of maximum temperatures seems to be a perfect candidate.

1.4.2 Closeness under tail equivalence property

An interesting property of all three types of DA $D(G_k)_{k=1,2,3}$ we have derived, is that of those *closed under tail-equivalence*. This is useful for characterizing tail's types of the distributions falling in the pertaining DA. In this sense,

1. For the **Gumbel** DA, let $F \in D(G_{1,\alpha})$. If H is another df such that, for some $b > 0$,

$$\lim_{x \uparrow x_*} \frac{\bar{F}(x)}{\bar{H}(x)} = b, \quad (1.28)$$

then $H \in D(G_{1,\alpha})$. This emphasizes exponential type of the tails for H in the Gumbel DA.

2. For the **Fréchet** DA, let $F \in D(G_{2,\alpha})$. If H is another df such that, for some $c > 0$,

$$\lim_{x \rightarrow \infty} \frac{\bar{F}(x)}{\bar{H}(x)} = c, \quad (1.29)$$

then $H \in D(G_{2,\alpha})$.

3. For the **Weibull** DA, let $F \in D(G_{3,\alpha})$. If H is another df such that, for some $c > 0$,

$$\lim_{x \uparrow x_*} \frac{\bar{F}(x)}{\bar{H}(x)} = c, \quad (1.30)$$

then $H \in D(G_{3,\alpha})$.

This emphasizes the polynomial decay for the tails of the distributions falling in the Fréchet or in the Weibull DA.

1.4.3 Domain of attraction of the GEV

The conditions that have been stated for the three preceding DA can be restated under a "unified" framework for the GEV distribution defined in (1.12). For a given df F that is sufficiently smooth, by letting the sequences b_n , a_n , and the shape parameter such that

$$b_n = F^\leftarrow(1 - n^{-1}), \quad a_n = r(b_n) \quad \text{and} \quad \xi = \lim_{n \rightarrow \infty} r'(x),$$

then, $a_n^{-1}(X_{(n)} - b_n)$ has the GEV as nondegenerate limiting distribution which density is denoted in Table 1.1. This is a sufficient condition. Among many characterizations, we present the following.

Theorem 1.10. *Let F be the df of a sequence $\{X_i\}$ iid. For $u(\cdot) > 0$ measurable and $\xi \in \mathbb{R}$, $F \in D(GEV)$ if and only if :*

$$\lim_{v \uparrow x_*} \Pr \left\{ \frac{X - v}{u(v)} > x \mid X > v \right\} := \lim_{v \uparrow x_*} \frac{\bar{F}(v + x \cdot u(v))}{\bar{F}(v)} = \begin{cases} (1 + \xi x)_+^{-\xi^{-1}}, & \xi \neq 0; \\ e^{-x}, & \xi = 0. \end{cases} \quad (1.31)$$

□

We will see in Chapter 2 that it defines the "Peaks-Over-Threshold" model.

1.5 Return Levels and Return Periods

After having defined the theoretical properties of distributions pertaining to the GEV family precisely, we are now interested in finding a quantity that could significantly improve the interpretability of such models. *Return levels* play a major role in environmental analysis. For such tasks, it is usually more convenient to interpret EV models in terms of insightful return levels rather than individual parameter estimates.

Assuming for this introductory example the block-length is one year -as usually assumed in meteorological analysis-, let consider the *m-year return level* r_m which is defined as the high quantile for which the probability that the annual maximum exceeds this quantile is $(\lambda \cdot m)^{-1}$, where λ is the mean number of events that occur in a year. For yearly blocks, we have $\lambda = 1$ which will facilitate the interpretation. We call m the *return period* and define it to a reasonable degree of accuracy as the expected time between the occurrence of two so-defined high-quantiles. For example, under stationary assumption, if the 100-year return level is $37^\circ c$ for the sequence of annual maximum temperatures, then $37^\circ c$ is the temperature that is expected to be reached on average once within a period of 100 years. More precisely, you can see it such that r_m is exceeded by the annual maximum in any particular year with probability m^{-1} .

Let $\{X_{(n),y}\}$ denote the iid sequence of n random variables representing the annual maximum for a particular year y . From (1.12), we have

$$\begin{aligned} F(r_m) &:= \Pr\{X_{(n),y} \leq r_m\} = 1 - 1/m \\ &\Leftrightarrow \left[1 + \xi \left(\frac{r_m - \mu}{\sigma}\right)\right]^{-\xi^{-1}} = \frac{1}{m}. \end{aligned}$$

Hence, by inverting this relation, and by letting $y_m = -\log(1 - m^{-1})$, we can retrieve the quantile of the GEV, namely the *return level* r_m

$$r_m = \begin{cases} \mu + \sigma \xi^{-1} (y_m^\xi - 1), & \xi \neq 0; \\ \mu + \sigma \log(y_m), & \xi = 0. \end{cases} \quad (1.32)$$

Having estimated the model (that will be the subject of [Section 1.6](#)), we can replace the estimated parameters $\hat{\theta} = (\hat{\mu}, \hat{\sigma}, \hat{\xi})$ in (1.32) to obtain an estimate of the m -year return level.

However, we recall that the definition of return period is easily misinterpreted and the one given above is thus not universally accepted. To address this issue, it is important to distinguish stationary from nonstationary sequences. [Section 3.3](#) investigates the return periods and return levels more precisely by relaxing the independence assumption (stationary) and then under a climate change environment (nonstationary). In order to check the accuracy of the fitted model, [Section 1.7.1](#) present the *return level plot*.

1.6 Inference

As already stated, a great advantage for the modeling of GEV is that we actually do not have to find the normalizing sequences to estimate the parameters of the model. Hence, this section presents the main (frequentists) methods of inference for the GEV. These are mostly based on the likelihood ([Section 1.6.1](#)) but we will also present other methods that are widely used to estimate GEV parameters (probability weighted moment estimator in [Section 1.6.2](#)). There exist estimators for the EVI ξ only, and these will be addressed in [Section A.5](#). After all, we will heavily rely on Bayesian inference in [Chapter 4](#).

1.6.1 Likelihood-based Methods

The most usual inference we will consider is Maximum Likelihood (ML). It is intuitive to understand though its implementation could bring some problems. Depicted by [Smith \[1985\]](#), the potential difficulty when using likelihood methods for GEV concerns the regularity conditions that are required for the usual asymptotic properties associated with the Maximum Likelihood Estimator (MLE) to be valid. Such conditions are not satisfied by the GEV model because the endpoints of the GEV distribution are functions of the parameter value⁴. Depending on the value of the EVI ξ , the special cases are :

1. $\boxed{\xi < -1}$: MLE's are unlikely to be obtainable.
2. $\boxed{\xi \in (-1, -0.5]}$: MLE's are usually obtainable but standard asymptotic properties do not hold.
3. $\boxed{\xi > -0.5}$: MLE's are regular, in the sense of having the usual asymptotic properties.

In practice, problematic cases ($\xi \leq -0.5$) are rarely encountered in most environmental problems. This corresponds to distributions in the Weibull family with very short bounded upper tail, see for example the red density in Figure 1.1 or Figure C.1, or directly in the Shiny application where we see what defines the borders of the problematic case. The 'bell' of the curve becomes very narrow. In the problematic cases, Bayesian inference that does not depend on these regularity conditions may be preferable. We will see in [Part II](#) that the distribution of the yearly maximum temperature is upper bounded which lead us to consider Bayesian inference in [Chapter 4](#).

Other forms of likelihood-based methods have also emerged to remedy this problem of instability for low values of ξ . Close to a Bayesian formulation, *penalized ML* method has been proposed by [Coles and Dixon \[1999\]](#) which adds a penalty term to the likelihood function to "force" the shape parameter to be > -1 , values closer to -1 being more penalized. We will use this concept in Section ?? to circumvent issues of these likelihood computations in nonstationary sequences, and to add more flexibility through a deep architecture.

We are now considering a sequence $\{Z_i\}_{i=1}^n$ of independent random variables sharing each the same GEV distribution. Let $\mathbf{z} = (z_1, \dots, z_n)$ denote the vector of observations. From the densities of the GEV distribution $g_\xi(z)$ defined in Table 1.1, we can derive the log-likelihood $\ell = \log [L(\mu, \sigma, \xi; \mathbf{z})]$, for the two different cases $\xi \neq 0$ or $\xi = 0$ respectively:

1.

$$\ell(\mu, \sigma, \xi \neq 0 ; \mathbf{z}) = -m \log \sigma - (1 + \xi^{-1}) \sum_{i=1}^n \log \left[1 + \xi \left(\frac{z_i - \mu}{\sigma} \right) \right]_+ - \sum_{i=1}^n \left[1 + \xi \left(\frac{z_i - \mu}{\sigma} \right) \right]_+^{-\xi^{-1}}, \quad (1.33)$$

2.

$$\ell(\mu, \sigma, \xi = 0 ; \mathbf{z}) = -m \log \sigma - \sum_{i=1}^n \left(\frac{z_i - \mu}{\sigma} \right) - \sum_{i=1}^n \exp \left\{ - \left(\frac{z_i - \mu}{\sigma} \right) \right\}. \quad (1.34)$$

Maximization of this pair of equations with respect to $\boldsymbol{\theta} = (\mu, \sigma, \xi)$ leads to the MLE with respect to the entire GEV family. Note that there is no analytical solution and hence, it must be numerically optimized.

⁴See paragraph below equation (1.17).

From standard MLE theory, we know that the estimated parameter vector $\hat{\theta}$ will be approximately multivariate normal. Inference such as confidence intervals can thus be applied, relying on this approximate normality of the MLE. Hence, problems of this method arise when the approximate normality cannot hold. The underlying inferences will not be sustainable. Whereas Zhou [2010] closed the discussion on the theoretical properties of the MLE, another method is usually more preferable for inference, the *profile likelihood*.

Profile Likelihood

In general, the normal approximation to the true sampling distribution of the respective estimator is poor. *Profile likelihood* inference is often more convenient when a single parameter is of interest. Let's denote it θ_j . Now let's consider the parameter vector $\theta = (\theta_j, \theta_{-j}) = (\mu, \sigma, \xi)$ typically in EVT in a stationary context, where θ_{-j} corresponds to all components of θ except θ_j . Hence, θ_{-j} can be seen as a vector of nuisance parameters. The profile log-likelihood for θ_j is defined by

$$\ell_p(\theta_j) = \arg \max_{\theta_{-j}} \ell(\theta_j, \theta_{-j}). \quad (1.35)$$

Henceforth for each value of θ_j , the profile log-likelihood is the maximised log-likelihood with respect to θ_{-j} , i.e. with respect to all other components of θ but not θ_j . Note that θ_j can be of dimension higher than one (e.g. in a nonstationary context).

Another interpretation is related to the χ^2 distribution and the equality with the hypothesis testing the Gumbel case. Details can be found in Beirlant et al. [2006, pp.138]. Applications of likelihood inferences will be provided in [Section 6.1](#).

1.6.2 Other Estimator : Probability-Weighted-Moments

Introduced by Greenwood et al. [1979], the *Probability-Weighted-Moments* (PWM) of a random variable X with df F , are the quantities

$$M_{p,r,s} = \mathbb{E}\left\{X^p[F(X)]^r[1 - F(X)]^s\right\}, \quad (1.36)$$

for real p, r and s . From (1.36), we can retrieve the PWM estimator from specific choices of p, r and s .

1.7 Model Diagnostics : Goodness-of-Fit

After having fitted a statistical model to data, it is important to assess its accuracy in order to infer reliable conclusions from this model. Ideally, we aim to check that our model fits well the whole population, e.g. the whole distribution of maximum temperatures, i.e. all the past and future temperature maxima... As this cannot be achieved in practice, it is common to assess a model with the data that were used to estimate this model. The aim here is to check that the fitted model is acceptable for the available data.

As these concepts are generally known, we let in [Appendix A.4](#) a reminder of *quantile* and *probability plots* applied in the world of extremes.

1.7.1 Return Level Plot

Section 1.5 introduced the concept of return levels and its intuitive interpretations. We will use this quantity as a diagnostic tool for model checking. Approximate confidence intervals for the return levels can be obtained by the delta method which relies on the asymptotic normality of the MLE and hence produces symmetric confidence intervals.

Standard errors of the estimates

We expect the standard errors to increase with the return period. Indeed, it is less accurate to estimate 100-year than a 2-year return level. As r_m is a function of the GEV parameters, we use the *delta method* to approximate the variance of \hat{r}_m . Specifically,

$$\text{Var}(\hat{r}_m) \approx \nabla r'_m V \nabla r_m,$$

with V the variance-covariance matrix of the estimated parameters $(\hat{\mu}, \hat{\sigma}, \hat{\xi})'$ and

$$\begin{aligned} \nabla r'_m &= \left[\frac{\partial r_m}{\partial \mu}, \frac{\partial r_m}{\partial \sigma}, \frac{\partial r_m}{\partial \xi} \right] \\ &= \left[1, \xi^{-1}(y_m^{-\xi} - 1), \sigma \xi^{-2}(1 - y_m^{-\xi}) - \sigma \xi^{-1} y_m^{-\xi} \log y_m \right], \end{aligned} \tag{1.37}$$

with $y_m = -\log(1 - m^{-1})$ and the gradient being evaluated at the estimates $(\hat{\mu}, \hat{\sigma}, \hat{\xi})$.

A problem for the so-computed standard errors when considering long-range return levels is that they can increase so drastically with the return period such that the confidence intervals of the *return level plot* can become difficult to work with. To address this issue we will construct intervals on the basis of the *profile* log-likelihood. Finally, note that this inference relies on the model adequacy and hence, more uncertainty should be given if the model fit is not perfect.

Profiled likelihood Return levels

Usual likelihood methods are not the most accurate for inference in EVT. The problem is that confidence intervals computed in the usual method, with standard errors computed by the Delta method in (1.37), relying on the normal approximation, is not reliable for inference on return levels. This is due to severe asymmetries that are often observed in the likelihood surface for return levels, especially for large quantiles, see e.g. [Bolívar et al. \[2010\]](#).

Profile likelihood method is hence more accurate for confidence intervals as it better captures the skewness generally associated with return level estimates. We are now specifically interested in computing the profile log-likelihood for the estimation of the return level r_m . To do that, we present a method which consists of three main steps :

1. To include r_m as a parameter of the model, by (1.32) we can rewrite μ

$$\mu = r_m - \sigma \xi^{-1} \left[\left(-\log\{1 - m^{-1}\} \right)^{-\xi} - 1 \right].$$

as a function of ξ, σ and r_m . By plugging it in the log-likelihood in (1.33)-(1.34), we obtain the new GEV log-likelihood $\ell(\xi, \sigma, r_m)$ as a function of r_m .

2. We maximise this new likelihood $\ell(\xi, \sigma, r_m = r_m^-)$ at some fixed low value of $r_m = r_m^- \leq r_m^+$ with respect to the nuisance parameters (ξ, σ) to obtain the profiled log-likelihood

$$\ell_p(r_m = r_m^-) = \arg \max_{(\xi, \sigma)} \ell(r_m = r_m^-, (\xi, \sigma)).$$

We choose arbitrarily large value of the upper range r_m^+ , and conversely for starting point of r_m^- .

3. Repeat the previous step for a range of values of r_m such that $r_m^- \leq r_m \leq r_m^+$ and then choose r_m which attain the maximum value of $\ell_p(r_m)$.

Doing this little algorithm gives the (profiled log-likelihood) *return level plot*.

Interpretation

Generally plotted against the return period on a logarithmic scale, the return levels has different shapes depending on the value of the shape parameter ξ , namely :

- If $\xi = 0$, then return level plot will be **linear**.
- If $\xi < 0$, then return level plot will be **concave**.
- If $\xi > 0$, then return level plot will be **convex**.

This can be understood as we have seen that $\xi < 0$ implies an upper endpoint and heavy left tail while $\xi > 0$ implies the converse. Henceforth, the "increasing rate" of the return level will decrease as the return period increases for $\xi < 0$ as it cannot go too far away beyond the upper endpoint, and the converse holds for $\xi > 0$. Figure 6.2 can already help to visualize shape of the plot in our case ($\xi < 0$).

CHAPTER 2

PEAKS-OVER-THRESHOLD METHOD

Contents

2.1	Preliminaries	24
2.2	Characterization of the Generalized Pareto Distribution	24
2.2.1	Outline proof of the GPD and justification from GEV	25
2.2.2	Dependence of the scale parameter	26
2.2.3	Three different types of GPD : Comparison with GEV	26
2.3	Return Levels	27
2.4	Inference : Parameter Estimation	28
2.5	Inference : Threshold Selection	28
2.5.1	Standard Threshold Selection Methods	28
2.5.2	Varying Threshold : Mixture Models	30

This new chapter will focus on another major approach of EV models by modeling only the excess over a certain threshold. This approach is very popular in practice as it can handle all the extremes with more flexibility and not only the maximum of one block. From this fact, numerous techniques have emerged and we will quickly navigate the main ideas.

In [Section 2.1](#), we will intuitively introduce the approach that will help us to formally characterize the resulting distribution of interest in [Section 2.2](#). Then, [Section 2.3](#) will present the concept of return levels applied to this concept. Next, we will assess the maximum temperature threshold in a statistical sense in [Section 2.5](#) by reviewing available methods, regardless common suggested thresholds of $25^{\circ}c$ or $30^{\circ}c$ from meteorologists.

Unfortunately, the resulting analysis of this chapter will not be present in [Part II](#) because it would have made the text become too voluminous. But empirical results (code and html reports) will remain available in the [repository](#)¹ which structure is explained in [Appendix D](#). Moreover, *point process* will not be covered for the same reason but we remind that this is a powerful and flexible method that summarizes the two techniques considered in the two first chapters, and it should then not be missed.

This chapter is mainly based on [Coles \[2001, chap.4 and 7\]](#), [Beirlant et al. \[2006, chap.4\]](#), [Reiss and Thomas \[2007, chap.5\]](#) and [Embrechts et al. \[1997, chap.5\]](#), and other relevant articles.

¹<https://github.com/proto4426/PissoortThesis/>

2.1 Preliminaries

Threshold models relying on the *Peaks-Over-Threshold* (POT) method propose an alternative to the blocking method seen in the [previous Chapter](#). Focusing exclusively on observations greater than a pre-specified *threshold* provides a natural way to expose extreme values. POT solves the issue of choosing a single observation per data block, but makes the trade-off at the expense of threshold determination and independence issues since cold days are more likely to be followed by cold days, etc ; more details follow in [Chapter 3](#). The notion of "extremes" is therefore intrinsically different.

Let $\{X_j\}$ be a sequence of n iid random variables with marginal df F , shown in Figure 2.1 representing our application's data. Next we look at observations exceeding a threshold u (blue) that must be lower than the right endpoint (1.17) of F . The aim here is to find the child distribution that is depicted in red, say H , from the parent distribution F depicted in grey. It will allow us to model the exceedances $Y = X - u$ with H expressed as

$$H(y) = \Pr\{X - u \leq y \mid X > u\}.$$

Throughout this chapter we will aim to model this empirical distribution.

Threshold models can be seen as the conditional survival function of the exceedances Y , knowing that the threshold is exceeded, according to [Beirlant et al. \[2006, pp.147\]](#) :

$$\Pr\{Y > y \mid Y > 0\} = \Pr\{X - u > y \mid X > u\} = \frac{\bar{F}(u + y)}{\bar{F}(u)}. \quad (2.1)$$

Or similarly, in terms of the exceedance df $F^{[u]}(x) = \Pr\{X \leq u + x \mid X > u\}$, see [Reiss and Thomas \[2007, pp.25-29\]](#) or following [Charras-Garrido and Lezaud \[2013\]](#) and [Rosso \[2015\]](#), using the conditional probability law.

If the parent distribution F was known, the threshold exceedances distribution could be computed (2.1). But, as in the method of block maxima, F is unknown in practice. We will still rely on approximations². Whereas [Theorem 1.1](#) were used to find an approximate distribution for block maxima, we will attempt here to approximate the distribution of the exceedances $H(y)$.

2.2 Characterization of the Generalized Pareto Distribution

Similarly to the GEV (1.12) in the limit for the block maxima, we look for a limit distribution for exceeding a certain threshold. As for max-stability in [Definition 1.2](#), another formulation can be given for POT models and will help derive a theorem.

²We quote here the well-known "All models are wrong, but some are useful" from George Box & Draper (1987), *Empirical model-building and response surfaces*, Wiley, p.424

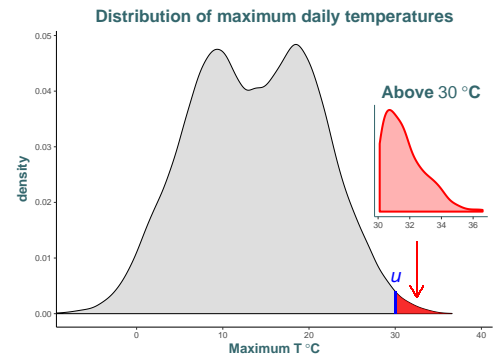


Figure 2.1: Kernel density estimates for the whole series (grey) and for the series of excess over the threshold of $u = 30^\circ\text{C}$ (red). More information on the data will be given in [Part II](#).

Definition 2.1 (POT-stability). *The dfs H are the only continuous one such that, for a certain choice of constants a_u and b_u ,*

$$F^{[u]}(a_u x + b_u) = F(x).$$

△

We can now state the key theorem discovered by [Balkema and Haan \[1974\]](#) and [Pickands \[1975\]](#).

Theorem 2.1 (Pickands–Balkema–de Haan). *Let $\{X_j\}$ be the sequence of n iid random variables having marginal df F for which [Theorem 1.1](#) holds. Then,*

$$\Pr\{X - u \leq y \mid X > u\} \longrightarrow H_{\xi, \sigma_u}(y), \quad u \rightarrow x_*. \quad (2.2)$$

It means that for large enough u , the df of $Y = X - u > 0$, conditional on $X > u$, is approximately $H_{\xi, \sigma_u}(y)$ where $H_{\xi, \sigma_u}(y)$ is the Generalized Pareto Distribution (GPD) :

$$H_{\xi, \sigma_u}(y) = \begin{cases} 1 - \left(1 + \frac{\xi y}{\sigma_u}\right)_+^{-\xi^{-1}}, & \xi \neq 0; \\ 1 - \exp\left\{-\frac{y}{\sigma_u}\right\}, & \xi = 0. \end{cases} \quad (2.3)$$

□

The scale parameter is denoted σ_u to emphasize its dependency with the specified threshold u :

$$\sigma_u = \sigma + \xi(u - \mu), \quad (2.4)$$

where we notice the absence of location parameter μ in (2.3) as it appears in (2.4).

2.2.1 Outline proof of the GPD and justification from GEV

In the following sections we describe a meaningful yet not too technical way of retrieving the GPD.

Outline Proof of [Theorem 2.1](#) :

- From [Theorem 1.1](#), we have for the distribution of the maximum, for large enough n ,

$$F_{X(n)}(z) = F^n(z) \approx \exp\left\{-\left[1 + \xi\left(\frac{z - \mu}{\sigma}\right)\right]^{-\xi^{-1}}\right\}, \quad (2.5)$$

with $\mu, \sigma > 0$ and ξ the GEV parameters. Hence, by taking logarithm on both sides, we get

$$n \ln F(z) \approx -\left[1 + \xi\left(\frac{z - \mu}{\sigma}\right)\right]^{-\xi^{-1}}. \quad (2.6)$$

- We also have that, from Taylor expansion, $\ln F(z) \approx -[1 - F(z)]$ as both sides go to zero as $z \rightarrow \infty$. Therefore, substituting into (2.6), we get the following for large u :

$$1 - F(u + y) \approx n^{-1} \left[1 + \xi \left(\frac{u + y - \mu}{\sigma} \right) \right]^{-\xi^{-1}}.$$

where we added the term $y > 0$ to retrieve something in the form of (2.1).

- Finally, by mathematical manipulation, as $u \rightarrow x_*$:

$$\begin{aligned} \Pr\{X > u + y \mid X > u\} &= \frac{\bar{F}(u + y)}{\bar{F}(u)} \approx \frac{n^{-1} [1 + \xi \sigma^{-1} (u + y - \mu)]^{-\xi^{-1}}}{n^{-1} [1 + \xi \sigma^{-1} (u - \mu)]^{-\xi^{-1}}} \\ &= \left[1 + \frac{\xi \sigma^{-1} (u + y - \mu)}{1 + \xi \sigma^{-1} (u - \mu)} \right]^{-\xi^{-1}} \\ &= \left[1 + \frac{\xi y}{\sigma_u} \right]^{-\xi^{-1}}, \end{aligned} \quad (2.7)$$

By simply taking the survivor of (2.7), we retrieve

$$\begin{aligned} \Pr\{X - u \leq y \mid X > u\} &= 1 - \Pr\{X > u + y \mid X > u\} \\ &= 1 - \left(1 + \frac{\xi y}{\sigma_u} \right)_+^{-\xi^{-1}}, \end{aligned} \quad (2.8)$$

which is $GPD(\xi, \sigma_u)$ as required. □

More insights come from [Reiss and Thomas \[2007\]](#), pp.27-28] with analysis of rates of convergence. Examples of how to retrieve the GPD from specific distributions are available in [Coles \[2001\]](#), pp.77].

2.2.2 Dependence of the scale parameter

We chose to express the scale parameter as σ_u to emphasize its dependency with the threshold u . If we increase the threshold, say to $u' > u$, then the scale parameter will be adjusted :

$$\sigma_{u'} = \sigma_u + \xi(u' - u), \quad (2.9)$$

and in particular, this adjusted parameter $\sigma_{u'}$ will increase if $\xi > 0$ and decrease if $\xi < 0$. If $\xi = 0$, there would be no change in the scale parameter³. Also, we consider it noteworthy that as for the GEV, the scale parameter σ_u for GPD models differs from the standard deviation since it governs the “size” of the excess, as mentioned in ?, pp.20. The issue of threshold selection will be discussed in [Section 2.5](#).

2.2.3 Three different types of GPD : Comparison with GEV

One should remark the similarity with the GEV distributions. Indeed, parameters of the GPD of the threshold excesses are uniquely determined by the corresponding GEV parameters of block maxima. Hence, the shape parameter ξ of the GPD is equal to that of the corresponding GEV and, most of all,

³Consistent with the well-known *memoryless property* of the exponential distribution H_{0,σ_u}

it is invariant. In block maxima, the GEV parameters would shift for a different block length, while in POT the GPD parameters are not affected by the choice of the threshold due to the self-compensation arising in (2.9).

Hence, as for the block-maxima approach, there are also three possible families of the GPD depending on the value of the shape parameter ξ which determines the qualitative behaviour of the corresponding GPD. [Hosking and Wallis \[1987\]](#), [Singh and Guo \[1995\]](#)

- **First** type $H_{0,\sigma_u}(y)$ comes by letting the shape parameter $\xi \rightarrow 0$ in (2.3), giving :

$$H_{0,\sigma_u}(y) = 1 - \exp\left(-\frac{y}{\sigma_u}\right), \quad y > 0. \quad (2.10)$$

One can easily notice that it corresponds to an **exponential** df and hence light-tailed with parameter $1/\sigma_u$, namely $Y \sim \exp(\sigma_u^{-1})$.

- **Second** and **third** types, i.e. when $\xi < 0$ and $\xi > 0$ (resp.), differ only by their support :

$$H_{\xi,\sigma_u}(y) = 1 - \left(1 + \frac{\xi y}{\sigma_u}\right)^{-\xi^{-1}}, \quad \text{for } \begin{cases} y > 0, & \xi > 0; \\ 0 < y < \sigma_u \cdot |\xi|^{-1}, & \xi < 0. \end{cases} \quad (2.11)$$

Therefore, if $\xi > 0$ the corresponding GPD is of **Pareto**-type, hence is heavy-tailed, and has no upper limit while if $\xi < 0$, the associated GPD has an upper bound $y_* = u + \sigma_u/|\xi|$ and is then of **Beta**-type. Special case arise when $\xi = -1$ where the pertaining distribution becomes Uniform($0, \sigma_u$), result coming from [Grimshaw \[1993, pp.186\]](#).

The **density** of the GPD is written here as

$$h_{\xi,\sigma_u}(y) = \begin{cases} \frac{1}{\sigma_u} \left(1 + \xi \frac{y}{\sigma_u}\right)^{-\xi^{-1}-1}, & \xi \neq 0; \\ \sigma_u^{-1} \cdot e^{-y}, & \xi = 0. \end{cases} \quad (2.12)$$

In the example of Figure 2.1, we can see that the red density seems to have an upper bound around 36.5°C . thence, we can conclude that this distribution should be of Beta-type. Part II will confirm that $\xi < 0$.

After looking at the behaviour of the density of these functions, we will procure a more comprehensive view by defining some examples of how to retrieve these different types of Generalized Pareto Distributions.

2.3 Return Levels

Presented in [Section 1.6](#) for block maxima, return levels are also useful in POT to bring valuable information. However, unlike for block maxima, the quantiles of the GPD cannot be as readily interpreted as return levels because the observations no longer derive from predetermined *blocks* of equal length. Instead, it is now required to estimate the *probability of exceeding the threshold* $\zeta_u = \Pr\{X > u\}$, from which a natural estimator is $\hat{\zeta}_u = k/n$ with k the number of points exceeding u . We can now retrieve the return level r_m , i.e. the *value that is exceeded on average once every m observations*. This is given by

$$r_m = \begin{cases} u + \sigma_u \xi^{-1} [(m\zeta_u)^\xi - 1], & \xi \neq 0; \\ u + \sigma_u \log(m\zeta_u), & \xi = 0. \end{cases} \quad (2.13)$$

provided m is sufficiently large. Computations are very similar as for the GEV in [Section 1.7.1](#).

Interpretation

Whereas the interpretation of the plot in function of the shape parameter value is the same as for the block-maxima method (see [Section 1.8](#)), it is more convenient to replace the value of m by $N \cdot n_y$ in (2.13), where n_y is the number of observations per year, to give return levels on an annual scale. This method allows us to obtain the *N-year return level* which is now commonly defined as the level expected to be exceeded once every N years.

2.4 Inference : Parameter Estimation

We will not develop likelihood techniques here as it ressembles that of GEV in [Section 1.6](#), and requires numerical techniques as well.

The two approaches we have encountered so far, i.e. block-maxima and POT share the same parameter ξ . Therefore, it is not necessary to differentiate between these methods for the sole estimate of the shape parameter. We give in [Appendix A.5](#) some of the most used methods to estimate the EVI.

Finally, methods dedicated to POT exist to estimate the parameters of the GPD. For example, they can include the probability-weighted-moment (PWM) which is formulated differently as for GEV in [Section 1.6.2](#), see e.g. [Ribereau et al. \[2016\]](#). The L -moment estimator is also important, especially for rainfall application, where [Hosking and Wallis \[1997\]](#) emphasized that L -moment method came historically as a modification of the PWM estimator.

2.5 Inference : Threshold Selection

Threshold selection is crucial in a POT context. It involves a *bias-variance trade-off*, that is :

- *Lower threshold* will induce *higher bias* due to model misspecification. In other words, the threshold must be sufficiently high to ensure that the asymptotics underlying the GPD approximation are reliable.
- *Higher threshold* will imply higher estimation uncertainty, i.e. *higher variance* of the parameter estimate as the sample size is reduced for high threshold.

2.5.1 Standard Threshold Selection Methods

Applications of all the subsequent methods can be viewed in Section 3.1 of the **Summary1_intro.Rmd** in the **/vignettes** folder of the [repository](#). Vignette can be downloaded in html from the compressed file in the same folder. Recall that all empirical results of this chapter will not be included in this thesis.

Based on Mean Residual Life

The *mean residual life* function or *mean excess* function is defined as

$$mrl(u_0) := E(X - u_0 \mid X > u_0) = \frac{\int_{u_0}^{x_*} \bar{F}(u) du}{\bar{F}(u_0)}, \quad (2.14)$$

for X having survival function $\bar{F}(u_0)$ computed at u_0 . It denotes in an actuarial context the expected remaining quantity or amount to be paid out when a level u_0 has been chosen. However, there are also interesting and reliable applications in an environmental context. Moreover, this function yields valuable properties about the tail of the underlying distribution of X . In fact, we expect that :

- If $mrl(u_0)$ is constant, then X is exponentially distributed.
- If $mrl(u_0)$ ultimately increases, then X has a heavier tail than the exponential distribution.
- If $mrl(u_0)$ ultimately decreases, then X has a lighter tail than the exponential distribution.

This can be particularly interesting for our purpose when considering threshold models. For this case, we have the excesses $\{Y_i\}$ that follow a GPD (2.3) and which are generated by the sequence $\{X_i\}$. From the theoretical mean of this distribution, we retrieve (provided $\xi < 1$)

$$\begin{aligned} mrl(u) &:= E(X - u \mid X > u) = \frac{\sigma_u}{1 - \xi} \\ &= \frac{\sigma_{u_0} + \xi u}{1 - \xi}, \end{aligned} \quad (2.15)$$

from dependence of the scale parameter σ with the threshold u , see (2.9). Hence, we remark that $mrl(u)$ is linearly increasing in u , with gradient $\xi \cdot (1 - \xi)^{-1}$ and intercept $\sigma_{u_0} \cdot (1 - \xi)^{-1}$. Furthermore, we can estimate empirically this function by

$$\widehat{mrl}(u) = \frac{1}{n_u} \sum_{i=1}^{n_u} (x_{[i]} - u), \quad (2.16)$$

where the $x_{[i]}$ denote the i-th observations out of the n_u that exceed u .

Mean residual life plot The *mean residual life plot* results from combining the linearity detected between $mrl(u)$ and u in (2.15) with (2.16). Therefore, worthwhile information can be retrieved from the locus of the points :

$$\left\{ \left(u, \frac{1}{n_u} \sum_{i=1}^{n_u} (x_{[i]} - u) \right) : u < x_{max} \right\}. \quad (2.17)$$

Even if its interpretation is not straightforward, this graphical procedure will give insights for the choice of a suitable threshold u_0 to model extremes via a GPD, that is the threshold u_0 above which we can detect linearity in the plot. Relying on this well-chosen threshold u_0 , the GPD approximation should be correct, even though its interpretation is subjective. Furthermore, information in the far right-hand-side of this plot is unreliable. Variability is high due to the limited amount of data above high thresholds.

Based on the stability of the parameter's estimates

Due to its simplicity, *stability plots of the parameter's estimates* is one of the preferred tools for practitioners. The aim is to plot MLE's of the parameters against different values for the threshold. In theory, MLE's are independent of the threshold choice, and hence the threshold is chosen at the lowest value for which the MLE's remain near-constant.

But this method is also criticized, especially owing to its lack of interpretability, and the pointwise confidence interval strongly dependent across the range of thresholds. Other techniques have thus been proposed, see e.g. [Wadsworth \[2016\]](#) which suggests complementary plots with greater interpretability, with a likelihood-based procedure allowing for automated and a more formal threshold selection. In short, this new method relies on the independent-increments structure of MLE and makes use of likelihood ratio tests to identify the threshold that significantly provides the best fit to the data. Thresholds are then compared iteratively, and significance is assessed by simulations.

Based on the Dispersion Index Plot

As mentioned, methods considered above involve substantial amount of subjectivity. Following [Ribatet \[2006\]](#), the *Dispersion Index* (DI) plot is particularly useful for time series. Point process that we have not developed here, can be used to characterize the excess over a threshold as a Poisson process. Hence, $\mathbb{E}[X] = \text{Var}[X]$. The DI statistic introduced by [Cunnane \[1979\]](#) is defined by $DI = s^2 \cdot \lambda - 1$, where s^2 is the intensity of the Poisson process and λ is the mean number of events in a block.

Based on L-Moments plot

L-Moments are linear combinations of the ordered data values. From the GPD, we have that

$$\tau_4 = \tau_3 \cdot \frac{1 + 5\tau_3}{5 + \tau_3}, \quad (2.18)$$

where τ_4 is the *L-Kurtosis* and τ_3 is the *L-Skewness*. See e.g. [Hosking and Wallis \[1997\]](#) for more details on L-moments or [Peel et al. \[2001\]](#) for a known application of this method in hydrology.

We can then construct the *L-Moment plot* which consist of the points :

$$\left\{ (\hat{\tau}_{3,u}, \hat{\tau}_{4,u}) : u \leq x_{\max} \right\} \quad (2.19)$$

where $\hat{\tau}_{3,u}$ and $\hat{\tau}_{4,u}$ are estimations of L-kurtosis and L-skewness based on u and x_{\max} is the maximum observation. Note that interpretation of this plot is often tedious.

2.5.2 Varying Threshold : Mixture Models

The so-called "fixed threshold" approaches (as renamed in [Scarrott and MacDonald \[2012\]](#), among others) considered so far have been criticized since it leads to a fixed and subjective threshold, sometimes also seen as an arbitrary choice where the uncertainty cannot be taken into account.

Hence, recent models have emerged that allow a dynamic view of the threshold. In *mixture models*, the threshold is either implicitly or explicitly defined as a parameter to be estimated, and in most cases

the uncertainty associated with the threshold choice can be naturally accounted for in the inferences. The model can be presented in a general way :

$$f(x) = (1 - \zeta_u) \cdot b_t(x) + \zeta_u \cdot g(x), \quad (2.20)$$

where $\zeta_u = \Pr\{X > u\}$ is now called the *tail fraction* and is a new parameter of the model, $b_t(x)$ is the density of the *bulk model* (i.e., the data that does not exceed the threshold) and $g(x)$ is the *tail model*, e.g. the GPD density. We ignored parameter dependence for clarity. There is abundant literature on the subject and numerous models have emerged, not necessarily parametric, see e.g. [Dey and Yan \[2016, chap.3\]](#) for the univariate case. The guiding principle in choosing EV mixture models is to combine a flexible bulk model with a reliable tail fit which is robust to the bulk data. These two components are not independent as they share common information about the threshold.

Serious issues arise in these models, for example regarding the discontinuity that often occurs in the density function at the junction between the bulk and the tail model. Alternative models have emerged to force continuity on the density but still, mixture models are often regarded as over-complex with respect to the benefits these models can offer in practice. Research is in great progress but we think improvements have still to be made before yielding straightforward modeling and valuable results.

CHAPTER 3

RELAXING THE INDEPENDENCE ASSUMPTION

Contents

3.1	Stationary Extremes	33
3.1.1	The extremal index	34
	Clusters of exceedances	34
	New parameters	34
	Return levels	35
3.1.2	Modelling in Block Maxima	35
3.2	Non-Stationary Extremes	35
3.2.1	Block-Maxima	36
3.3	Return Levels : New Definitions	38
3.4	Neural Networks for Nonstationary Series : GEV-CDN	39
3.4.1	Generalized Maximum Likelihood	40
3.4.2	Architecture of the GEV-CDN Network	41
3.4.3	Prevent Overfitting : Bagging	42
3.4.4	Confidence Intervals : Bootstrapping Methods	42

In most environmental applications, the independence assumption made in the first chapters is questionable and never completely fulfilled. From hydrological process as stated in Milly et al. [2008] to temperature data where climate warming is a famous issue, such theoretical assumptions that have been previously made are not sustainable in practice. First, Section 3.1 will provide tools that enable EV models to hold in presence of a limited long-range dependence. Section 3.2 will allow EV modeling under nonstationary processes allowing us for instance to study the possible increasing behavior of the maximum temperatures. Whereas Section 3.3 redefined return levels under those less restricted cases, Section 3.4 will introduce a new flexible way to model nonstationary extremes under a redefined Multi Layer Perceptron framework providing inference techniques that minimize chance of overfitting.

This chapter is mostly based on Coles [2001, chap.5-6], Beirlant et al. [2006, chap.10] and Reiss and Thomas [2007, chap.7], and other relevant articles.

3.1 Stationary Extremes

So far, we considered the maximum $X_{(n)} = \max_{1 \leq i \leq n} X_i$ being composed of independent random variables only. Now, we are interested by modeling $X_{(n)}^* = \max_{1 \leq i \leq n} X_i^*$ where $\{X_i^*\}$ will now denote a *stationary* sequence of n random variables sharing the same marginal df F as the sequence $\{X_i\}$ of independent random variables.

Definition 3.1 (Stationary process). *We say that the sequence $\{X_i\}$ of n random variables is (strongly) stationary if, for $h \geq 0$ and $n \geq 1$, the distribution of the lagged random vector $(X_{1+h}, \dots, X_{n+h})$ does not depend on h .* \triangle

It corresponds to physical processes whose stochastic properties are homogeneous but which may be dependent. There exist other formulations of *stationarity* but we stick to this general definition.

This dependence can take many forms and hence we need to relax the independence condition. Let $F_{i_1, \dots, i_p}(u_1, \dots, u_p) := \Pr\{X_{i_1} \leq u_1, \dots, X_{i_p} \leq u_p\}$ denote the joint df of X_{i_1}, \dots, X_{i_p} for any arbitrary positive integers (i_1, \dots, i_p) .

Definition 3.2 ($D(u_n)$ dependence condition from Leadbetter [1974]). *Let $\{u_n\}$ be a sequence of real numbers. We say that the **$D(u_n)$ condition** holds if for any set of integers $i_1 < \dots < i_p$ and $j_1 < \dots < j_q$ such that $j_1 - i_p > \ell$, we have that*

$$|F_{i_1, \dots, i_p, j_1, \dots, j_q}(u_n, \dots, u_n; u_n, \dots, u_n) - F_{i_1, \dots, i_p}(u_n, \dots, u_n) \cdot F_{j_1, \dots, j_q}(u_n, \dots, u_n)| \leq \beta_{n,\ell}, \quad (3.1)$$

where $\beta_{n,\ell}$ is nondecreasing and $\lim_{n \rightarrow \infty} \beta_{n,\ell_n} = 0$ for some sequence $\ell_n = o(n)$. \triangle

This condition ensures that, when the sets of variables are separated by a relatively short distance, typically $s_n = o(n)$, the long-range dependence between such events is limited in a sense that is sufficiently close to zero to have no effect on the limit extremal laws. This result is remarkable in the sense that, provided a series has limited long-range dependence at extreme levels (i.e., where $D(u_n)$ condition holds), maxima of stationary series follow the same distributional limit laws as those of independent series.

Theorem 3.1 (Limit distribution of maxima under $D(u_n)$, Leadbetter [1974]). *Let $\{X_i^*\}$ be a stationary sequence of n iid random variables. If there exists sequences of constants $\{a_n > 0\}$ and $\{b_n\}$ such that $D(u_n)$ condition holds with $u_n = a_n x + b_n$ for every real x , and*

$$\Pr\{X_{(n)}^* \leq u_n\} \longrightarrow G^*(x), \quad n \rightarrow \infty, \quad (3.2)$$

where G^* is a non-degenerate df, then G^* is a member of the GEV family as presented in Theorem 1.1. \square

Theorem 3.2 (Leadbetter et al. [1983]). *Let $\{X_i^*\}$ be a stationary sequence and let $\{X_i\}$ be a iid sequence of n random variables. We have under regularity conditions,*

$$\Pr\{a_n^{-1}(X_{(n)} - b_n) \leq x\} \longrightarrow G(x), \quad n \rightarrow \infty,$$

for normalizing sequences $\{a_n > 0\}$ and $\{b_n\}$, where G is non-degenerate, if and only if

$$\Pr\{a_n^{-1}(X_{(n)}^* - b_n) \leq x\} \rightarrow G^*(x), \quad n \rightarrow \infty,$$

where G^* is the limiting df coming from a stationary process, defined by

$$G^*(x) = G^\theta(x), \quad (3.3)$$

for some constant $\theta \in (0, 1]$ called the **extremal index**.

□

It is evident from (3.3) that the maximum of a stationary series will have a tendency to decrease.

3.1.1 The extremal index

The *extremal index* is an important indicator quantifying the extent of extremal dependence, that is the degree at which the assumption of independence is violated. From (3.3), it is clear that $\theta = 1$ lead to an independent process, but the converse does not hold. The case $\theta = 0$ will not be considered as it is too "far" from independence and brings problems. Moreover, results of [Theorem 3.2](#) would not hold.

Formally, it can be defined as

$$\theta = \lim_{n \rightarrow \infty} \Pr\left\{\max(X_2, \dots, X_{p_n}) \leq u_n \mid X_1 \geq u_n\right\}, \quad (3.4)$$

in the POT approach, where $p_n = o(n)$ and the sequence u_n is such that $\Pr\{X_{(n)} \leq u_n\}$ converges. Hence, θ can be thought for example as the probability that an exceedance over a high threshold is the final element in a *cluster of exceedances*.

Clusters of exceedances

From (3.4) and in a POT context, extremes have the tendency to occur in clusters whose *mean cluster size* is θ^{-1} at the limit. Equivalently, θ^{-1} can be viewed as the factor with which the mean distance between cluster is increased. This problem of temporal dependence make inference based on the likelihood invalid. We name two methods that can be used to circumvent this issue :

- **Filtering out** an (approximate) independent sequence of threshold exceedances.
- **Declustering** : compute the maximum value in each cluster and then we model these clusters maximums as independent GP random variable. In this approach, we remove temporal dependence but we do not estimate it. However, information is discarded and this could be a substantial loss in meteorological applications, for instance to determine heat or cold waves.

New parameters

When $0 < \theta \leq 1$, we have from [Theorem 3.2](#) that G^* is an EV distribution but with different scale and location parameters than G . If we note by (μ^*, σ^*, ξ^*) the parameters pertaining to G^* and those from

G kept in the usual way, we have the following relationships, when $\xi \neq 0$

$$\mu^* = \mu - \sigma\xi^{-1}(1 - \theta^\xi), \quad \text{and} \quad \sigma^* = \sigma\theta^\xi. \quad (3.5)$$

In the Gumbel case ($\xi = 0$), we simply have $\sigma^* = \sigma$ and $\mu^* = \mu + \log \theta$. The fact that $\xi^* = \xi$ induce that the two distributions G^* and G will have the same form, following [Theorem 3.2](#).

Return levels

Because of clustering, notion of return levels is more complex and the dependence appear in the definition of return levels for excess models :

$$r_m = u + \sigma\xi^{-1}[(m\zeta_u\theta)^\xi - 1]. \quad (3.6)$$

Hence, we see that ignoring dependence will lead to an overestimation of return levels. For example, we have that :

- If $\theta = 1$, then the *100-year-event* has probability 0.368 of not appearing in the next 100 years.
- If $\theta = 0.1$, the event has probability of 0.904 of not appearing in the next 100 years.

Return levels will be redefined in [Section 3.3](#) for the stationary case.

3.1.2 Modelling in Block Maxima

With dependent series, modeling by means of GEV as in [Chapter 1](#) can be used in a similar way since the shape parameter ξ^* will remain invariant. The difference is that the effective number of block maxima $n^* = n\theta$ will be reduced and hence convergence in [extremal Theorem 1.1](#) will be slower. Indeed, approximation is expected to be poorer and this will be exacerbated with increased levels of dependence in the series. Efforts must be made to either try to increase n for example by reducing the block length, or make sure the model fit is convincing with diagnostic tools presented in [Section 1.7](#).

3.2 Non-Stationary Extremes

Whereas [previous Section](#) relaxed the first "i" of the "iid" assumption made during [Chapter 1](#) and [2](#) by allowing temporal dependence under stationary process, this section will now tackle the "**id**" part, i.e. assumption that the observations are identically distributed. The stationarity assumption is not likely to hold for climatological data such as temperatures. For instance, the most obvious departure from stationarity is the presence seasonal patterns as seen in [Figure C.2](#) with higher spread in spring or in autumn for example. Seasonal concerns should disappear for very high thresholds in excess models but this is not a valid argument since the number of data would become very small. For a sufficiently large block size in block maxima, meteorological seasons should not be an issue.

Furthermore, the aim of this thesis will focus on the modeling of the possible trend in order to assess the climate warming. Our modeling will hence more focus on the analysis of different parametrizations for the mean by allowing the location parameter μ to vary with time. Even if it seems less interesting, we

will also allow the scale parameter to vary in order to check if the annual maxima have varying spread over time. We will avoid to vary ξ with time in order to stay in the same EV family of distributions.

There are no new general theory for nonstationary processes in previous section and we will then use a pragmatic approach of combining standard EV models with statistical modeling. We will only discuss the approach in block maxima but the extrapolation to POT is straightforward for inference, model comparison and diagnostics.

3.2.1 Block-Maxima

As we continue to consider yearly blocks, we do only face nonstationary concerns for the trend which could probably be imputed to the Global Warming. The evidence of seasonality arising when we decrease the block lengths is an issue in block maxima. For example if one consider daily maximum temperatures, seasonality will be present. However, we loose information by taking yearly blocks only as we do not use all the information since at least one half of the daily temperatures from October to March will not be used. To overcome this issue, dataset could be divided and different models can be applied on sub-blocks of the data, for example on the month July and August and fitting a GEV model with block length of 62 days and do similar analysis with other months. This will provide us a set of GEV models that will describe different aspects of the process. In fact, this method would lead to some kind of a "manual" nonstationary GEV modeling.

Inference for GEV

In a nonstationary context, ML is preferred for its adaptability to changes in model structure. In a general setting, we let a nonstationary GEV model describe the distribution Z_t for $t = 1, \dots, m$:

$$Z_t \sim \text{GEV}(\mu(t), \sigma(t), \xi(t)), \quad (3.7)$$

where each of $\mu(t), \sigma(t), \xi(t)$ are expressed as

$$\theta(t) = b(X' \beta), \quad (3.8)$$

for a specified inverse link function $b(\cdot)$ where θ denotes either μ, σ or ξ , β denote the complete vector of parameters, and X is the design matrix. In our example, Z_t will describe the annual maximum temperature of year t for $m = 116$ years. As already stated, it will not be recommended to allow ξ to vary with time. Examples of parametric expressions from (3.8) will be given in [Section 6.2.1](#).

If $g(z_t; \mu(t), \sigma(t), \xi(t))$ denotes the GEV density ([Table 1.1](#)) with parameters $\mu(t), \sigma(t), \xi(t)$ evaluated at z_t , the log-likelihood of the model (3.7) is, provided $\xi(t) \neq 0 \forall t$,

$$\begin{aligned} \ell(\beta) &= \sum_t^m \log g(z_t; \mu(t), \sigma(t), \xi(t)) \\ &= - \sum_t^m \left\{ \log \sigma(t) + [1 + \xi^{-1}(t)] \log \left[1 + \xi(t) \cdot \sigma^{-1}(t) \cdot (z_t - \mu(t)) \right]_+ \right. \\ &\quad \left. + \left[1 + \xi(t) \cdot \sigma^{-1}(t) \cdot (z_t - \mu(t)) \right]_+^{-\xi^{-1}(t)} \right\}, \end{aligned} \quad (3.9)$$

where the notation $y_+(t) = \max\{y(t), 0\}$ holds for all t . The parameters $\mu(t)$, $\sigma(t)$, $\xi(t)$ are replaced by their respective expressions from (3.8). If $\xi(t) = 0$ for any t , we replace the likelihood by using the limit $\xi(t) \rightarrow 0$ in (3.9) as in Table 1.1. Numerical techniques are then used to maximize (3.9) in order to yield the MLE of β and evaluate standard errors.

Model Comparisons

In order to compare our models, that is for example to check whether a trend is statistically significant, or if the nonstationary models provide an improvement over the simpler (stationary) model, we will use two techniques :

1. The *deviance statistic* which is defined as

$$D = 2\{\ell_1(\mathcal{M}_1) - \ell_0(\mathcal{M}_0)\}, \quad (3.10)$$

for two nested models $\mathcal{M}_0 \subset \mathcal{M}_1$, where $\ell_1(\mathcal{M}_1)$ and $\ell_0(\mathcal{M}_0)$ are the maximized log-likelihoods (3.9) under models \mathcal{M}_1 and \mathcal{M}_0 respectively. Asymptotically, the distribution of D is χ_k^2 with k degrees of freedom representing the difference of parameters between model \mathcal{M}_1 and \mathcal{M}_0 . Comparisons of D with the χ_k^2 critical value will guide our decision.

2. It is sometimes preferable to rely on other criterion, for example when the number of models to be compared is large or their construction is not straightforward. We will make use of the *Bayesian Information Criterion* (BIC) and the *Akaike Information Criterion (corrected)* (AIC_c). For n observations and p parameters, we define

$$\text{BIC} = -2\ell + p \log(n), \quad \text{AIC}_c = -2\ell + 2p + \frac{2p(p+1)}{n-p-1}. \quad (3.11)$$

Used by Cannon [2010], these two criterion both have a likelihood term which represent the quality of fit of the model and a term which penalizes the complexity of the model represented by its number of parameters to be estimated. These two criterion are advised for small samples and to prevent overfitting (i.e., fitting to noise instead of the true underlying process). BIC will penalize more heavily models that are more complex.

The basic principle of parsimony holds for both methods. In the first method, it is incorporated in the statistical test since the critical value χ_k^2 will increase with k , the difference of complexity of two models. In the second method, it is directly included in the criterion since the partial derivative with p is positive for both criterion(3.11) and these are to be minimized.

We will use the first technique in Section 6.2.1 to make successive comparisons of parametric models that we propose for the location parameter. We will then summarize all the results in Table 6.6 in the following Section by means of BIC and AIC_c, taking all relevant models into account.

Model Diagnostics

When the "best" model is selected following the method, it is still necessary to assess that the model fits well enough the data at hand that we can infer conclusions about some aspect of the population. We will

use tools seen in the independent (or stationary) case, the quantile and the probability plots presented in [Appendix A.4](#). From the inhomogeneous distribution across years, it is needed to standardize the data. For example, when model (3.7) is estimated, the *standardized variables* \tilde{Z}_t are

$$\tilde{Z}_t = \hat{\xi}^{-1}(t) \cdot \log \left\{ 1 + \hat{\xi}(t) \cdot \hat{\sigma}^{-1}(t) \cdot (Z_t - \hat{\mu}(t)) \right\}, \quad (3.12)$$

each having standard Gumbel distribution (1.9). This yield the *residual probability plot* :

$$\left\{ \left(i/(m+1), \exp(-e^{-\tilde{z}_{(i)}}) \right) : i = 1, \dots, m \right\}, \quad (3.13)$$

with the Gumbel as reference, and the *residual quantile plot* :

$$\left\{ \left(\tilde{z}_{(i)}, -\log(-\log(i/(m+1))) \right) : i = 1, \dots, m \right\}. \quad (3.14)$$

The choice of the Gumbel as reference distribution can be discussed but this is a reasonable choice regarding its place in EVT. Figure 6.3 in [Appendix C](#) will present such plots.

3.3 Return Levels : New Definitions

Whereas we already defined return levels in [Section 1.5](#) for independent sequences, we will now give a more general definition for return levels.

Stationarity

Under assumption of a stationary sequence, the return level is the same for all years. The m -year return level r_m is associated with a return period of m years. Let $X_{(n),y}$ denote the annual maximum for a particular year y . Assuming $\{X_{(n),y}\} \stackrel{iid}{\sim} F$, there are two main interpretations for return periods in this context, following [Amir AghaKouchak \[2013, chap.4\]](#) :

- 1. Expected waiting time until an exceedance occurs** : let T be the year of the first exceedance. Recalling $F(r_m) = \Pr\{X_{(n),y} \leq r_m\} = 1 - 1/m$, we write

$$\begin{aligned} \Pr\{T = t\} &= \Pr\{X_{(n),1} \leq r_m, \dots, X_{(n),t-1} \leq r_m, X_{(n),t} > r_m\} \\ &= \Pr\{X_{(n),1} \leq r_m\} \dots \Pr\{X_{(n),t-1} \leq r_m\} \Pr\{X_{(n),t} > r_m\} \quad \boxed{\text{iid assumption}} \\ &= \Pr\{X_{(n),1} \leq r_m\}^{t-1} \Pr\{X_{(n),1} > r_m\} \quad \boxed{\text{stationarity}} \\ &= F^{t-1}(r_m)(1 - F(r_m)) \\ &= (1 - 1/m)^{t-1}(1/m). \end{aligned}$$

We easily recognize that T has a geometric distribution with parameter m^{-1} . Hence, its expected value is $1/m^{-1} = m$, showing that the expected waiting time for an m -year event is m years.

- 2. Expected number of events in a period of m years is exactly 1** : to see that, we define

$$N = \sum_{y=1}^m \mathbb{I}(X_{(n),y} > r_m)$$

as the random variable representing the number of exceedances in m years, with \mathbb{I} the indicator function. Hence, each year is a "trial", and from the fact that $\{X_{(n),y}\}$ are iid, we can compute the probability that the number of exceedances in m -years is k by

$$\Pr\{N = k\} = \binom{m}{k} (1/m)^k (1 - 1/m)^{m-k},$$

where we retrieve $N \sim \text{Bin}(m, 1/m)$ and hence N has an expected value of $m \cdot m^{-1} = 1$.

Non-stationarity

As demonstrated in [Amir AghaKouchak \[2013\]](#), Section 4.2], we can retrieve the same two interpretations of return period as for a stationary process. However, mathematical derivations go beyond the scope of this thesis. Moreover, from definition of non-stationary process, as parameter(s) will be function of time, return levels will also change over time. This will have big impacts on modeling, since an inappropriate model will lead to inappropriate return levels, as we will see to a certain extent in Figure 6.4. We will now try more complex models in order to improve this fit.

3.4 Neural Networks for Nonstationary Series : GEV-CDN

In the era of Artificial Intelligence and Machine Learning or even the trendy term "Deep Learning", it is interesting to see how artificial Neural Networks (NN) can effectively deal with nonstationarity in EVT for the block-maxima approach. In practice, assumptions made by models (3.8) may not be accurate enough, in the sense that it could not take the complex temporal relationship with GEV parameters. One could for example expect to have particular relationships between the covariates¹ and the GEV parameters. Only considering parametric models in location or scale could thus be seen as too restrictive. For example, [Kharin and Zwiers \[2005\]](#) allowed for nonlinear trends in temperature extremes by making simulations over a 110-year transient global climate to estimate linear trends in the three GEV parameters based on a series of overlapping 51-year time windows.

Here, we follow an automated approach allowing to take into account all possible relationships through a flexible modeling approach. The well-known result from [Hornik et al. \[1989\]](#) says that provided enough data, hidden units and an appropriate optimization, NN's can capture any smooth dependencies of the parameters given the input, and hence, it can theoretically capture any conditional continuous density, be it asymmetric, multimodal, or heavy-tailed. This can be particularly interesting as we do not have particular prior knowledge on the form of the underlying process of annual maximum temperatures. NN's have this facility of being capable of automatically modeling any non-stationary relationships without explicitly specify it a priori, including interactions between covariates. As demonstrated by the reference article of [Cannon \[2010\]](#), physical process such as rainfall or other meteorological data have a tendency to show nonlinearities and so NN's become interesting. However from its flexibility, attention must be given to the danger of overfitting the data. Another pitfall is its

¹Here we will still consider the time itself only but we could have other time-varying covariates.

lack of interpretation of the relationships retrieved by the model between inputs and outputs but it bears noting that sensitivity analysis methods as in [Cannon and McKendry \[2002\]](#) could be used to identify the form of nonlinear relationships between covariates and GEV distribution parameters or quantiles.

We will use a *conditional density estimation network* (CDN), which is a probabilistic variant of the *multilayer perceptron* (MLP). An extensive review of the MLP can be found for example in [Hsieh and Tang \[1998\]](#) in the context of meteorological or climatological predictions. Parameters will be estimated via generalized maximum likelihood.

Parametric or nonparametric ? It is always a difficult task to state whether Neural Networks (NN) are parametric models or not. NN are somewhere in the gray area between a *parametric* and a *nonparametric* model, in the sense that it assumes a GEV distribution from the output layer defined by the three parameters of interest, while it also allows for a fabulous flexibility coming from the hidden layers which lead to think that these are rather nonparametric. Note that all transformations applied inside the network are in general parametric and nonlinear. However, this terminological question is not very relevant and this will not impact the particular modeling.

3.4.1 Generalized Maximum Likelihood

In [Section 1.6.1](#) we introduced the concept of penalized likelihood. The idea is that the MLE's may diverge for some values of ξ , especially when sample size is small. To resolve this problem, [Martins and Stedinger \[2000\]](#) suggest the use of a prior distribution for the shape parameter ξ of the GEV model such that the most probable values of the parameter are included. This method extend the usual ML and is called the *Generalized Maximum Likelihood* (GML). In this method, the penalty is in the form of a prior distribution on ξ :

$$\pi(\xi) \sim \text{Beta}(\xi + 0.5; c_1, c_2), \quad (3.15)$$

in which ξ is limited to the range $-0.5 \leq \xi \leq 0.5$ to limit the search space of ξ during optimization to the support of the shifted beta prior. It is recommended by the authors to set c_1 and c_2 to 6 and 9 respectively, resulting in a Beta density function with a mode at -0.1 and $\approx 90\%$ of the probability concentrated between -0.3 and 0.1 . However, these two values can be tuned depending on the application or relying on results of preceding inferential methods, based on the characteristics of the Beta distribution. For a sequence $\mathbf{x} = x_1, \dots, x_n$ of observations, the GML estimator corresponds to the mode of the empirical posterior distribution, i.e. the *generalized-likelihood*

$$\text{GL}(\mu, \sigma, \xi | \mathbf{x}) = L(\mu, \sigma, \xi | \mathbf{x}) \cdot \pi(\xi), \quad (3.16)$$

where $L(\cdot)$ can be the log-likelihood $\ell(\cdot)$ [\(3.9\)](#). When dealing with nonstationary processes [El Adlouni et al. \[2007\]](#) have proven that GML estimators are likely to outperform the usual ML's. This method will be used in the GEV-CDN framework also because it is more flexible and will avoid issues of usual likelihood computations.

3.4.2 Architecture of the GEV-CDN Network

The MLP architecture of the general GEV-CDN framework is pictured in Figure 3.1. Given a set of covariates $\{x_i(t), i = 1, \dots, I\}$ at time t , outputs are evaluated following these steps :

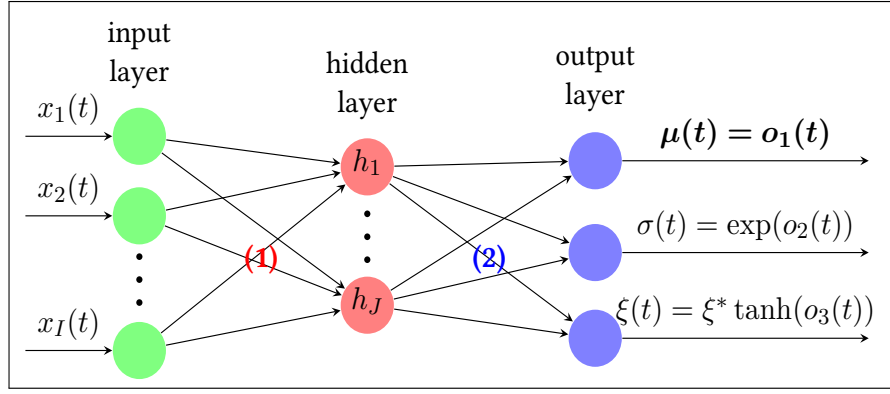


Figure 3.1: General framework of the fully-connected nonstationary GEV-CDN based on Cannon [2010]. The input layer will still the time itself in our application, i.e. $x_i(t) = t, \forall i = 1, \dots, I$ but it can be other covariates. The hidden layer represent additional complexity incorporated in the model and the output layer represent the three GEV parameters. (1) and (2) represent the functional relationships (3.17)-(3.18) between layers.

- The j -th hidden layer node h_j is given by

$$h_j(t) = m\left(\sum_{i=1}^I x_i(t) \cdot w_{ji}^{(1)} + b_j^{(1)}\right), \quad (3.17)$$

with $m(\cdot)$ the hidden layer activation function, $w_{ji}^{(1)}$ and $b_j^{(1)}$ are the input-hidden layer weight and bias. The function $m(\cdot)$ is often sigmoidal to allow the GEV-CDN mapping to be nonlinear but it can be the identity function for a strictly linear mapping.

- The value of the k -th output is given by

$$o_k(t) = \sum_j^J h_j(t) \cdot w_{kj}^{(2)} + b_k^{(2)}, \quad k = 1, 2, 3, \quad (3.18)$$

where $w_{kj}^{(2)}$ is the hidden-output layer weight and $b_k^{(2)}$ is the hidden-output layer bias.

- The GEV parameters are obtained by applying the output-layer activation functions $g_k(\cdot)$ denoted in Figure 3.1. As usual, the function $g_2(\cdot)$ is to force σ to take positive values and $g_3(\cdot)$ is to constraint ξ to lie within $[-\xi^*, \xi^*]$. Again, we notice that it is not recommended to allow ξ to vary with time.

A hierarchy of models can be defined by varying the structure of the CDN (number of hidden layers, which activation function $m(\cdot)$ and weights connections) and compared by the selection criterion such as the BIC or AIC_c discussed in (3.11).

3.4.3 Prevent Overfitting : Bagging

Bootstrap aggregating or *bagging* is an ensemble method² used in many state-of-the-art machine learning algorithms such as Random Forests discovered by Breiman [2001]. This technique is praised in Machine Learning for its performance as it decreases variance of predictions (or estimates) and hence reduce the risk of overfitting. This method works by generating additional data with repetitions from the original dataset to produce multisets of the same size. The individual multisets' outputs having equal weights are then combined by averaging the ensemble members. This process is also known as *model averaging*. Indeed, by increasing the size of original data you cannot improve the model predictive force, but just decrease its variance.

Carney et al. [2005] have successfully applied this averaging method in the context of CDN and Cannon [2010] says it is worth exploring for GEV-CDN models. He implemented it soon after in its R package GEVcdn. *Early stopping* stopping can be added as a computationally intensive means of controlling overfitting as it stops training prior to convergence of the optimization algorithm and hence allow to reduce the complexity of the model.

Other techniques are available to prevent overfitting. First used by MacKay [1992], *weight penalty regularization* is popular and available in the GEV-CDN framework as a means of limiting the effective number of parameters. The amount of weight penalty is controlled via a Gaussian prior on the magnitude of the input-hidden layer weights. Optimal value for the variance of the Gaussian prior must be set relying on some form of split-sample or cross validation scheme.

3.4.4 Confidence Intervals : Bootstrapping Methods

Like the estimated parameters themselves, the standard errors may not be reliable for small samples. One way to improve the accuracy of the standard errors is to use *bootstrap*. Discovered by Efron [1979], this can be used for EV dfs including nonstationarity. The bootstrap samples are manufactured through Monte Carlo resampling of residuals to attend to the underlying assumption that original sample is iid. There exist a large panel of different bootstrap procedures to construct confidence intervals. For example, Khaliq et al. [2006] follows these steps for the residual bootstrap :

1. Fit a nonstationary GEV model to the data.
2. Transform residuals from the fitted model to be identically distributed :

$$\varepsilon(t) = \left[1 + \xi(t) \cdot \sigma^{-1}(t) \cdot (x(t) - \mu(t)) \right]^{-\xi^{-1}(t)},$$

where $\varepsilon(t)$ is the t -th transformed residual.

3. Resample $\varepsilon(t)$ with replacement to form the bootstrapped set $\{\varepsilon^{(b)}(t), t = 1, \dots, n\}$.
4. Rescale the bootstrapped residuals by inverting the transformation :

$$x^{(b)}(t) = \mu(t) - \sigma(t) \cdot \xi^{-1}(t) \cdot (\varepsilon^{(b)}(t) - 1). \quad (3.19)$$

²For climatologists, *ensemble models* are different but of major utility, especially to make weather forecasting, see for example Suh et al. [2012] among others.

5. Fit a new nonstationary GEV model to the bootstrapped samples (3.19) and estimate the parameters and quantiles from the fitted model.
6. Repeat steps 1 to 5 a large number of times B.

Cannon [2010] found that *parametric* bootstrap outperformed the *residual* bootstrap in the GEV-CDN framework, but he did not consider alternative bootstrap approaches such as the *bias-adjusted percentile* which might yield better calibrated confidence intervals. Empirical Monte-Carlo comparisons of coverage from all available methods considered so far would be interesting. Furthermore, the incoming chapter will introduce other methods to construct intervals in a strictly Bayesian approach relying also on Monte-Carlo sampling.

CHAPTER 4

BAYESIAN EXTREME VALUE THEORY

Contents

4.1	Prior Elicitation	45
4.1.1	Non-informative Priors	46
4.1.2	Informative Priors	47
4.2	Bayesian Computation : Markov Chains	47
4.2.1	Algorithms	47
4.2.2	Hamiltonian Monte Carlo	48
4.2.3	Computational efficiency comparison	48
4.3	Convergence Diagnostics	48
4.3.1	Proposal Distribution	49
4.3.2	The problem of auto and cross-correlations in the chains	50
4.4	Posterior Predictive	50
4.5	Bayesian Predictive Accuracy for Model Validation	51
4.5.1	Cross-validation for predictive accuracy	51
4.6	Bayesian Inference ?	52
4.6.1	Bayesian Credible Intervals	52
4.6.2	Distribution of Quantiles : Return Levels	53
4.7	Bayesian Model Averaging	53
4.8	Bayesian Neural Networks	53

see evdbayes pdf package r

Attention : π ou f ??????

We let useful relevant tools regarding bayesian inference in Appendix ??

This chapter is mostly based on [Coles \[2001, sec. 9.1\]](#), [Beirlant et al. \[2006, chap.11\]](#) and [Reiss and Thomas \[2007, chap.1-4\]](#), and other relevant articles.

Definition 4.1 (Posterior distribution). Let $\mathbf{x} = (x_1, \dots, x_m)$ denote the observed data of a random variable X distributed according to a distribution with density

$$\pi(\theta|\mathbf{x}) = \frac{\pi(\theta) \cdot L(\theta|\mathbf{x})}{\int_{\Theta} \pi(\theta) \cdot L(\theta|\mathbf{x}) \cdot d\theta} \propto \pi(\theta) \cdot L(\theta|\mathbf{x}) \quad (4.1)$$

where $L(\cdot)$ denotes the likelihood function, as in ?? but there it was the log-likelihood !!! and θ usually denotes the multidimensional set of parameters in EVT, $\theta = (\mu, \sigma, \xi)$, at least in a univariate stationary context. \triangle

Unlike other chapters, we will directly write θ as a 3D vector, unless stated differently. This allows not to overload the equations and to facilitate readability.

1. Whenever it is possible, it allows to introduce other source of knowledge coming from the domain at-hand, by the elicitation of a prior. The counter-argument of this advantage is that it also introduces (improper ?) subjectiveness.
2. "accounting for parameter and threshold uncertainty is perhaps handled most easily in the Bayesian paradigm" [Dey and Yan, 2016, pp.106]

As such, It permits an elegant way of making future predictions which is one of the most(?) important issue in EVT.

3. Bayesian framework can overcome the regularity conditions of the likelihood inference (see section 4.1). Thus it usually provides a viable alternative in cases when MLE (for example) breaks down. And actually, we are not so far from the problematic situations depicted in section 3.1. Moreover, the Highest Posterior Probability (HPD) region is constructed so that... and there is no more need to fall to asymptotic theory as in conventional methods.
4. For an asymmetric distribution, the HPD interval can be a more reasonable summary than the central probability interval (see illustration ...). For symmetric densities, HPD and central intervals are the same while HPD is shorter for asymmetric densities. See Liu et al. [2015]....

As the dependence becomes stronger, the run length n must be larger in order to achieve the same precision. Dependence exists both within the output for a single parameter (autocorrelations) and across parameters (cross-correlations), we discuss this issue in section text.

4.1 Prior Elicitation

Sometimes viewed as advantage from the amount of information that can be retrieved, and sometimes viewed as a drawback due to the (rather unquantifiable) subjectivity that introduced, the construction of the prior is a key step in Bayesian analysis.

Priors are necessary in the Bayesian paradigm to be able to compute the posterior in (4.1). But, priors require the legitimate statement of domain's expert, to make this viewed the less subjective as possible

Prior may not be of great importance if the size (m) of the dataset is large. It can be seen from (4.1) where the amount of information contained in the data through $L(\theta|\mathbf{x})$ will be prominent compared to this contained in the prior through $\pi(\theta)$. Prior will have limited influence.

One is aware that this is not often the case in EVT cases. By design, we are dealing with rather small so-constructed datasets. And mostly for this reason, it could be important to incorporate additional information in this limited dataset through the prior distribution.

4.1.1 Non-informative Priors

Receive a correct and accepted advice from an expert is often difficult So, in many cases, we cannot inject information through the prior. We must then construct a prior which represent this lack of knowledge so that they do not influence posterior inferences.

There exists a vast amount of uninformative priors in the literature (see e.g. [Yang and Berger \[1996\]](#), [Ni and Sun \[2003\]](#)) This family of priors can be *improper*, i.e. priors for which the integral of $\pi(\theta)$ over the parameter space is not finite. It is valid to use improper priors only if the posterior target is proper.

Adjustments of these priors must always be thought in practical applications

Jeffrey's prior

is specified as

$$\pi(\theta) \propto \sqrt{\det I(\theta)}, \quad \text{where} \quad I_{ij}(\theta) = \mathbb{E}_\theta \left[-\frac{\partial^2 \log f(\mathbf{x}|\theta)}{\partial \theta_i \partial \theta_j} \right], \quad i, j = 1, \dots, d. \quad (4.2)$$

where $f(\mathbf{x}|\theta)$ is the density function of X. This prior is invariant to reparametrization, but has complex form for EV models, and it exists only when $\xi > -0.5$ in GEV models, where it is function of ξ and σ only.

MDI prior

Maximal Data Information priors

However, it has been showed by [Northrop and Attalides \[2016\]](#) that both Jeffrey and MDI priors give improper posterior when there are no truncation of the shape parameter, i.e. we must restrict the fact that $\pi(\theta) \rightarrow \infty$ as $\xi \rightarrow (-)\infty$ for Jeffreys (MDI), in order to obtain a proper posterior.

Vague priors

The last and often preferred alternative to construct uninformative priors is to use proper priors which are near flat, e.g. which are uniform or with exhibits large variance for the normal distribution.

In GEV we will take independent normal-distributed priors each with a large (tuned) variance. When these variances increase, we get at the limit

$$\pi(\theta) = \pi(\mu, \nu, \xi) \stackrel{(4.1)}{=} \pi(\mu) \cdot \pi(\nu) \cdot \pi(\xi) \propto 1, \quad (4.3)$$

where $\nu = \log \sigma$.

Taking multivariate normal distribution as prior has also been proposed (see) is often difficult as it involves 9 (hyper)parameters in total and this can be difficult

4.1.2 Informative Priors

STAN : "It can also be a huge help with computation to have less diffuse priors, even if they're not informative enough to have a noticeable impact on the posterior. "

Gamma Distributions for Quantile Differences

Beta Distributions for Probability Ratios

The Bayes Factor

4.2 Bayesian Computation : Markov Chains

Methods have been developed for sampling from arbitrary posterior distributions $\pi(\theta|x)$. Simulations of N values $\theta_1, \theta_2, \dots, \theta_N$ that are iid from $\pi(\theta|x)$ can be used to estimate features of interest.

But simulating from $\pi(\theta|x)$ is usually not achievable and this is why we need **Markov Chain Monte Carlo** (MCMC) techniques. We use it to simulate a markov chain $\theta_1, \theta_2, \dots, \theta_N$ that converge to the target distribution $\pi(\theta|x)$. This means that, after some *burn-in period* B , $\theta_{B+1}, \dots, \theta_N$ can be treated as random sample from $\pi(\theta|x)$.

Let's now (a bit weakly) define one of the most important results in Markov Chain theory.

Definition 4.2 (*First-order discrete-time Markov Property*). *Let k_0, k_1, \dots be the states associated to a sequence of time-homogeneous random variables, say $\{\theta_t : t \in \mathbb{N}\}$. The Markov property states that the distribution of the future state θ_{t+1} depends only on the distribution of the current state θ_t . In other words, given θ_t , we have that θ_{t+1} is independent of all the states prior to t . We can write this as*

$$\Pr\{\theta_{t+1} = k_{t+1} \mid \theta_t = k_t, \theta_{t-1} = k_{t-1}, \dots\} = \Pr\{\theta_{t+1} = k_{t+1} \mid \theta_t = k_t\}. \quad (4.4)$$

△

or see [Angelino et al. \[2016, section 2.2.3\]](#) for more in-depth results.

The samples are not independent, and the dependence influences the accuracy of the posterior estimates. As dependence becomes stronger, we must increase the run-length N to achieve the same accuracy.

4.2.1 Algorithms

We are looking for a so-generated chain that has a stationary distribution $\pi(\theta|x)$. This is the case if the chain is

1. *aperiodic*

2. *irreducible* or *ergodic*, that is if any state for θ can be reached with probability > 0 in a finite number of steps from any other state for θ .

"The Markov chains Stan and other MCMC samplers generate are *ergodic* in the sense required by the Markov chain central limit theorem, meaning roughly that there is a reasonable chance of reaching one value of theta from another." ?

With MH or Gibbs sampler, we need to tune individually the proposal standard deviations to reach a correct acceptance, and this is often done with trial-and-error methodology.

The performance of the standard Markov chain Monte Carlo estimators depends on how effectively the Markov transition guides the Markov chain along the neighborhoods of high probability. If the exploration is slow then the estimators will become computationally inefficient, and if the exploration is incomplete then the estimators will become biased [Betancourt \[2016\]](#). It is then necessary to consider other form of sampling...

4.2.2 Hamiltonian Monte Carlo

Package Rstan

[Neal and others \[2011\]](#) and [Betancourt and Girolami \[2015\]](#) are really

HMC permit to better exploit the properties of the target distribution to make informed jumps through neighborhoods of high probability while avoiding neighborhoods of low probability entirely.

4.2.3 Computational efficiency comparison

In modern statistical area, computing methods have been widely ... And this need for computations will rise in the future.

We will then compare our 3 methods too see if effectively

4.3 Convergence Diagnostics

When applying MCMC algorithms to estimate posterior distributions, it is vital to assess convergence of the algorithm to try to ensure that we reached the stationary target distribution. Let's now enumerate some of the key steps we must keep in mind when thinking about convergence, an hence reliable results.

1. A sufficient *burn-in period* $B < N$ must be chosen to ensure that the convergence to the posterior distribution $\pi(\theta|x)$ has occurred.
2. For the same reason, a sufficient number of simulations N to eliminate the influence of initial conditions and ensure accuracy in the estimations ((and then make sure than we are sampling from the target stationary (posterior) distribution)).
3. Several dispersed starting values must have been simulated to ensure we explored all the regions of high probability. This is particularly important when the target distribution is complex.
4. The chains must have good mixing properties, in the sense that the whole parameter space (...) A common technique that we will apply is to run different chains several times and then combine

a proportion of each chain (typically 50%) to get the final chain. This procedure wants to ensure a proper mixing behaviour. The potential scale reduction factor (Gelman diagnostic) is also a popular tool, see .

We must keep in mind that no convergence diagnostics can prove that convergence really happened and validate the "model". However, a combined use of several relevant diagnostics will be required to increase our confidence that convergence actually happened.

4.3.1 Proposal Distribution

The main ideas are :

- If the variance of the proposal distribution is too large, most proposals will be rejected :
ie the jumps through the chain are too large,
- If the variance of the proposal distribution is too low, then most proposals will be accepted

Both are harmful for the objective of an efficient "visit" of the whole parameter space.

Widely speaking, we consider 2 different types of algorithms in which it is preferable to target a certain acceptance rate. It is distinguished by the updating manner of the components of θ through the algorithm, i.e. the 3 univariate parameters of interest.

- When all components of θ are updated simultaneously, it is recommended to target an acceptance rate of around 0.20. [Roberts et al. \[1997\]](#) have shown that, under quite general conditions, the asymptotically optimal acceptance rate is 0.234. (for target density that has a symmetric product form) This quantity has been verified by [Sherlock et al. \[2009\]](#). It holds for the *Metropolis-Hastings* algorithm.
- When the components are updated one at a time, an acceptance rate of around 0.40 is recommended. It holds for the *Gibbs sampler* algorithm.

Let's (see ? for example for the first case)

Gelman-Rubin diagnostic : the \hat{R} statistic

As discussed in [item 4](#) above

Geweke diagnostic

Thinning

iteration k is stored only if $k \bmod \text{thin}$ is zero (and if k greater than or equal to the burn-in B).

This typically reduces the precision of posterior estimates, but it may represent a necessary computational saving.

4.3.2 The problem of auto and cross-correlations in the chains

There exists exists 2 problems of correlations in the output delivered by a MC.

- **Autocorrelation** is the
- **Cross-correlation**

4.4 Posterior Predictive

notation for posterior ? π or f

As discussed in item 2 above, prediction is of important interest in EVT, and this is "facilitated" in the Bayesian paradigm. This also permits a more straightforward quantification of the inferential uncertainty associated.

Definition 4.3 (Posterior Predictive density). *Let X_{m+1} denotes a (one-step-ahead) future observation with density $f(x_{m+1}|\theta)$. Then we define the Posterior Predictive density of a future observation X_{m+1} given \mathbf{x} as*

$$\begin{aligned} f(x_{m+1}|\mathbf{x}) &= \int_{\Theta} f(x_{m+1}, \theta|\mathbf{x}) \cdot d\theta = \int_{\Theta} f(x_{m+1}|\theta) \cdot \pi(\theta|\mathbf{x}) \cdot d\theta \\ &:= \mathbb{E}_{\theta|\mathbf{x}}[f(x_{m+1}|\theta)] \end{aligned} \tag{4.5}$$

where the last line emphasizes that we can evaluate $f(x_{m+1}|\mathbf{x})$ by averaging over the different possible parameter values.

△

The uncertainty in the model is reflected here through $\pi(\theta|\mathbf{x})$ while the uncertainty due to variability in future observations is also reflected through $f(x_{m+1}|\theta)$.

Definition 4.4 (Posterior Predictive probability). *The posterior predictive probability of X_{m+1} exceeding some threshold x is accordingly given by*

$$\begin{aligned} \Pr\{X_{m+1} > x | \mathbf{x}\} &= \int_{\Theta} \Pr\{X_{m+1} > x | \theta\} \cdot \pi(\theta|\mathbf{x}) \cdot d\theta \\ &= \mathbb{E}_{\theta|\mathbf{x}}[\Pr(X_{m+1} > x | \theta)] \end{aligned} \tag{4.6}$$

△

This quantity is often of interest in EVT as we are rather concerned with the probability of future unknown observable exceeding some threshold.

However, this quantity is difficult to obtain analytically. Hence, we will more rely on simulated approximations. Given a sample $\theta_1, \dots, \theta_r$ from the posterior $\pi(\theta|\mathbf{x})$, we use

$$\Pr\{X_{m+1} > x | \mathbf{x}\} \approx r^{-1} \sum_{i=1}^r \Pr\{X_{m+1} > x | \theta_i\}, \tag{4.7}$$

where $\Pr\{X_{m+1} > x \mid \theta_i\}$ follows directly from $f(x|\theta)$.

We will now analyse more in-depth the numerical computations in the Bayesian paradigm or how we can get numerically a sample of the posterior distribution.

4.5 Bayesian Predictive Accuracy for Model Validation

4.5.1 Cross-validation for predictive accuracy

When having large amount of data, we can use a well-known and widely used technique coming from Machine Learning. That is, dividing the dataset between a training (typically 75% of the whole set) and a test set containing the remaining observations. For example, having N draws $\theta^{(1)}, \theta^{(2)}, \dots, \theta^{(N)}$ coming from the posterior $\pi(\theta|x_{train})$, we can score each value using (?)

$$\log \left[N^{-1} \sum_{t(i)=1}^N f(x^*|\theta^{(t)}) \right]. \quad (4.8)$$

However, we often do not have large amounts of data. Henceforth, we can use the *cross-validation* technique which is more relevant in smaller dataset, but which is computationally more demanding. There exists several variants of them.

Leave-one-out cross-validation

The *Leave-One-Out* (LOO) cross-validation is the

K -fold cross-validation

[Vehrtari et al. \[2016\]](#)

Or we can use other criteria which avoid the computations. The basic approach is to use $\log f(x|\bar{\theta}) - p^*$ for N draws $\theta^{(1)}, \dots, \theta^{(N)}$ from $\pi(\theta|x)$. where p^* represents the effective number of parameters and $\bar{\theta}$ the posterior mean. Several methods exists using this idea. We will see the two most important.

Deviance Information Criterion

The *Deviance Information Criterion* (DIC) was first used by [Spiegelhalter et al. \[2002\]](#) and use the following estimate for the effective number of parameters

$$p^* = 2 \cdot \left(\log f(x|\bar{\theta}) - N^{-1} \sum_{t=1}^N \log f(x|\theta^{(t)}) \right) \quad (4.9)$$

It is defined on the deviance scale and smaller DIC values indicate better models.

$$\text{DIC} = 2 \log f(x|\bar{\theta}) - \frac{4}{N} \sum_{t=1}^N \log f(x|\theta^{(t)}) \quad (4.10)$$

Widely Applicable Information Criterion

The *Widely Applicable Information Criterion* (WAIC) is a more recent approach proposed by [Watanabe \[2010\]](#) and is given by

$$\text{WAIC} = 2 \sum_{i=1}^n [\log \{\mathbb{E}_{\theta|x} f(x_i|\theta)\}] - \mathbb{E}_{\theta|x} \log f(x_i|\theta) \quad (4.11)$$

or

$$\text{WAIC} = \sum_{i=1}^n \left[2 \log \left(N^{-1} \sum_{t=1}^N f(x_i|\theta^{(t)}) \right) - \frac{4}{N} \sum_{t=1}^N \log f(x_i|\theta^{(t)}) \right] \quad (4.12)$$

There exists for sure other several methods, as proposed by [Gelman et al. \[2014\]](#).

'LOO and WAIC have various advantages over simpler estimates of predictive error such as AIC and DIC but are less used in practice because they involve additional computational steps'

For each generated chains with dispersed starting values, we evaluate separately the information criteria. The discrepancies between the chains are small (?), which is a good sign.

4.6 Bayesien Inference ?

4.6.1 Bayesian Credible Intervals

The Bayesian *credible intervals* are inherently different from the frequentist's confidence intervals. In the Bayesian intervals, the bounds are treated as fixed and the estimated parameter as a random variable, while in the frequentist's setting, bound are random variables and the parameter is a fixed value.

There exist mainly two kinds of credible interval in the Bayesian sphere :

- The *Highest Probability Interval* (HPD) which is defined as the shortest interval containing $x\%$ of the posterior probability, e.g. if we want a 95% HPD interval (ξ_0, ξ_1) for ξ :

$$\int_{\xi_0}^{\xi_1} \pi(\xi|\mathbf{x}) d\xi = 0.95 \quad \text{with} \quad \pi(\xi_0|\mathbf{x}) = \pi(\xi_1|\mathbf{x}). \quad (4.13)$$

It is often the preferred interval as it gives the parameter's values having the highest posterior probability.

- The Quantile-based credible intervals or *equal-tailed interval* picks an interval which ensures a probability of being below this interval as likely as of being above it. For some posterior distribution which are not symmetric, this could be misleading, thus it is not the most recommended interval. (see ..) However, these are often easily obtained when we have a random smaple of the posterior... (?)

4.6.2 Distribution of Quantiles : Return Levels

The Markov chains generated can be transformed to estimate quantities of interest such as quantiles and hence return levels.

The values can be retrieved in the same manner as we have done in the GEV frequentist setting in (1.32). If the df F associated is GEV then $y_m = -\log(1 - m^{-1})$, and if F is GPD then $y_m = m^{-1}$.

r_m is the quantile corresponding to the upper tail probability $p = m^{-1}$.

We can use the values of the samples generated by the posterior to estimate features of this distribution. (... see edbayes)

4.7 Bayesian Model Averaging

4.8 Bayesian Neural Networks

Part II

Experimental Framework : Extreme Value Analysis of Maximum Temperatures

CHAPTER 5

INTRODUCTION TO THE ANALYSIS

Contents

Repository for the code : R Package	56
Visualization Tool : Shiny Application	56
5.1 Presentation of the Analysis : Temperatures from Uccle	57
5.2 First Analysis : Annual Maxima	57
5.2.1 Descriptive Analysis	57
5.2.2 First visualization with simple models	58
5.2.3 Deeper Trend Analysis : Splines derivatives in GAM	58
Pointwise vs Simultaneous intervals	59
Methodology	59
Final Results	61
5.3 Comments and Structure of the Analysis	62

Since we have theoretically defined useful concepts in EVT, we will now introduce the practical analysis of this thesis that consist of analyzing daily maximum temperatures in Uccle from 1901 to 2016. We already showed the distribution of these data in Figure 2.1 to introduce the POT approach. This chapter will present an introductory analysis of the annual maxima of these data. We chose annual maxima in order to later provide a convenient GEV modeling. We will then first use several techniques to analyze these data before going further into the EV models in the following chapters.

After a brief presentation of the repository which contains the R package created for this thesis and the structure for the scripts that contains the code that created all the analysis, we will briefly present the shiny applications created to enhance visualizations. Then, Section 5.1 will present data and their source(s). Section 5.2 will first describe data and compare models to represent the data before going further on the trend analysis with splines derivatives in a Generalized Additive Model to assess significance of the trend with correction for simultaneous tests and provide first aspects in the issue of Climate Warming without using extreme models.

This chapter will then not explicitly use techniques presented in the previous chapters. It will be mostly based on Ruppert et al. [2003] for the model presented in Section 5.2.3.

Repository for the code : R Package

The created **R package** can be easily downloaded from this **repository** :

<https://github.com/proto4426/PissoortThesis>

by following instructions in the README. It follows the standard structure of a usual R package (see e.g. [Leisch \[2008\]](#)) and makes use of the roxygen2 package for the documentation.

For your convenience, an external folder has been created in this repository containing all the scripts created during this thesis. It allows to reproduce all the results often with more details, tables or plots. It is located in the **/Scripts-R/** folder of the repository. Each script will be mentioned in its corresponding section. Further details on the repository structure can be found in [Appendix D](#).

Visualization Tool : Shiny Application

Shiny applications that have been developed can be run directly through the R environment after loading the package in your environment, by executing

```
runExample() # in the R console ,
```

choosing one application's name between the displayed propositions and write it inside (' '). So far, we have

- ('GEV_distributions') : application based on Figure 1.1 smoothly displaying the GEV and the influence of its parameters.
- ('trend_models') : application dedicated to annual maxima that can you can visualize with some preliminary methods (see [Section 5.2.2](#)).
- ('splines_draws') : application to simulate splines of GAM model that allow to visualize coverages of the pointwise and simultaneous confidence intervals. (see [Section 5.2.3](#)).
- ('neural_networks') : application for the GEVcdn allowing bagging to see the effects of all the (hyper)parameters, since the model's choice is still subjective... (see if we have time to finish !)

Moreover, a dynamic overview of the applications is available in the repository's README.

All-in-one : Dashboard For the reader's convenience, we have decided to gather all applications in a smooth *dahsboard*. Moreover, it is uploaded on a server at the following [URL¹](#) in order to provide a quick user-friendly overview through the rsconnect interface.

The rest of the analysis in this chapter will rely on `1intro_stationary.R` and `1intro_trends(splines).R` codes from the **/Scripts-R/** folder of the **repository**.

¹https://proto4426.shinyapps.io/All_dashboard/

5.1 Presentation of the Analysis : Temperatures from Uccle

Data used during this thesis comes from the "Institut Royal de Météorologie" (IRM) located in Uccle. We were provided official data used by meteorologists in Belgium. We wanted to have data that is reliable enough in order to be able to produce relevant results.

We were provided a set of databases from the IRM and decided to focus on temperature analysis in order to assess climate warming. Rainfall data analysis would have also been interesting in EVT.

The fact that the dataset begins only at year 1901 is due to homogeneity reasons since the measurement shelters evolved substantially compared to previous periods, especially in terms of measurement errors. For meteorological considerations and again for reasons of homogeneity, it is better to analyze the temperatures in *closed shelters*, following for example [Lindsey and Newman \[1956\]](#). Indeed, thanks to helpful advice from C.Tricot, climatologist at the IRM, temperatures in closed shelters have the advantage of not being too influenced by the solar radiation which artificially increases temperatures, especially in periods of *extreme* heats and thus high solar activity, and therefore in the studied case. For example, the maximum temperature of 36.6°C that occurred the 27th June 1947 in closed shelters was actually measured at 38.8°C in open shelters the same day.

Comparisons with freely available data

A similar dataset for Uccle is publicly available on the Internet². It was a project initially performed by the KMNI and which was used by [Beirlant et al. \[2006\]](#). However, we did not want to simply analyze that data as we did not know if it was trustworthy, for reasons mentioned above.

Afterwards, we compared these two datasets for years 1901 to 2001. We remark that there are large differences in these two datasets. For example, 54% of measurements are equal with those of the dataset in open shelters against 14.4% in the closed shelters. For this reason, we have confidence that the public dataset has temperatures measured in open shelters, which is not recommended. Hence, we conclude that large measurement errors can easily occur in unofficial data which emphasizes the necessity of reliable data in order to yield a reliable analysis.

5.2 First Analysis : Annual Maxima

5.2.1 Descriptive Analysis

The goal of this section is simply to display a global overview of the data. The code provided most of the descriptive analysis. To summarize most of the information, we have plotted a violin-plot and a density plot of the **daily** maximum temperatures in Figure C.2 in [Appendix C](#) where we divided data in each meteorological season to point out the differences. Per example, we can see that the spread is higher for autumn and spring.

Now, we will rather stick to the block-maxima approach by taking yearly blocks leaving us with $n = 116$ data which seems justifiable for further GEV analysis and the conditions to hold. We will discuss the choice of the block length further in the [next Chapter](#).

²<http://1stat.kuleuven.be/Wiley/Data/ecad00045TX.txt>

5.2.2 First visualization with simple models

We present the series of yearly maxima in Figure 5.1 where we introduce 3 **models for the trend** :

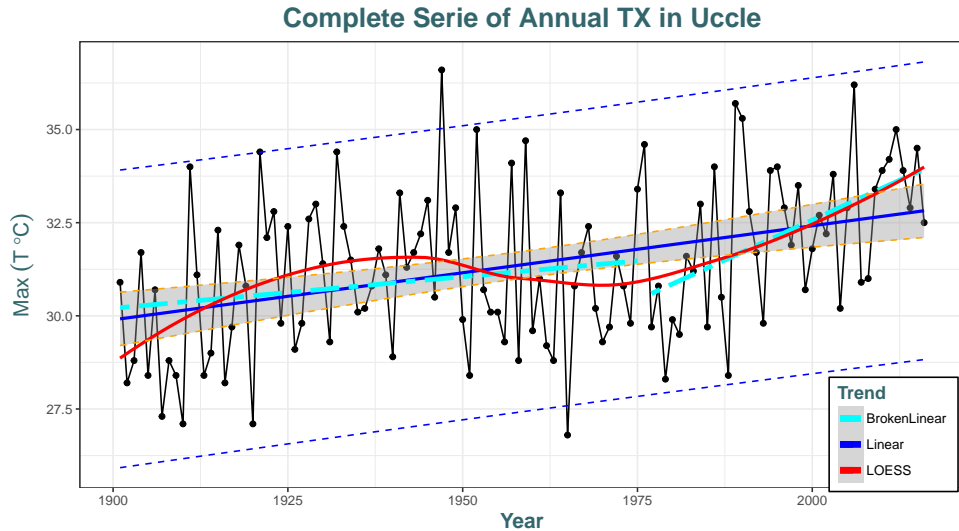


Figure 5.1: Yearly maxima together with three first models that represent the trend. Note that shaded grey area around the linear regression fit represent its 95% pointwise confidence interval on the fitted values (i.e., $\pm 1.96 \times \sigma_{\text{pred}}(\text{year})$) while blue dotted lines are prediction intervals taking also into account the prediction uncertainty.

- *Linear regression* is a **parametric** fit. We remark that it is slightly but significantly increasing over time ($p\text{-value} \approx 10^{-5}$). From this model, one rough interpretation we can deduce is that each year we expect the annual maximum temperature to increase by $\hat{b} = 0.025^\circ\text{C}$ ($\hat{\sigma}_{\hat{b}} = 0.005$).
- *Local Polynomial regression* or LOESS is a **nonparametric** fit. It tells us that the yearly maxima process is rather "smooth". The drop in the series visible around years 1950 to 1975 is probably due to noise rather than a real decrease or freezing of the maximum temperatures at this time. Moreover, it disappears if we change the parameter controlling the degree of smoothing. We will assess that more formally in the [next Section](#) with another nonparametric model.
- *Broken-linear regression* is a **parametric** fit. We wanted to emphasize visually the trend difference between the period [1901-1975] and [1976-2016]. These two periods have been chosen arbitrarily and we remark that period [1901-1952] has also a very high positive slope. We will study that in more details in [next Section](#).

These different models give us insights on the process we will study throughout the rest of this thesis. We will not develop further the results of each model as this is not the subject of this thesis and we are more interested in assessing this trend and its statistical significance over time with a more interesting method.

5.2.3 Deeper Trend Analysis : Splines derivatives in GAM

Apart from the significant pointwise increasing linear trend, we did not find concrete results. Additionally, we see in the series in Figure 5.1 that a linear trend to the entire series could be considered as too

restrictive. Regarding the broken-linear trend for example, we would like to assess if there is indeed a difference in the slope of the trend over some time periods.

We assume the reader knows about *Generalized Additive Models* (GAM) developed by [Hastie and Tibshirani \[1986\]](#). We also assume the reader knows about *penalized splines* and *splines smoothing*. Theoretical explanations of these concepts can be found in [Ruppert et al. \[2003\]](#), chapter 3, 6 and 11] which will be the reference book of this section. Replacing covariates with smooth functions such as smoothing splines will result in a more flexible nonparametric model. We will also follow the simulation-based Bayesian approach of [Marra and Wood \[2012\]](#) that compares coverage properties of intervals.

Pointwise or Simultaneous confidence intervals ?

For this analysis, we deem important to differentiate the two types of intervals for a better understanding of the actual meaning of "confidence interval". A special example is the grey area around the linear fit in Figure 5.1 which represents a 95% interval for the regression line (and not for the data), taking into account variability in the data. If we repeatedly sample over and over and take the predicted values, then the new linear fit will be in the grey zone approximately 95% of the time.

Let \mathcal{X} denote the set of x values of interest, i.e. $\mathcal{X} = [1901, 2016]$ in our case and $f(\cdot)$ is the model of interest, e.g. the linear regression, or the GAM model that we will fit. Hence, we define

- A **pointwise** $100(1 - \alpha)\%$ confidence interval $\{[L(x), U(x)] : x \in \mathcal{X}\}$ approximately satisfies

$$\Pr\{L(x) \leq f(x) \leq U(x)\} \geq 1 - \alpha, \quad \forall x \in \mathcal{X}. \quad (5.1)$$

- A **Simultaneous** $100(1 - \alpha)\%$ confidence interval must satisfy

$$\Pr\{L(x) \leq f(x) \leq U(x), \forall x \in \mathcal{X}\} \geq 1 - \alpha. \quad (5.2)$$

In the linear regression example of Figure 5.1, from the pointwise confidence intervals we can say that, $f(1920)$ has 95% chance to lie within [29.8, 31.1] and $f(2016)$ has also 95% to lie within [32.1, 33.6] but it is a fallacy to say that both are contained in these intervals at the same time with 95% confidence. The corresponding simultaneous intervals (blue dotted lines) are quite larger, [26.4, 34.3] and [36.8, 28.8] for years 1920 and 2016 respectively.

For the interested reader, theoretical details on how to mathematically derive simultaneous intervals are available in [Ruppert et al. \[2003\]](#), pp.142-144].

Methodology

- We have fitted a simple GAM model on the annual maxima relying on the `mgcv` package from [Maindonald and Braun \[2006\]](#).
- Figure C.3 in [Appendix C](#) shows the correlation structure of the serial normalized residuals. As selection of a model for the residuals is not trivial from this figure, we fitted several time series models for the residuals. It is not necessary to consider too complex models, therefore 2 additional degrees of freedom are sufficient. Results are in Table C.1 in [Appendix C](#) where we see that

BIC will prefer the independent model for the residuals but the AIC won't. Parsimony being important, we chose the independent model to draw plots with simultaneous intervals but we will also keep MA(1) for comparisons. Likelihood ratio tests validated our choice. Diagnostics of the model presented in Figure C.4 in [Appendix C](#) are correct.

- As we took a Gaussian (identity) link, our model can hence be written as

$$Y_{\text{GAM}}(\text{year}) = \alpha + f_{(k)}(\text{year}) + \epsilon, \quad \epsilon \sim \text{WN}. \quad (5.3)$$

where f is modelled by smoothing splines, ϵ can be MA(1) and Y represent annual TX. We set the dimension of the basis k for the spline to 20 to ensure a reasonable degree of smoothness as there is modest amount of non-linearity in the series and we did not perform cross-validation as it will not influence the results that much.

- To account for uncertainty, we simulated $M = 10^4$ draws (quite fast) from the posterior of the GAM model in (5.3). Hence, the confidence intervals (or bands) that we compute will be of the form of Bayesian credible intervals, discussed in [Section 4.6.1](#) and which is highlighted by [Marra and Wood \[2012\]](#). 50 posterior draws are displayed in Figure 5.2 displaying pointwise (in yellow) and simultaneous (in red) intervals. We point out that pointwise intervals are too narrow.

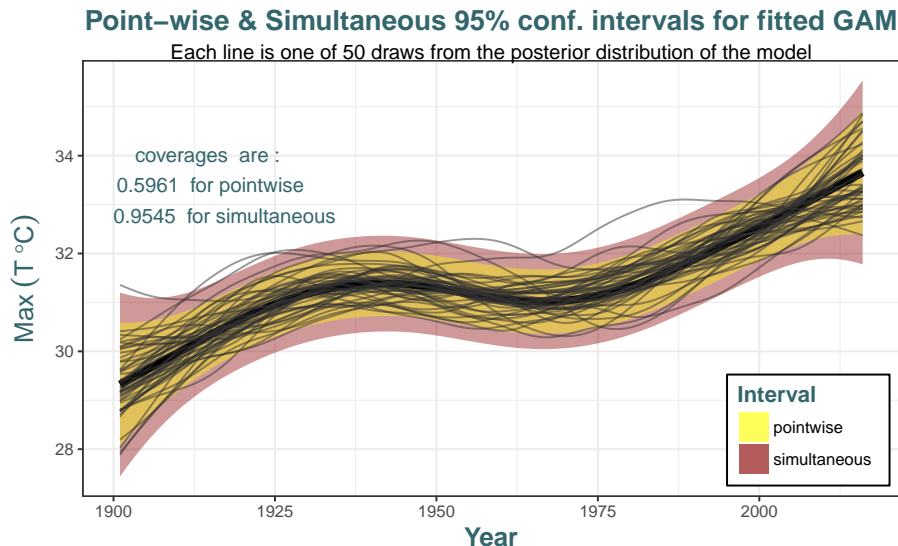


Figure 5.2: Draws from the posterior distribution of the model. Notice the large uncertainty associated to the posterior draws (grey lines). The coverages are calculated for $M = 10^4$ simulations.

Coverage Analysis

We would like to highlight the inadequacy of the pointwise intervals. Hence, we computed posterior draws of the fitted GAM and we counted how many draws lied within each interval.

We clearly see that the coverages indeed converge to the true value 95% of the confidence level for the simultaneous intervals when M becomes very large, while it converges rather to $\approx 60\%$ for the pointwise intervals.

Table 5.1: Proportion of the M posterior simulations which are covered by the confidence intervals

Coverage at 95%	$M = 20$	$M = 100$	$M = 10^3$	$M = 10^5$
<u>Pointwise</u>	40%	63%	61.1%	59.463%
<u>Simultaneous</u>	80%	91%	94.9%	95.019%

Shiny application has been build from this graph for better visualization of the impact of the number of simulations on the confidence intervals and how their coverage varies, both visually and quantitatively. Finally, note that the results are similar if we do the experiment on the first derivatives $f'(\cdot)$ of the splines rather than on the splines themselves.

Final Results

We see two significant increases in the trend fitted by GAM in Figure C.5 in Appendix C when we do not use simultaneous intervals. The decrease pointed out in Figure 5.1 with LOESS between 1945 and 1970 is hence not significant and probably due to randomness.

Some remarks from the two plots in Figure 5.3, considering now splines derivatives :

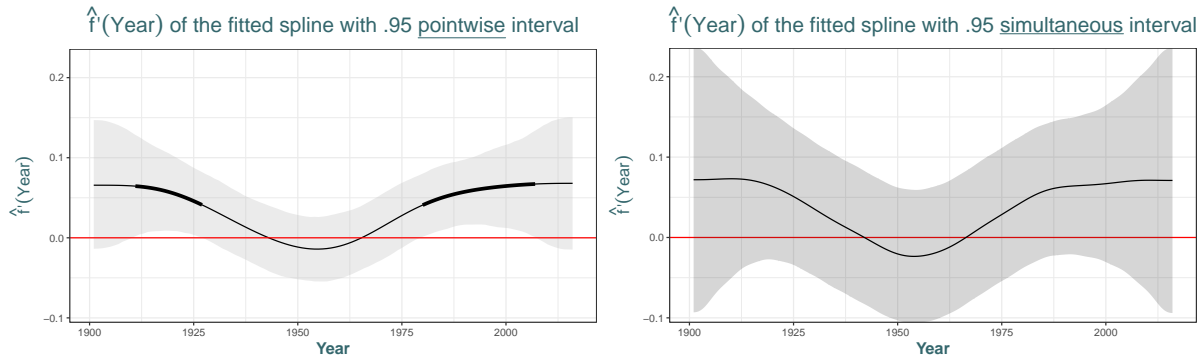


Figure 5.3: Plots of the first derivative $f'_{(20)}(\text{year})$ of the estimated splines on the retained GAM model. Grey area represents 95% confidence bands. Sections of the spline where the confidence interval does not include zero are indicated by thicker lines.

- Together with the series in Figure 5.1, we can make the link between the trend behavior of the series and the splines' first derivatives which accurately models the slope behavior of the trend.
- We notice the increasing trend with decreasing slope, i.e. $f''_{(20)}(\text{year}) < 0$, until year ≈ 1945 where it becomes negative. Then the slope increases and the trend starts to increase again near 1962. This upward trend in the series of annual maxima for this last period brings light to the climate change we are currently facing. However, we see that we are now at a "critical point" since several years, i.e. $f''_{(20)}(\text{year}) \approx 0$, meaning that the trend is likely linear.
- Whereas the pointwise confidence interval includes significant regions, i.e. 0 is not included in the interval, the simultaneous interval that is accounting for the increase in uncertainty, has no significant regions. Therefore, we cannot conclude that there has been any significant increase in the annual maximum temperatures in any period.

5.3 Comments and Structure of the Analysis

We have found that there is indeed an upward (linear) trend for the series of yearly maxima but it is not significant once applied the correction for simultaneous intervals. Hence, a nonstationary analysis is worth to be continued. After this introductory analysis, we will go through with the specific subject of this thesis, the extreme value analysis. Hence, next chapter will first present a stationary GEV analysis and then allow nonstationarity in various ways.

POT As you have seen, the analysis in POT or in GEV involves different methods and different subsets of data. In this text, we will not display the results of the POT analysis for readability purposes. Henceforth, we will focus on the GEV analysis only. But note that the POT analysis is available on the same [repository](#) as presented above. [Appendix D](#) summarizes its contents.

Moreover, we have also conducted some analysis by dividing the dataset by seasons, by hot or cold months (July-August or January-February), etc. We have also analyzed annual minimum temperatures and found a less pronounced trend than for maxima. Interesting comparisons are also available on the [repository](#), but we will focus on a GEV analysis on yearly maxima.

CHAPTER 6

ANALYSIS IN BLOCK MAXIMA

Contents

Block-length	64
R packages for EVT	64
6.1 Inference of the Stationary Model	64
6.1.1 Return Levels	65
6.1.2 Diagnostics	66
6.1.3 Stationary Analysis	67
POT	68
6.2 Parametric Nonstationary Analysis	68
6.2.1 Comparing Different Models	68
6.2.2 Selected Model, Diagnostics and Inference	69
6.3 Improvements with Neural Networks	71
6.3.1 Models and Results	71
6.3.2 Bagging	73
6.3.3 Inference : Confidence intervals by Bootstrap	74
6.4 Comments and Comparisons with POT	74

This chapter introduces the core subject of this thesis, the stationary and nonstationary GEV analysis for the annual maximum temperatures in Uccle. It will use concepts borrowed from [Chapter 1](#) and [Chapter 3](#). POT analysis of [Chapter 2](#) will be mentioned but all results are let in the code.

In [Section 6.1](#), we will present first GEV inferences assuming stationarity. It relies on `1intro_stationary.R` code from the `/Scripts-R/` folder of the [repository](#). [Section 6.2](#) will introduce the nonstationary analysis with parametric models and relies on `2Nonstationary.R` code while [Section 6.3](#) allows for more complex models from deep architectures and relying on `2NeuralsNets.R` code.

Whereas some Bayesian concepts will be used in this section such as use of *prior distributions* for the EVI to limit its domain when estimating it with a likelihood-based method, or to regularize weights of Neural Networks in [Section 6.3](#), we will still call all these methods as "frequentists". A strict Bayesian analysis will be made in the [next Chapter 7](#) and comparisons will be provided.

Block-length

The block-length selection is crucial in a GEV analysis. It is important to choose a block-length which is large enough for the limiting arguments supporting the GEV approximation (1.8) to be valid, or a large bias in the estimates could occur. But, a large block-length implies less data to work with, and thus a large variance of the estimates. A compromise must be found as pointed out in [Chapter 1](#). Here, we chose yearly blocks. It is justifiable not only for the above reason but for their interpretability and ease of use. Note that this will cause wastage of data since we will not use 6 month (from October to March) in the analysis since they never had an annual maximum. An idea to prevent this wastage could be to fit several GEV models on some subsets of the dataset divided by a seasonal criterion, but it would also generate other issues.

R packages in EVT

A bunch of packages exist for modeling extreme values in R. We have explored and used most of them to do the following analysis, and made some comparisons. Regarding classical EVT analysis, we must name the following :

- ▷ `ismev`, `evd`, `extRemes` (good for a wide nonstationary analysis with POT and nice tutorials, see e.g. [Gilleland and Katz \[2016\]](#)), `POT` (see [Ribatet \[2006\]](#)), `evir`, `fExtremes`, ...

Since lots of the package are doing the same analysis but with different methods, we decided to rely mostly on `ismev` as it is the package used in the book of [Coles \[2001\]](#).

6.1 Inference of the Stationary Model

The whole content of [Chapter 1](#) is important to understand the concepts used in this section but we will now be mostly based on inferential methods discussed in [Section 1.6](#), return levels in [Section 1.5](#) and diagnostics in [Section 1.7](#).

Maximum Likelihood

We estimate the MLE's relying on packages cited above, but also by checking it manually, that is by numerically solving the minimization of the negative log-likelihood. This can be done with the `n1m` routine using the Newton-Raphson algorithm of [Dennis and Schnabel \[1987\]](#). This algorithm is based on an approximation of the log-likelihood by a quadratic function which is the second order Taylor series approximation of the log-likelihood for a given point. Estimates and standard errors are shown in Table 6.1.

Table 6.1: MLE's of the three GEV parameters assuming a independent (stationary) context.

	Location μ	Scale σ	Shape ξ
Estimates (s.e.)	30.587 (0.216)	2.081 (0.155)	-0.254 (0.067)

The important thing to note from Table 6.1 is the value of the **shape** parameter which is negative. It means that we are under a Weibull-type of the GEV family. From Figure 1.1 the corresponding density

has the form of the red line, having a finite right endpoint. Moreover, a likelihood ratio test will confirm this in Table 6.4, comparing the fitted EV-Weibull with a Gumbel distribution.

The Weibull-type implies that the fitted distribution have an estimated right endpoint of $\hat{x}_* = \hat{\mu} - \hat{\sigma} \cdot \hat{\xi}^{-1} = 38.77^\circ c$. Comparing this value with the maximum value of the annual series ($36.6^\circ c$) tells us that this model takes into account the uncertainty since there are only 116 years of data. Hence, it allows return levels¹ to go beyond $36.6^\circ c$, for very long return periods. This will be highlighted in Figure 6.2 (right plot) where we remark there is still a probability mass beyond the minimum and the maximum values of the series from the fitted model.

Profile log-likelihood intervals These intervals are often preferred for individual parameters to handle the poor normal approximation of the MLE. Results provided by the `ismev` package are in Figure C.6 let in Appendix C. These intervals are constructed in the following way : search for the horizontal line and then subtract the maximum log-likelihood by half the corresponding upper quantile of the χ^2_{df} for $df = 1$ parameter of interest. We notice that :

- Even at 99% confidence, the interval for $\hat{\xi}$ does not contain 0 supporting that the distribution is left heavy-tailed and right bounded.
- 95% intervals for the location and scale parameters are [30, 31] and [1.8, 2.4] respectively.
- The intervals do not present much asymmetries. In fact, these will be more relevant for return levels as we will see in the [next Section](#).

Probability-Weighted-Moments

It is always a good practice to check whether different methods lead to significantly different results. A second estimator we have seen is the *probability-weighted-moments*. Results are shown in Table 6.2.

Table 6.2: Stationary GEV parameters estimated by PWM.

	Location μ	Scale σ	Shape ξ
Estimates	30.552	2.115	-0.232

We directly see that these results are very close to the MLE's of Table 6.1, in particular for the EVI ξ . This gives us confidence to be actually under a Weibull-type GEV model. For convenience and for their properties, we will only keep the MLE's to work with in the following.

6.1.1 Return Levels

First presented in Section 1.5, return levels are very appreciated by the practitioners for inference in an environmental EVT context. Usual likelihood intervals relying on the normal approximation are not reliable for return levels. Hence, we decided to compute the profile likelihood intervals and compare both values in Table 6.3.

The interpretation we can make from Table 6.3 is that, for example, the estimated 100-year return level is $36.23^\circ c$ which is the temperature which will be exceeded on average once every 100 years.

¹Since we recall that they are quantiles of the fitted distribution.

Table 6.3: The m -year return level estimates and 95% intervals. Last line computes the length's differences between the normal and the profile likelihood intervals.

	2-year	10-year	100-year	1000-year
Estimates	31.315	34.153	36.229	37.982
Normal interval	(30.88, 31.75)	(33.63, 34.67)	(35.21, 37.25)	(35.67, 39.04)
Profile likelihood interval	(31.16, 31.68)	(33.95, 34.74)	(35.54, 37.84)	(36.58, 40.25)
Difference of lengths	0.348	0.247	-0.260	-0.294

Note however that very long term extrapolation should be tempered by caution since we only have 116 years of data and predicting far beyond this value will become unreliable. We clearly see the shift of the profile likelihood confidence intervals compared with the normal intervals. This can also be seen on the return level plot in Figure 6.2 where we clearly see blue dots going higher than red lines for higher return periods. Moreover, we see that the profile likelihood intervals are more precise for small return periods, i.e. approximately until half the total number of annual data, and then profile likelihood intervals become wider than normal intervals. This illustrates how profile likelihood intervals better take into account the uncertainty of long-term predictions. Hence, in addition to arguments already provided, uncertainty but also climate warming lead us to have a preference for profile likelihood intervals which, quite surprisingly, are not used by default in EV packages such as `ismev`.

6.1.2 Diagnostics

Section 1.7 provided us tools to check the accuracy of the fitted model. The goal is to check that the model \hat{F} fitted by MLE is accurate enough for the true distribution F which is estimated by the empirical df (A.11). First, we present the quantile and the probability plots in Figure 6.1.

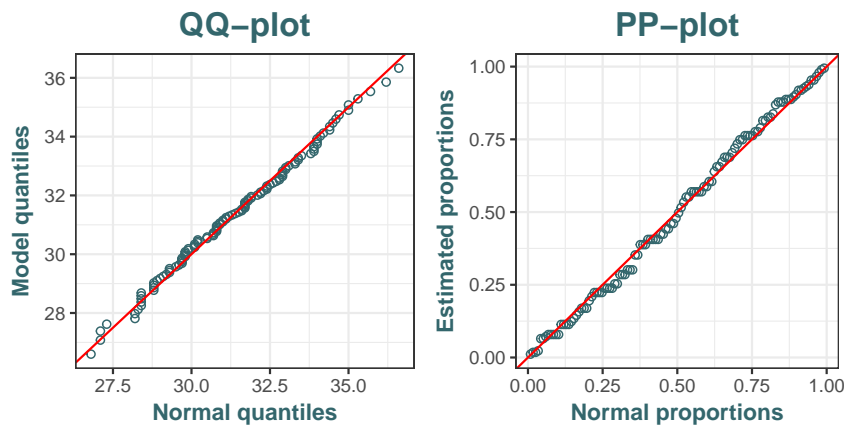


Figure 6.1: Quantile (left) and probability (right) plots for the stationary GEV model fitted by MLE.

Both plots show points lying very close to the unit diagonal, showing the empirical df is very close to the fitted model and hence putting confidence that our model fits our data accurately. Right plot of Figure 6.2 has a similar interpretation and leads to the same conclusion, although the fitted model has a higher peak.

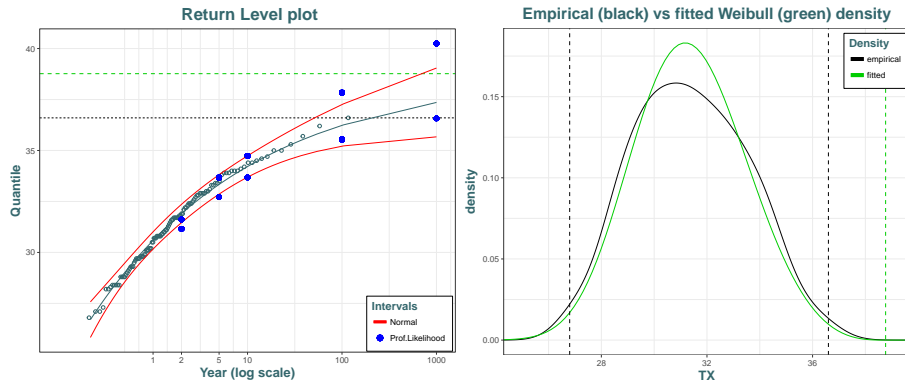


Figure 6.2: (Left) Return level plot with red lines representing normal confidence intervals, and blue points the individual profile likelihood intervals for return levels. Horizontal dotted line represent the right endpoint of the fitted model in green and the maximum of the series in black. (Right) kernel density in black compared with the density of the fitted model in green, with dotted lines representing the **endpoints** of the empirical distribution, and green dotted lines still represent the same right endpoint of the fitted EV-Weibull.

Return Level Plot

Another tool is available in EVT to check the fit of a model is the return level plot. It allows to compare observations with return levels coming from the EV-Weibull model fitted by MLE. Left plot of Figure 6.2 shows us a concave shape of the return levels with the return period which asymptotes to the right endpoint x_* of the model since $\xi < 0$. We remark that all points are very close the estimated return level and hence we have confidence that our model is suitable. Moreover, all these points are inside the normal confidence intervals (recall that profiled intervals are not suitable for very small return periods).

Whereas the estimated return level cannot go beyond x_* , we see that for very high return periods, the upper bound of the confidence intervals goes beyond this right endpoint of the fitted model. Again, this is justified since for such far periods, both intervals allow to go beyond the domain of the fitted model, with profile likelihood ones taking more uncertainty into account.

Profile Likelihood Intervals for Return Levels

We let the Figure C.7 in Appendix C which represents the profile log-likelihood intervals for three return periods, at the x -intersections between the blue line and the curve. We clearly visualize the asymmetries (positive skew) which are increasing for higher values of the return period. This was expected since the data at hand provide increasingly weaker information about high return levels of the process. We also displayed on the plots of Figure C.7 the return levels from Table 6.3, represented by the green lines, which were computed relying on another method from package `extRemes`. It is interesting to see how results can be slightly different.

6.1.3 Stationary Analysis

Section 3.1 proved that a dependent sequence can still have the GEV distribution in the limit of normalized maxima. This will only induce different location and scale parameters compared to the sequence as if it were independent. We can visualize the dependence in the series for example by hand of the autocorrelation functions. Corresponding plots are shown in Figure C.8 let in Appendix C where we

see that temporal dependence is light, but present. Actually, estimates shown in Table 6.1 implicitly take this dependence into account.

POT

Dependence is not a big concern for GEV but it is more problematic for POT. Indeed, by analyzing only data that are above a threshold (say 30°C), serial dependence in the data can be strong and observations will have the tendency to occur in clusters. We wanted to illustrate this with Figure C.9 in Appendix C which highlights this dependence with red lines corresponding to the historic heat waves of summers 1911 and 1976 in Uccle. Indeed, observations lying on the red lines are serially correlated since they occurred during a same period of extreme heat. It is not difficult to think that *hot days are more likely to be followed by hot days*.

Moreover, we estimated the extremal index θ by the method of Ferro and Segers [2003] to have an idea on the extent of this extremal dependence. We obtained $\hat{\theta} \approx 0.42$ and hence, one interpretation is that the extremes are expected to cluster by groups of mean size $0.42^{-1} \approx 2.4$. We can visualize from Figure C.9 that the points have indeed some tendency to form groups of size around 2. The next step (not displayed here) is to decluster the series.

6.2 Parametric Nonstationary Analysis

As depicted in the introductory Figure 5.1, even the assumption of stationarity is likely to be poor for our data. Whereas the oscillatory behavior caught by the LOESS model is probably due to noise rather than a true characteristic of the underlying process, the increasing trend is more alarming. Indeed, our flexible modeling of the trend in Section 5.2.3 confirmed that the trend is statistically significant for two periods when doing pointwise comparisons but it is inadequate since we proved that this method lead to coverages that did not match with the assumed confidence level. When controlling for simultaneous tests, significance of the trend completely disappeared. However, one could argue that these intervals are very large (looking back at Figures 5.2 or 5.3) and thus not precise. Hence, results are not clear regarding this trend and a nonstationary GEV analysis is worth carrying on.

6.2.1 Comparing Different Models

Our first approach will use the deviance statistic by sequentially comparing nested models. The number of degrees of freedom (df) represent the number of parameters in the model (i.e., its complexity). The parametric models we will first compare are :

1. *Gumbel* : most simple EV-model with unrestricted domain and only 2 parameters as $\xi = 0$.
2. *stationary* : EV-Weibull model fitted in Table 6.1 by MLE.
3. *linear in $\mu(t)$* : allowing a nonstationary location parameter with $\mu(t) = \beta_0 + \beta_1 \cdot t$.
4. *quadratic in $\mu(t)$* : allowing a nonstationary location parameter with $\mu(t) = \beta_0 + \beta_1 \cdot t + \beta_2 \cdot t^2$.
5. *linear in $\mu(t)$ and $\sigma(t)$* : same as Model 3 for the location but with nonstationary scale $\sigma(t) = \exp(\alpha_0 + \alpha_1 \cdot t)$. The use of the inverse link $b(\cdot) = \exp(\cdot)$ is to ensure positivity of $\sigma \forall t$.

6. *cubic in $\mu(t)$* : nonstationary location parameter with $\mu(t) = \beta_0 + \beta_1 \cdot t + \beta_2 \cdot t^2 + \beta_3 \cdot t^3$. Note that computational singularities occurred for the likelihood computation of this model (or more complex ones). This came from a problem of solving the hessian to compute the covariance matrix of the parameters since there were too much linear dependencies in the hessian. We simply solved this by decreasing the tolerance, but this shows us that a linear model with so much polynomial terms is not recommended.

As explained in [Section 3.2](#), it is not recommended to model ξ as a smooth function of time. The p-values from the sequential pairwise comparisons have been computed with respect to the best retained model. Results are shown in Table [6.4](#).

Table 6.4: Comparisons of nested GEV models with nonstationary parameters. Significant p-values at level 5% are shown in bold.

Model	ℓ	df	p-value
Gumbel	-256.84	2	
stationary	-251.75	3	0.14%
linear in $\mu(t)$	-241.81	4	0.001%
quadratic in $\mu(t)$	-241.48	5	42%
linear in $\mu(t)$ and $\sigma(t)$	-241.69	5	63%
cubic in $\mu(t)$	-241.37	6	65%

The model that is chosen by this procedure in Table [6.4](#) is Model [3](#) which allows a linear model for the location parameter. The choice is clearly emphasized by likelihood ratio tests and hence we put confidence that a nonstationary GEV model with a linearly increasing trend from the location has strong supports. In the [next Section](#) we will allow for more flexibility in the model's parameters.

6.2.2 Selected Model, Diagnostics and Inference

Having selected the best model, we will now give the estimates of the new parameters before assessing the accuracy of this new model in order to provide reliable inferences through return levels.

Model

Table [6.5](#) shows the parameters and standard errors for the selected nonstationary GEV model estimated by MLE.

Table 6.5: MLE's of the nonstationary GEV parameters of Model [3](#) with a linear trend on $\mu(t) = \beta_0 + \beta_1 \cdot t$.

	Location β_0	Location β_1	Scale σ	Shape ξ
Estimates (s.e.)	29.13 (0.38)	0.0254 (0.005)	1.87(0.14)	-0.21 (0.06)

We remark that ξ is in the same range as previous stationary model. The parameter β_1 says that the location parameter $\mu(t)$ is expected to increase by 0.025 each year, starting at $\beta_0 = 29.13$ until $29.13 + 0.025 \cdot 116 = 32.07$ where 116 is the number of years of data. Extrapolation, say in year 2050 for example, would then lead to a distribution $\text{GEV}(32.93, 1.87, -0.21)$, other parameters being held constant.

Diagnostics

Section 3.2.1 showed how diagnostic tools such as quantile and probability plots can still be used in a nonstationary context, with some transformations, i.e. the observations must be standardized to have a Gumbel distribution. Results are shown in Figure 6.3 for the selected model.

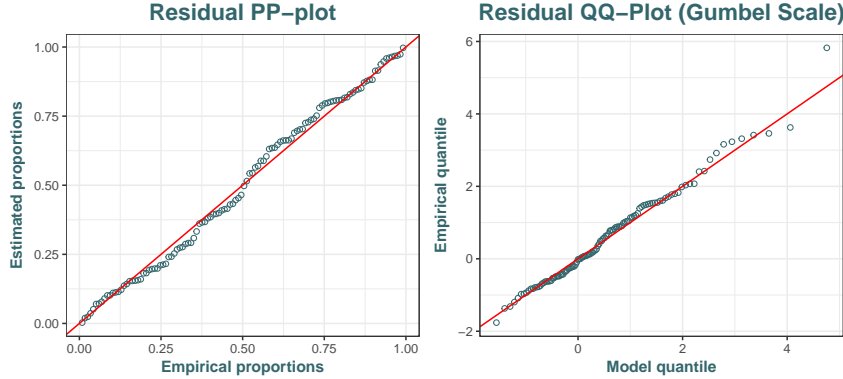


Figure 6.3: (left) Residual probability plot and (right) residual quantile plot on the Gumbel scale for the nonstationary GEV model allowing for a linear trend in the location parameter fitted by MLE.

We appreciate that the fit seems accurate. Note that problems for large quantiles in the residual QQ-plot is not problematic.

Return Levels

We will still use the return levels as our reference tool to make inference in EVT, even in presence of nonstationarity. Since the distribution will change every year (by a right shift of the location), the return levels will also change each years. Hence, we plot return levels against years by choosing a 10-year return period which corresponds to the 90% quantile of the fitted GEV distribution. This is shown in Figure 6.4.

We clearly see the linear pattern of the return levels with t explained by the linear model for $\mu(t)$. The x -axis has been carefully chosen to have the best interpretation. 36 years are in the range of data and then return levels are extrapolated from the model. The maximum prediction horizon of length 183 corresponds to the reach of 40°C for the 10-year return level.

Quite interestingly, we see that the fitted return level after $n = 116$ years where n is the number of data is 38.3°C which is actually quite higher than the maximum 36.6°C of the series. This return level means that, in year 2132, we will expect a maximum temperature of 38.3°C to be reached in a period of 10 years. Note that such far extrapolation, especially those right to the number of data (dotted red line), should be made with caution. Moreover, we can-

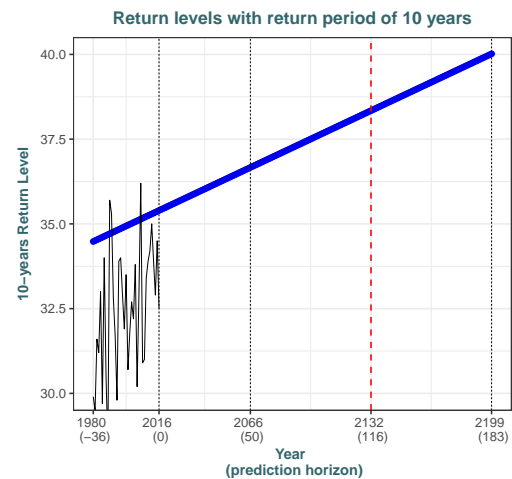


Figure 6.4: Return levels (in blue) of the nonstationary GEV model allowing linear trend on $\mu(t)$. Dotted red line represent horizon after $n = 116$ years and black lines represent the series [1980 – 2016].

not know in practice whether or not it is believable for the upward linear trend in annual maximum temperatures to continue to be valid beyond the range of data.

6.3 Improvements with Neural Networks

New advances in EVT allow to consider more flexible approaches allowing to consider much more models. Indeed, we have seen that a linear model in the location parameter is significant against the other parametric models of Table 6.4, but we did not consider enough models to be able to sustain this conclusion.

As discussed in Section 3.4, Neural Networks (NN) allow through a complex process to capture complex relationships between the input (time) and the outputs (the 3 GEV parameters). We will follow the approach of Cannon [2010] and its package GEVcdn using an extension of the multi layer perceptron, the GEV Conditional Density Network (GEV-CDN).

Model parameters are estimated from weights and biases via GML using a quasi-Newton BFGS optimization algorithm and appropriate relationships, i.e. refer to Figure 3.1 for the complete architecture. To avoid convergence to a shallow local minimum of the error surface, the algorithm is run 100 times with different initial values. The selected model is the one that minimizes an appropriate cost-complexity criteria (AIC_c or BIC). Different structures are tested with combinational cases of stationary and nonstationary parameters of the GEV distribution, or linear and nonlinear architecture of the CDN.

6.3.1 Models and Results

NN's are meant to approximate any functions with very good accuracy. It incorporates thus all the parametric models considered so far. We allowed the shape parameter ξ to vary with time in order to consider all possible models but even if this is not advised for EV models since it allows the form of the fitted distribution to change with time. Anyways, it will not change the final result.

From Figure 3.1 which represent the fully connected architecture, the hierarchy of models we will consider is, by ascending complexity :

1. Stationary GEV model as in Table 6.1, but now fitted by GML.
2. Nonstationary GEV model with linear trend on the location.
3. Nonstationary GEV model with linear trend on the location and the scale parameters.
4. Nonstationary GEV model allowing complete linear relationships for the location, scale and shape parameters.
- 5.-9. The preceding nonstationary models allowed linear relationships between time and the parameters since the activation function $m(\cdot)$ used to compute the hidden layer nodes (3.17) was the identity link. Now, since $m(\cdot)$ is a (logistic) sigmoid function, the relationships can be nonlinear. The degree of complexity of the nonlinear relationships, i.e. number of degrees of freedom of the model, is controlled by the number of hidden layers. We also implemented the hyperbolic tangent as activation function but it has not improved the results.

Models 2 to 4 allow thus **linear** relationships of the parameters with time while the following Models 5 to 9 can handle nonlinear relationships. We did not consider nonstationary models for the sole $\sigma(t)$ parameter as it would not correspond to the goal of this thesis, in the sense that allowing changes in scale but not in location would not be relevant.

We picked the recommended values of 6 and 9 for the parameters c_1 and c_2 (resp.) of the Beta prior (3.15) for ξ to compute the generalized likelihood (3.16). Moreover, Cannon [2010] recommended to use between 1 and maximum 3 hidden layers due to the relatively small sample size $n = 116$ and the danger to quickly overfit. Table 6.6 displays the results for maximum 2 hidden layers.

Table 6.6: Comparisons of nonstationary GEV-CDN models fitted by GML. Linear models have the identity activation function and the nonlinear models have the logistic sigmoid activation function.

	model	AIC _c	BIC	hidden	df
Linear	stationary	-19.6	-11.5	0	3
	$\mu(t)$	-37.4	-26.7	0	4
	$\mu(t), \sigma(t)$	-35.4	-22.2	0	5
	$\mu(t), \sigma(t), \xi(t)$	-34.2	-18.4	0	6
Nonlinear	$\mu(t)$	-35.4	-19.6	1	6
	$\mu(t), \sigma(t)$	-36.2	-17.9	1	7
	$\mu(t), \sigma(t), \xi(t)$	-34	-13.3	1	8
	$\mu(t)$	-37.4	-14.3	2	9
	$\mu(t), \sigma(t)$	-32.5	-4.7	2	11
	$\mu(t), \sigma(t), \xi(t)$	-38.4	3.9	2	13

Relying on the BIC, this Table 6.6 actually emphasizes the finding of Table 6.4. This criterion is justified because the AIC_c does not penalize enough complex models and we want a parsimonious model since NN models are likely to overfit. Indeed, the AIC_c selected the most complex model, with 2 hidden layers and 13 df. Moreover, likelihood ratio tests always chose Model 2 ; and with p-value = 10^{-4} when compared with the complex model chose by AIC_c.

For Model 2 selected by BIC, Table 6.7 shows the parameters estimated by GML from the estimation of the weights $w^{(1)}$ and $w^{(2)}$ with (3.17)-(3.18).

Table 6.7: Estimation by GML of the nonstationary parameters from the GEV-CDN Model 2 allowing a linear trend on the location $\mu(t) = \beta_0 + \beta_1 \cdot t$.

	Location β_0	Location β_1	Scale σ	Shape ξ
Estimates	29.11	0.0253	1.84	-0.185

We remark that Table 6.5 lead to very similar results. Small differences are actually due to the method of estimation since we used GML here while the parametric nonstationary analysis in Table 6.5 used ML. Scale and shape parameters are of the same order of magnitude, and the same conclusions can be drawn since we used the identity activation function with no hidden layers. Whereas this model does not actually use the power of NN's, the advantage of this model is its ease of use. Nonlinear relationships retrieved from hidden layers are indeed difficult to interpret. Some quantiles of the model are shown on the left plot of the following Figure 6.5.

6.3.2 Bagging

A solution presented in [Section 3.4.3](#) to prevent overfitting is *bagging*. Since the linear model is not complex enough to require bagging, and the support for the linear model was not straightforward when looking for example at the AIC_c , we will now allow for nonlinearities that will be smoothly handled by the bagging process. From [Table 6.6](#), we chose 2 hidden layers to keep the model relatively simple, and we only allowed the location and scale parameters to vary with time for the same reasons as above.

We made use of parallel computing through the `foreach` and `doParallel` framework since this method is computationally intensive and it is important to have a reliable number M of bootstrap resamples for the method to be effective. It decreased computation time by a factor of ≈ 2.5 and allowed us to have $M = 1000$ resamples in only ≈ 158 seconds². We tried to estimate the parameters in [Table C.2 in Appendix C](#).

From the nonlinear relationships introduced in the model, it was actually not possible to estimate accurately the parameters $\mu(t)$ and $\sigma(t)$. Sensitivity analysis methods such as proposed by [Cannon and McKendry \[2002\]](#) are recommended to yield more accurate estimates of the parameters. We remark that, the scale parameter is (slightly) but constantly decreasing with time, while we expected that the climate warming would actually lead to more variable extremes.

Results of the generated quantiles are shown on the right plot of [Figure 6.5](#). We also made available in [Figure C.10 in Appendix C](#) a graph which gathers results that could help to better visualize differences in quantiles.

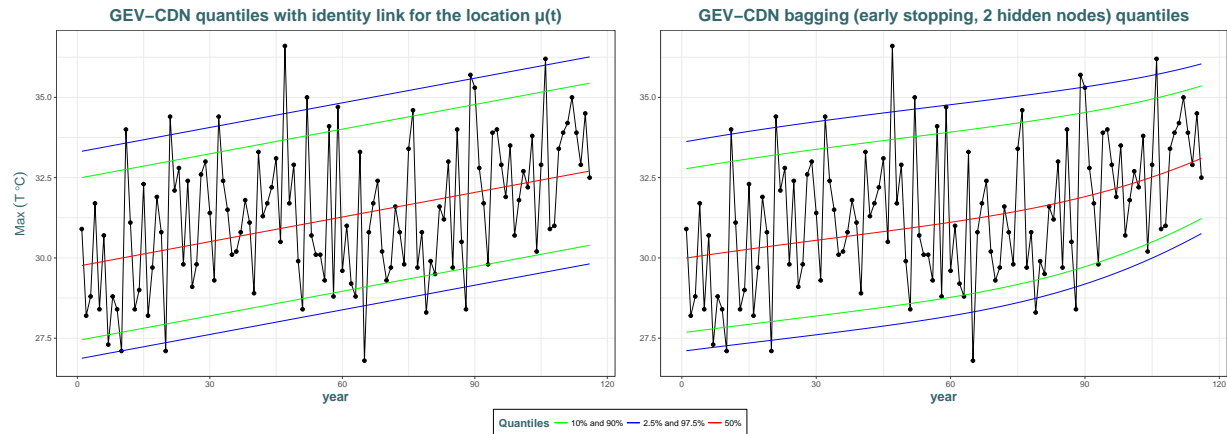


Figure 6.5: (Left) observations with quantiles from Model 2 estimated in [Table 6.5](#). (Right) observations with same quantiles coming from the nonstationary and nonlinear bootstrap aggregated model with $M = 1000$ resamples. Note that in a stationary context, the 50%, 90% and 95% quantiles represent return levels with return periods of 2, 10 and 20 years respectively.

From [Figure 6.5](#) we can clearly see the introduced nonlinear relationships in the two parameters $\mu(t)$ and $\sigma(t)$ with time from the two hidden layers. Compared with the left plot where the nonstationary link is linear and in $\mu(t)$ only, it seems that the ensemble model leads to an accelerate increasing rate at the end of the series, especially for low quantiles. It seems appropriate since the warming seems actually to accelerate for this period, and it fits with the findings of [Section 5.2.3](#). More formal comparisons could be made, for example [Cannon \[2010\]](#) compared predicted quantiles of the model with the empirical

²All computations are made on a i7-7700HQ 2.8GHz 20gb ddr4.

quantiles and computed the root mean squared error.

Note that the displayed values of the quantiles that are different for each year and represent return levels, can also be seen as confidence intervals, similar to credible intervals seen in the Bayesian paradigm in [Section 4.6.1](#).

In order to reduce the risk of overfitting, a technique that is commonly used is *weight penalty regularization*. In the GEVcdn framework, it works by controlling the variance σ_w^2 of a gaussian prior on the weights. Ideally, this value should be controlled by cross validation. It means that we have to find the value of σ_w that provide the best fit relying some criterion but this method rules out the use of the selection criterion such as BIC or AIC_c since the effective number of model parameters will no longer be equal to the number of weights in the GEV CDN model. We chose $\sigma_w = 2$ to limit the risk of overfitting. At the limit when σ_w goes to zero, we checked that results are the same as for nonstationary GEV-CDN in location with no hidden layers, i.e. left plot of Figure [6.5](#).

Finish the shiny application !!!!

6.3.3 Inference : Confidence intervals by Bootstrap

Bootstrap is an effective technique to compute quantile-based confidence intervals when we cannot rely on approximations. As for bagging, we did the computations in parallel. We took $B = 1000$ resamples in only 74 seconds for the residual bootstrap method. We used the residual bootstrap as presented [Section 3.4.4](#) since it is the method recommended by [Kharin and Zwiers \[2005\]](#). The results are shown in Figure [6.6](#) for all three GEV parameters. Left plots come from the 2.5% and 97.5% quantiles of Model [2](#) (Table [6.7](#)) and right plots are for the bagged nonlinear GEV-CDN model considered in the previous section (Table [C.2](#)).

These models have been chosen from previous sections. We did not extrapolate beyond the range of data. We compared results with the parametric bootstrap from Figure [C.11](#) let in [Appendix C](#) but we remark no significant differences. Graphs of the differences between two methods (i.e. residuals) does not yield additional concerns and are thus left at the end of `2NeuralsNets.R`. We think a coverage analysis is thus not relevant.

We clearly remark the flexibility introduced in the location and scale parameters intervals with the incorporated hidden layers. Stationary parameters have constant confidence lines as expected. Regarding the shape parameter ξ , we see that the value of 0 is near to be outside the EV-Weibull type for the complex model. Moreover, we remark this interval is quite wider with this model, but it is also the case for other parameters. We also note the decreasing behavior of the intervals for the scale parameters. This explains, to a certain extent, the decreasing quantiles intervals widths at the end of the series of right plot of Figure [6.5](#).

6.4 Comments and Comparisons with POT

During all this chapter, we considered time as the sole covariate. We recall that quite other covariates could have been included to improve the nonstationary analysis. To name a few : *Southern Oscillation Index* (a proxy for El Niño), the CO₂ concentration, etc. Most of these are time-dependent.

There are plenty of ways to analyze and we considered some of them. Moreover, sometimes our choices were subjective and thus in some ways debatable and this is the reason why we wanted to

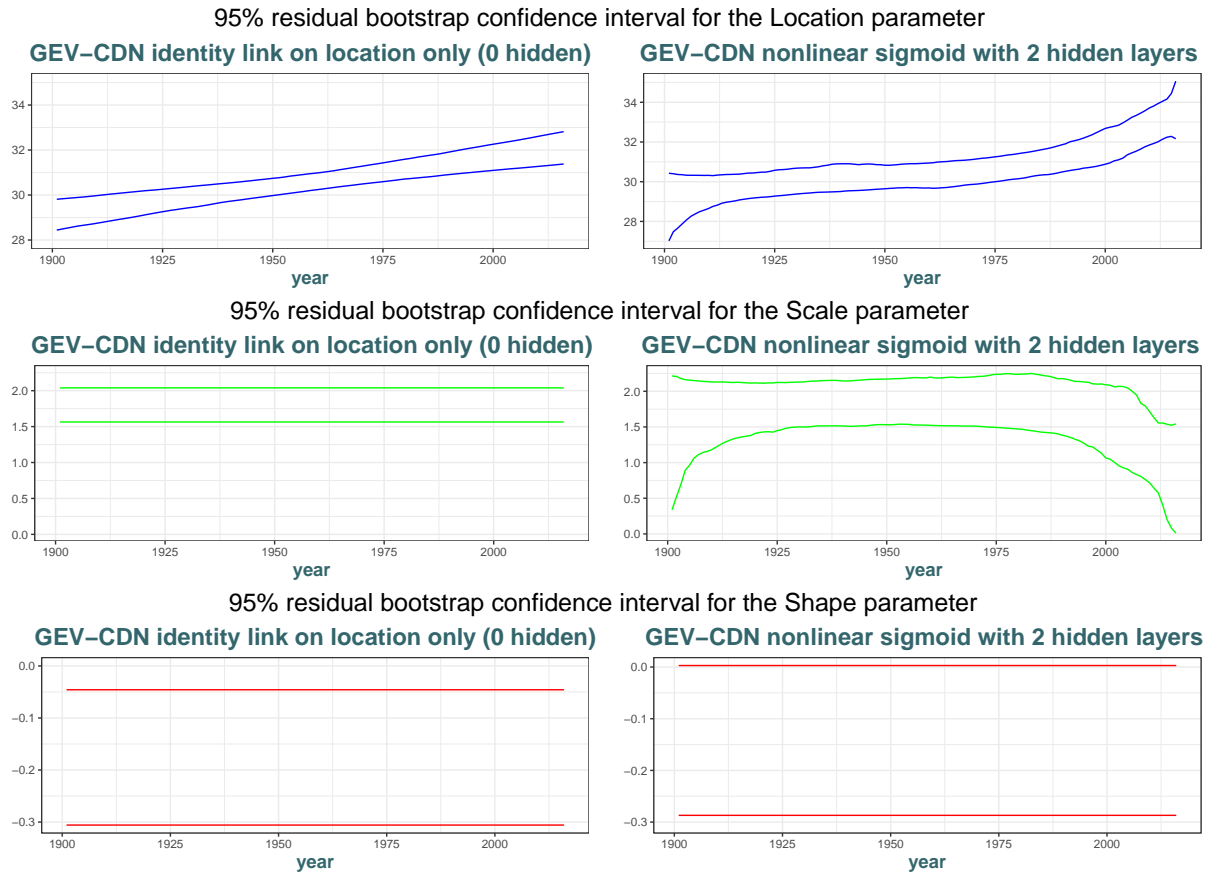


Figure 6.6: Residual bootstrap 95% intervals computed with the GEV-CDN model allow a linear nonstationary location parameter only (left), and for the nonlinear nonstationary model in location and scale parameters only with 2 hidden layers (right).

provide the user automated methods to easily redo analysis and visualize the effects of changing some of the (hyper)parameters.

The other approach we have seen is in [Chapter 2](#) is the POT and results were consistent with GEV for the EVI ξ in the stationary and nonstationary analysis. For the nonstationary analysis, we considered for example varying thresholds and seasonal models. A few results of nonstationary analysis in a POT approach are presented in Section 4.1 of the `Summary1_intro.html` file in the `/vignettes` folder of the [repository](#). Threshold selection were quite an issue.

CHAPTER 7

BAYESIAN ANALYSIS IN BLOCK MAXIMA

Contents

Note on the available R package : <code>evdbayes</code>	77
7.1 From Our Functions (R package)	77
7.2 From HMC algorithm using STAN language	77
7.3 Ratio of Uniform : <code>revdbayes</code> package	77
7.4 Comparisons	77
7.4.1 STAN	77
7.5 Comparison with frequentists results	78

This analysis relies on all the codes which filenames start by "Bayes" from the /**Scripts-R**/ folder of the [repository](#). All the functions created that are used and are also made available through the package are in /R/BayesFunc.R. Moreover, the /vignettes/Summary_Bayesian.html file in the [repository](#) present a big part of the analysis in details.

"It is often the case that more than one model provides an adequate fit to the data. Sensitivity analysis determines by what extent posterior inferences change when alternative models are used" book risk analysis other section pp.2.

"The basic method of sensitivity analysis is to fit several models to the same problem. Posterior inferences from each model can then be compared."

Note on the available R package : **evdbayes**

The **evdbayes** is the only package available on CRAN for (see Ribatet [2006]) which is a very old package. We had problems to understand both its structure and the famous "black-box" It only use the Metropolis Hastings algorithm.

Note that efforts should put to the new **revdbayes** R package which use the ratio-of-uniforms method is an other acceptance-rejection type of simulation algorithm. ([Section 7.3](#)

7.1 From Our Functions (R package)

7.2 From HMC algorithm using STAN language

The problem is maybe from [1.6.1](#). The parameter ξ is relatively near the region that could be problematic, causing convergence issues.

7.3 Ratio of Uniform : **revdbayes** package

<https://cran.r-project.org/web/packages/revdbayes/vignettes/revdbayes-vignette.html>

From the **revdbayes**

Helped with **rust**

7.4 Comparisons

Hartmann and Ehlers [2016] We can calculate the effective sample size (ESS) using the posterior samples for each parameter :

$$\text{ESS} = N \cdot (1 + 2 \sum_k \gamma(k))^{-1} \quad (7.1)$$

where N is still the number of posterior samples and $\gamma(k)$ are the monotone lag k sample autocorrelations. ?. We can thus interpret this as the number of effectively independent samples.

7.4.1 STAN

Benefits :

- Allows more flexibility (?) through the mathematical formulation of the formula
- It is really smoother and clearer (straightforward) for this kind of problems

Drawbacks :

- New language with all the problems/errors arising when learning it.

7.5 Comparison with frequentists results

In this first analysis, we rely on

Conclusion

During this thesis, we have statistically assessed the presence of a trend in the extreme temperatures in Uccle. We first detected that the trend is significative by the method of linear regression. We also discovered that the best fitted GEV model is the one with a linear trend in the location parameter.

"A key issue in applications is that inferences may be required well beyond the observed tail of the data, and so an assumption of stability is required." [Davison et al. \[2012\]](#)

"Another approach would be to use something other than time as the covariate in the model. For instance, one could imagine linking temperature data directly to CO₂ level rather than time. However, linking to a climatological covariate makes extrapolation into the future more difficult, as one would need to extrapolate the covariate as well. No obvious climatological covariate comes to mind for the Red River application."

Timescale-uncertainty effects on extreme value analyses seem not to have been studied yet. For stationary models (Sect. 6.2), we anticipate sizable effects on block extremes—GEV estimates only when the uncertainties distort strongly the blocking procedure. For nonstationary models (Sect. 6.3), one may augment confidence band construction by inserting a timescale simulation step (after Step 4 in Algorithm 6.1) [Mudelsee \[2014, pp.262\]](#)

!!!! not put too much references in the text !!!!

A project to give analysis in time live could be implemented, with values being stocked each days/year !

be prudent that all "methods" are listed (numbered) in (each) ToC

add square brackets [] for cite ?

Careful for boldsymbol, especially in bayesian

PissoortThesis:: Behind our functions

[MOTS DEXPLICATIONS SUR TTES LES FORMULES (domain attraction condition, etc...)]

Finish (Bayesian) documentation in the package.

See new graphs for stats desc. (in appendix), from workshop exam.

Create Gif animations for the github readme

Appendix

APPENDIX A

STATISTICAL TOOLS FOR EXTREME VALUE THEORY

A.1 Tails of the distributions

Heavy-tailed

Definition A.1 (Heavy-tails). *The distribution of a random variable X with distribution function F is said to have a heavy right tail if*

$$\lim_{n \rightarrow \infty} e^{\lambda x} \Pr\{X > x\} = \lim_{n \rightarrow \infty} e^{\lambda x} \bar{F}(x) = \infty, \quad \forall \lambda > 0. \quad (\text{A.1})$$

△

More generally, we can say that a random variable X has heavy tails if $\Pr\{|X| > x\} \rightarrow 0$ at a polynomial rate. In this case, note that some of the moments will be undefined.

Definition A.2 (Fat-tails). *The distribution of a random variable X is said to have a fat tail if*

$$\lim_{x \rightarrow \infty} \Pr\{X > x\} = x^{-\alpha}. \quad (\text{A.2})$$

△

Definition A.3 (Long-tails). *The distribution of a random variable X with distribution function F is said to have a long right tail if $\forall t > 0$,*

$$\lim_{x \rightarrow \infty} \Pr\{X > x + t | X > x\} = 1 \Leftrightarrow \bar{F}(x + t) \sim \bar{F}(x) \quad \text{as } x \rightarrow \infty. \quad (\text{A.3})$$

△

Definition A.4 (Light-tails). *Conversely, we say that X has light tails or exponential tails if its tails decay at an exponential rate, i.e.*

$$\lim_{x \rightarrow \infty} \Pr\{|X| > x\} = e^{-x} \quad (\text{A.4})$$

△

An intuitive example of a distribution with exponential tails such as the exponential distribution.

A.2 Convergence concepts

Convergence in distribution

Definition A.5 (Convergence in distribution). *We say that a sequence X_n with df F_n converges in distribution to X with df F , if*

$$F_n(x) := \Pr\{X_n \leq x\} \longrightarrow \Pr\{X \leq x\} := F(x), \quad (\text{A.5})$$

at all continuity points of F . \triangle

It means that, for large n , $\Pr\{X_n \leq t\} \approx \Pr\{X \leq t\}$. We denote this by $X_n \xrightarrow{d} X$.

Convergence in probability

Definition A.6 (Convergence in probability). *We say that a sequence X_n converges to X in probability if, $\forall \epsilon > 0$,*

$$\Pr\{|X_n - X| > \epsilon\} \rightarrow 0, \quad n \rightarrow \infty. \quad (\text{A.6})$$

\triangle

Hence, it means that the probability of the difference between X_n and X goes to 0 as n is large. We denote this by $X_n \xrightarrow{P} X$.

An example of application of this convergence is the *Weak Law of Large Numbers*.

Theorem A.1. [Weak Law of Large Numbers] *Let a sequence of R.V. $\{X_i\}_{i,i}$ be defined of the same probability space with mean μ and variance $\sigma^2 < \infty$. Then, we know that the difference between \bar{X}_n and μ will go to 0 in probability, i.e. $\bar{X}_n \xrightarrow{P} \mu$.* \square

But this law actually makes a stronger convergence, following [Kolmogorov et al. \[1956\]](#), that is an *almost sure convergence*

Almost Sure Convergence

This is the type of stochastic convergence that is most similar to pointwise convergence known from elementary real analysis.

Definition A.7 (Almost Sure convergence). *We say that a sequence of random variables X_n converges almost surely (or with probability one) to X if*

$$\Pr\{X_n = X\} = 1, \quad n \rightarrow \infty. \quad (\text{A.7})$$

\triangle

We can denote this by $X_n \xrightarrow{\text{a.s.}} X$. This means that the values of X_n approach the value of X , in the sense that events for which X_n does not converge to X have probability 0.

Well other forms of convergence do exist, but these ones are the most important in regard to EVT. However, the reader may refer e.g. to ? for more in-depth results.

A.3 Varying functions

Definition A.8 (Regularly varying function). *Let's consider the survival \bar{F} . We say that this survival function \bar{F} is **regularly varying** with index $-\alpha$ if*

$$\lim_{x \rightarrow \infty} \frac{\bar{F}(xt)}{\bar{F}(x)} = t^{-\alpha}, \quad t > 0. \quad (\text{A.8})$$

We write it $\bar{F} \in R_{-\alpha}$.

△

Definition A.9 (Slowly varying function). *We say that a function f is **slowly varying** with index $-\alpha$ if*

$$\lim_{x \rightarrow \infty} \frac{f(tx)}{f(x)} = 1, \quad t > 0. \quad (\text{A.9})$$

△

We remark that a slowly varying function is a regularly varying function with index 0.

A.4 Diagnostic Plots : Quantile and Probability Plots

From [Beirlant et al. \[1996\]](#), pp.18-36], together with the nice view of [Coles \[2001\]](#), pp.36-37], we present two major diagnostic tools which aim at assessing the fit of a particular model (or distribution) against the real distribution coming from the data used to construct the model. These are called the *quantile-quantile* plot (or *qq*-plot) and the *probability* plot (or *pp*-plot).

These diagnostics are popular by their easy interpretation and by the fact that they can both have graphical (i.e. subjective, qualitative, quick) view but also a more precise (i.e. objective, quantitative, rigorous) analysis can be derived, for example from the theory of linear regression.

For these two diagnostic tools, we use the order statistics as seen (1.1) but now we rather consider an **ordered sample** of independent **observations** :

$$x_{(1)} \leq x_{(2)} \leq \cdots \leq x_{(n)} \quad (\text{A.10})$$

coming from a population from which we fit the estimated model (distribution) \hat{F} and where $x_{(1)}$ (resp. $x_{(n)}$) is thus the minimum (resp. maximum) observation in the sample. We also define the **empirical distribution function**

$$\tilde{F}(x) = \frac{i}{n+1}, \quad x_{(i)} \leq x \leq x_{(i+1)}. \quad (\text{A.11})$$

\tilde{F} is an estimate of the true distribution F and hence, by comparing \hat{F} and \tilde{F} , it will help us to know if the fitted model \hat{F} is reasonable for the data.

Quantile plot

Given a ordered sample as in (A.10), a *qq*-plot consists of the locus of points

$$\left\{ \left(\hat{F}^{\leftarrow} \left(\frac{i}{n+1} \right), x_{(i)} \right) : i = 1, \dots, n \right\}. \quad (\text{A.12})$$

This graph compares the ordered quantiles $\hat{F}^{\leftarrow} \left(\frac{i}{n+1} \right)$ of the fitted model \hat{F} against the ordered observed quantiles, i.e. the ordered sample from (A.10). We used the continuity correction $\frac{i}{n+1}$ to prevent problems at the borders. Note that a disadvantage of Q-Q plots is that the shape of the selected parametric distribution is no longer visible [Beirlant et al. \[2006, pp.63\]](#)

Probability plot

Given the same sample in (A.10), a *probability plot* consists of the locus of points

$$\left\{ \left(\hat{F}(x_{(i)}), \frac{i}{n+1} \right) : i = 1, \dots, n \right\}. \quad (\text{A.13})$$

This graph compares the estimated probability of the ordered values $x_{(i)}$, thus from the fitted model \hat{F} , against the probability coming from the empirical distribution as in (A.11).

From these two graphical diagnostic tools, the interpretation is the same and we will consider that \hat{F} fits well the data if the plot looks linear, i.e. the points of the plots lie close to the unit diagonal.

Besides the fact that the probability and the quantile plots contain the same information, they are expressed in a different scale. That is, after changing the scale to probabilities or quantiles (with probability or quantile transforms), one can gain a better perception and both visualizations can sometimes lead contradictory conclusions, especially in the graphical inspection. Using both is thus preferable to make our model's diagnostic more robust.

A.5 Estimators Based on Extreme Order Statistics for EVI

The following estimators allow to estimate the EVI ξ .

Pickands estimator

First introduced by [Pickands \[1975\]](#), this method can be applied $\forall \xi \in \mathbb{R}$ to give

$$\hat{\xi}_k^P = \frac{1}{\ln 2} \ln \left(\frac{X_{n-\lceil k/4 \rceil + 1, n} - X_{n-\lceil k/2 \rceil + 1, n}}{X_{n-\lceil k/2 \rceil + 1, n} - X_{n-k+1, n}} \right), \quad (\text{A.14})$$

where we recall that $\lceil x \rceil$ denotes the integer (ceil) part of x .

A condition for the consistency of this estimator is that k must be chosen such that $k/n \rightarrow 0$ as $n \rightarrow \infty$. This condition will hold for the following estimators based on order statistics.

A problem with this intuitive estimator is that its asymptotic variance is very large (see e.g. [Dekkers and Haan \[1989\]](#)) and depends highly on the value of k . To improve this, we can quote the estimator of [Segers \[2001\]](#) which is globally more efficient.

The following estimators are only valid for $\xi > 0$. In general in EVT, this condition should hold

(rainfall data, finance, risk analysis,...) but in our application we know that ξ is likely to be negative and hence, the following estimators cannot be used.

Hill estimator

This is probably the most simple EVI estimator thanks to the intuition behind its construction. There exists plenty of interpretations to construct it (see e.g. [Beirlant et al. \[2006\]](#), pp.101-104]). It is defined as

$$\xi_k^H = k^{-1} \sum_{i=1}^k \ln X_{n-i+1,n} - \ln X_{n-k,n}, \quad k \in \{1, \dots, n-1\}. \quad (\text{A.15})$$

Following e.g. [de Haan and Resnick \[1998\]](#), this estimator is consistent under certain conditions. Besides that, this estimator has several problems :

- instability with respect to the choise of k .
- Severe bias due to the heavy-tails of the distribution and thus the slowly varying component which influences negatively.
- Inadequacy with shifted data.

Hence, this estimator should be carefully used.

Moment estimator

Introduced by [Dekkers et al. \[1989\]](#), this estimator is a direct generalization of the Hill estimator presented above. It is defined as

$$\hat{\xi}_k^M = \hat{\xi}_k^H + 1 - \frac{1}{2} \left(1 - \frac{(\hat{\xi}_k^H)^2}{\hat{\xi}_k^{H(2)}} \right)^{-1}, \quad (\text{A.16})$$

where

$$\hat{\xi}_k^{H(2)} = k^{-1} \sum_{i=1}^k (\ln X_{n-i+1,n} - \ln X_{n-k,n})^2.$$

This estimator is also consistent.

APPENDIX B

BAYESIAN METHODS

B.1 Algorithms

B.1.1 Metropolis–Hastings Algorithm

The *Metropolis–Hastings* algorithm is one of the first and of the pioneering algorithm discovered by [Hastings \[1970\]](#) to compute MCMC for Bayesian analysis.

Algorithm 1: The Metropolis–Hastings Algorithm

1. Pick a starting point θ_0 and fix some number N of simulations.

2. **For** $t = 1, \dots, N$ **do**

(a) Sample proposal θ_* from a proposal density $p_t(\theta_* | \theta_{t-1})$,

(b) Compute the ratio

$$r = \frac{\pi(\theta_* | \mathbf{x}) \cdot p_t(\theta_{t-1} | \theta_*)}{\pi(\theta_{t-1} | \mathbf{x}) \cdot p_t(\theta_* | \theta_{t-1})} = \frac{\pi(\theta_*) \cdot \pi(\mathbf{x} | \theta_*) \cdot p_t(\theta_{t-1} | \theta_*)}{\pi(\theta_{t-1}) \cdot \pi(\mathbf{x} | \theta_{t-1}) \cdot p_t(\theta_* | \theta_{t-1})}.$$

(c) Set

$$\theta_t = \begin{cases} \theta_* & \text{with probability } \alpha = \min(r, 1); \\ \theta_{t-1} & \text{otherwise.} \end{cases}$$

This algorithm remains valid when π is only proportional to a target density function and thus it can be used to approximate [4.1](#).

Note that the proposal density is often chosen to be symmetric so that we will just sample under a "simple Metropolis" algorithm where r is thus simplified to be only the ratio of the posterior densities, $r = \frac{\pi(\theta_* | \mathbf{x})}{\pi(\theta_{t-1} | \mathbf{x})}$.

We can shortly summarize the *pros* and *cons* this algorithm :

- *PROS* : Very easy to program and works even for relatively complex densities.
- *CONS* : Can be very inefficient, in the sense that it will require lots of iterations before the stationary target distribution will be reached. This requires some tuning to the algorithm through

B.1.2 Gibbs Sampler

The *Gibbs Sampler* can be seen as a special case of the Metropolis-Hastings algorithm. Suppose our parameter vector θ can be divided into d subvectors $(\theta_1, \dots, \theta_d)$, and let's say in our case that each of these "subvectors" represent a single parameter, thus typically one of the three (μ, σ, ξ) , for the simplest case so that $d = 3$ in this model. At each $t = 1, \dots, N$, the Gibbs sampler samples the subvectors $\theta_t^{(j)}$ conditional on both the data \mathbf{x} and the remaining subvectors $\theta_{t-1}^{(-j)}$ at their current values. Therefore, we have $\theta_{t-1}^{(-j)} = (\theta_t^{(1)}, \dots, \theta_t^{(j-1)}, \theta_{t-1}^{(j+1)}, \dots, \theta_{t-1}^{(d)})$ and each $\theta_t^{(j)}$ is sampled from $\pi(\theta^{(j)} | \theta_{t-1}^{(-j)}, \mathbf{x})$.

Algorithm 2: PSEUDOCODE of the Gibbs Sampler

1. Pick a starting point θ_0 and fix some number N of simulations.

2. **For** $t = 1, \dots, N$ **do**
For $j = 1, \dots, d$ **do**

- (a) Sample proposal θ_* from a proposal density $p_{t,j}(\theta_*^{(j)} | \theta_{t-1}^{(j)})$,
- (b) Compute the ratio

$$\begin{aligned} r &= \frac{\pi(\theta_*^{(j)} | \theta_{t-1}^{(-j)}, \mathbf{x}) \cdot p_{t,j}(\theta_{t-1}^{(j)} | \theta_*^{(j)})}{\pi(\theta_{t-1}^{(j)} | \theta_{t-1}^{(-j)}, \mathbf{x}) \cdot p_{t,j}(\theta_*^{(j)} | \theta_{t-1}^{(j)})} \\ &= \frac{\pi(\theta_t^{(1)}, \dots, \theta_t^{(j-1)}, \theta_*^{(j)}, \theta_{t-1}^{(j+1)}, \dots, \theta_{t-1}^{(d)} | \mathbf{x}) \cdot p_{t,j}(\theta_{t-1}^{(j)} | \theta_*^{(j)})}{\pi(\theta_t^{(1)}, \dots, \theta_t^{(j-1)}, \theta_{t-1}^{(j)}, \theta_{t-1}^{(j+1)}, \dots, \theta_{t-1}^{(d)} | \mathbf{x}) \cdot p_{t,j}(\theta_*^{(j)} | \theta_{t-1}^{(j)})}, \end{aligned}$$

(c) Set

$$\theta_t^{(j)} = \begin{cases} \theta_*^{(j)} & \text{with probability } \alpha = \min(r, 1); \\ \theta_{t-1}^{(j)} & \text{otherwise.} \end{cases}$$

(better signs for conditional bar "|" !!!!!!!

This algorithm depends on being able to simulate from $\pi(\theta^{(j)} | \theta_{t-1}^{(-j)}, \mathbf{x})$ which is often impossible. However, one can use Metropolis-Hastings to $\pi(\theta^{(j)} | \theta_{t-1}^{(-j)}, \mathbf{x})$, giving the above.

A special case arise if one can simulate directly so that $r = 1$, i.e. we take $p_{t,j}(\theta_*^{(j)} | \theta_{t-1}^{(j)}) = \pi(\theta_*^{(j)} | \theta_{t-1}^{(-j)}, \mathbf{x})$. (The proposal $p_{t,j}(\cdot)$ is also often symmetric, i.e. $p_{t,j}(\theta_*^{(j)} | \theta_{t-1}^{(j)}) = p_{t,j}(\theta_{t-1}^{(j)} | \theta_*^{(j)})$. But it cannot be simplified in the equation.)

It is important for our tasks to tune the average probability of acceptance to be roughly between 0.4 and 0.5 (see e.g. [Gelman et al. \[2013, chapter 11\]](#)) so that the so-generated markov-chain has desirable properties. This is done by setting the standard deviation $\sigma(j)$ of the univariate normal distribution taken for $p_{t,j}(\theta_*^{(j)} | \theta_{t-1}^{(j)})$. Whereas our $\theta^{(j)}$ are (often?) univariate, it is difficult to set each $\sigma^{(j)}$ to achieve average acceptance probabilities for all parameters. We will then use a trial-and-error approach.

Note also the increase of complexity with this sampler compared to the Metropolis-Hastings, where the nested loop implies that there are d iterations with each simulation.

pros and cons :

- *PROS* : Easy to program and, for some problems, it can also be very efficient. It is a pleasant way to split multidimensional problems into simpler (typically univariate) densities.
- *CONS* : Sometimes hard to compute analytically the conditional distributions. Not all densities can be split into pleasant conditionals equations.

Metropolis-within-Gibbs?

B.1.3 Hamiltonian Monte Carlo

<http://deeplearning.net/tutorial/hmc.html#hmc>

A difficulty we have faced and that we would like to point out for GEV models is (see p.316-317 STAN manual) t

"Most of the computation [in Stan] is done using Hamiltonian Monte Carlo. HMC requires some tuning, so Matt Hoffman up and wrote a new algorithm, Nuts (the "No-U-Turn Sampler") which optimizes HMC adaptively. In many settings, Nuts is actually more computationally efficient than the optimal static HMC! "

The *Hamiltonian Monte Carlo* (HMC)

"The Hamiltonian Monte Carlo algorithm starts at a specified initial set of parameters theta; in Stan, this value is either user-specified or generated randomly. Then, for a given number of iterations, a new momentum vector is sampled and the current value of the parameter θ is updated using the leapfrog integrator with discretization time and number of steps L according to the Hamiltonian dynamics. Then a Metropolis acceptance step is applied, and a decision is made whether to update to the new state (theta*; rho*) or keep the existing state" ?

? have demonstrated in similar application that HMC (and Riemann manifold HMC) are much more computationally efficient than traditional MCMC algorithms such as MH.

Definition B.1 (Total energy of a closed system : Hamiltonian function). *For a certain particle; Let $\pi(\theta)$ be the posterior distribution and let $\mathbf{p} \in \mathbb{R}^d$ denote a vector of auxiliary parameters independent of θ and distributed as $\mathbf{p} \sim N(\mathbf{0}, \mathbf{M})$. We can interpret θ as the position of the particle and $-\log \pi(\theta|\mathbf{x})$ describes its potential energy while \mathbf{p} is the momentum with kinetic energy $\mathbf{p}' \mathbf{M}^{-1} \mathbf{p} \cdot 2^{-1}$. Then the total energy of a closed system is the Hamiltonian function*

$$\mathcal{H}(\theta, \mathbf{p}) = -\mathcal{L}(\theta) + \mathbf{p}' \mathbf{M}^{-1} \mathbf{p} \cdot 2^{-1}, \quad \text{where } \mathcal{L}(\theta) = \log \pi(\theta). \quad (\text{B.1})$$

△

We define $\mathcal{X} = (\theta, \mathbf{p})$ as the *combined state* of the particle.

The unnormalized joint density of (θ, \mathbf{p}) is

$$f(\theta, \mathbf{p}) \propto \pi(\theta) \cdot \exp\{-\mathbf{p}' \mathbf{M}^{-1} \mathbf{p} \cdot 2^{-1}\} \propto \exp\{-\mathcal{H}(\theta, \mathbf{p})\}. \quad (\text{B.2})$$

Following Hartmann and Ehlers [2016], the idea is to use the Hamiltonian dynamics equations (not shown here for..) to model the evolution of a particle that keep the total energy constant. Introducing the auxiliary variables \mathbf{p} and using the gradients (..) will lead to a more efficient exploration of the parameter space

These differential equations cannot be solved so numerical integrators are required, for instance the "Störmer-Verlet" from ? which will introduce discretization. A MH step is then required to correct the error and ensure convergence. The new proposal $\mathcal{X}_* = (\theta_*, \mathbf{p}_*)$ will be accepted with probability

$$\alpha(\mathcal{X}, \mathcal{X}_*) = \min \left[\frac{f(\theta_*, \mathbf{p}_*)}{f(\theta, \mathbf{p})}, 1 \right] = \min \left[\exp \{ \mathcal{H}(\theta, \mathbf{p}) - \mathcal{H}(\theta_*, \mathbf{p}_*) \}, 1 \right]. \quad (\text{B.3})$$

As \mathbf{M} is symmetric positie definite, $\mathbf{M} = m\mathbf{I}_d$. Then we can summarize the [HMC algorithm](#) in the following, in its 'simplest' form :

marie est la best : $Moyenne = \frac{1}{n} \sum_{i=1}^n X_i$

Algorithm 3: The Hamiltonian Monte Carlo algorithm

1. Pick a starting point θ_0 and set $i = 1$.
 2. **Until** convergence has been reached **do**
 - (a) Sample $\mathbf{p}_* \sim N_d(\mathbf{0}, \mathbf{I}_d)$ and $u \sim U(0, 1)$,
 - (b) Set $(\theta_I, \mathbf{p}_I) = (\theta_{i-1}, \mathbf{p}_*)$ and $\mathcal{H}_0 = \mathcal{H}(\theta_I, \mathbf{p}_I)$,
 - (c) **repeat** L times
 - ▷ $\mathbf{p}_* = \mathbf{p}_* + \frac{\epsilon}{2} \nabla_{\theta} \mathcal{L}(\theta_{i-1})$
 - ▷ $\theta_{i-1} = \theta_{i-1} + \epsilon \cdot \mathbf{p}_*$
 - ▷ $\mathbf{p}_* = \mathbf{p}_* + \frac{\epsilon}{2} \nabla_{\theta} \mathcal{L}(\theta_{i-1})$,
 - (d) Set $(\theta_L, \mathbf{p}_L) = (\theta_{i-1}, \mathbf{p}_*)$ and $\mathcal{H}^{(1)} = \mathcal{H}(\theta_L, \mathbf{p}_L)$,
 - (e) Compute $\alpha[(\theta_I, \mathbf{p}_I), (\theta_L, \mathbf{p}_L)] = \min \left[\exp \{ H^{(0)} - H^{(1)} \}, 1 \right]$,
 - (f) **If** $\alpha[(\theta_I, \mathbf{p}_I), (\theta_L, \mathbf{p}_L)] > u$ **then** set $\theta_i = \theta_L$
else set $\theta_i = \theta_I$,
 - (g) Increment $i = i + 1$ and return to **step (a)**.
-

As you can see, it is not trivial. The basic idea to keep in mind is that jumping rules are much more efficient than for traditional algorithms because they learn from the gradient of the log posterior density, so they know better where to jump to. As a result, it can be MUCH more efficient.

Chains are expected to reach stationarity faster as it proposes moves to regions of higher probabilities.

pros and cons :

- **PROS :** Easy to program as we just have to write down the model. Very efficient in general, and works for all types of problems.

- *CONS* : Need to learn how to use STAN, less control over the sampler bu maybe it is for the best?

APPENDIX C

OTHER FIGURES AND TABLES

Regarding our future application, that is maximum temperatures, it is relevant to consider values of the location parameter μ around 30 degrees.

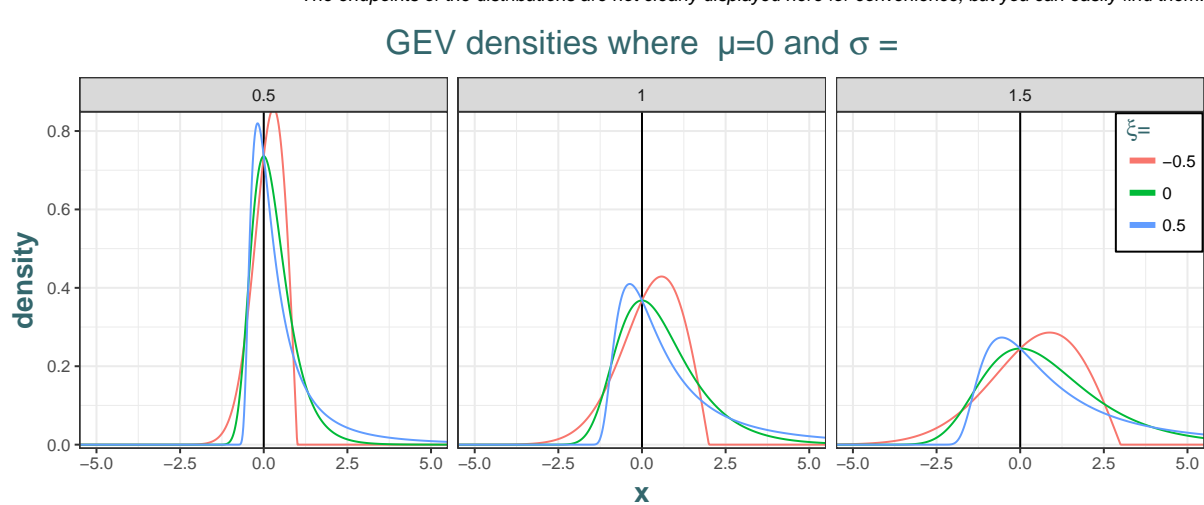
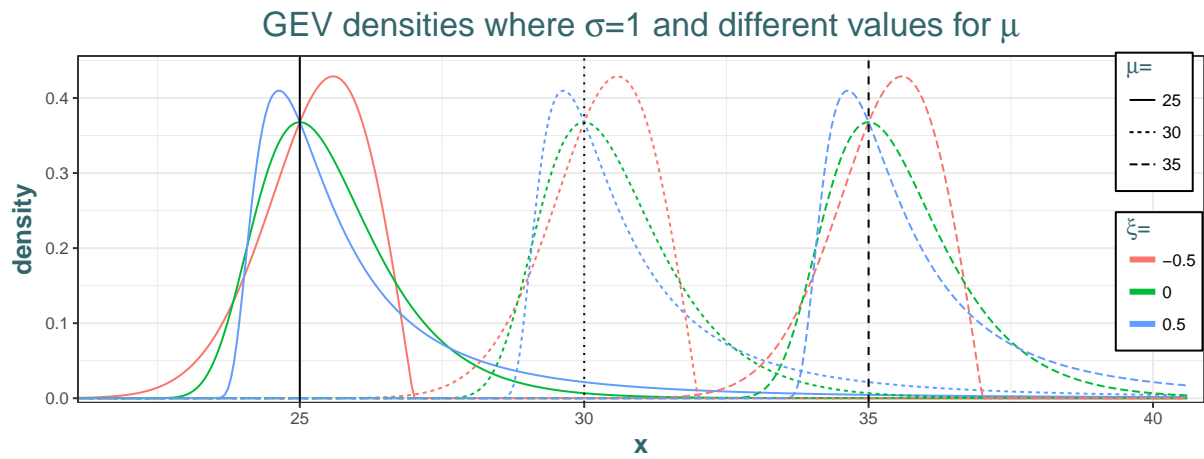


Figure C.1: GEV distribution for different values of the three parameters

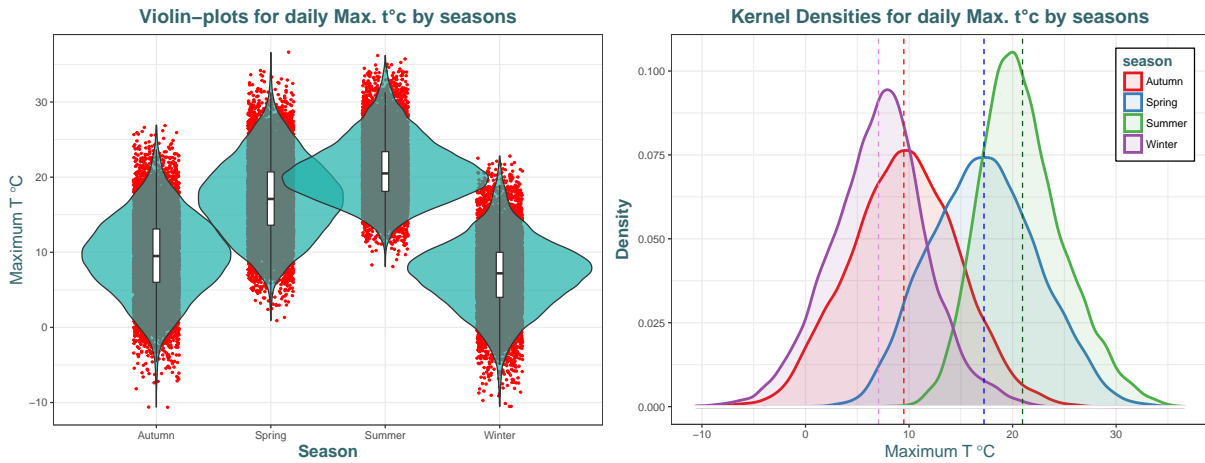


Figure C.2: Violin-plot and density plot for each seasons. (Right) vertical dotted lines represent the mean of each distribution.

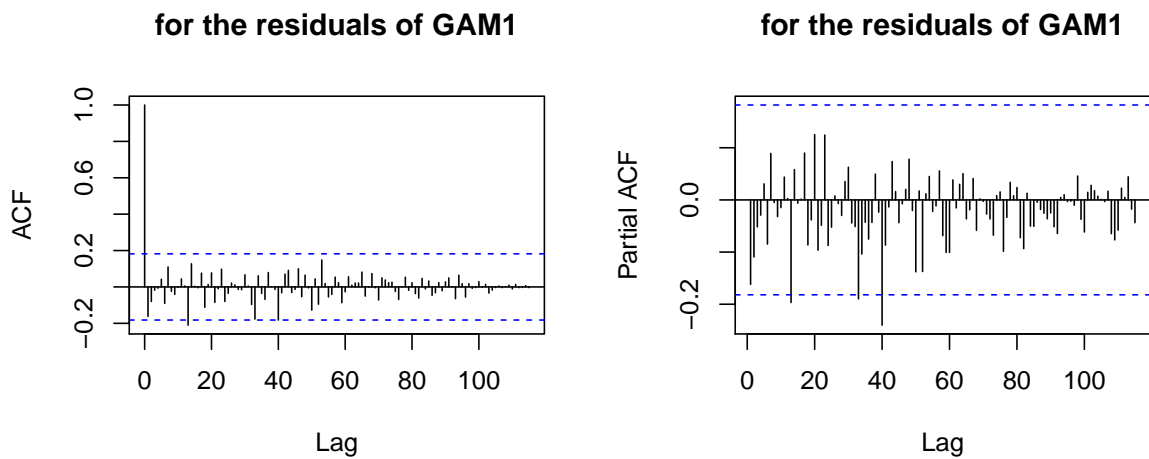


Figure C.3: ACF and PACF for the residuals of the fitted GAM model with assumed independent errors

Table C.1: Models' comparisons for the residuals of the GAM model based on AIC and BIC criterion.

	df	AIC	BIC
Uncorrelated	4	494.635	505.650
AR(1)	5	494.356	508.124
MA(1)	5	493.706	507.474
ARMA(1,1)	6	492.511	509.033
AR(2)	6	495.133	511.654
MA(2)	6	494.698	511.219

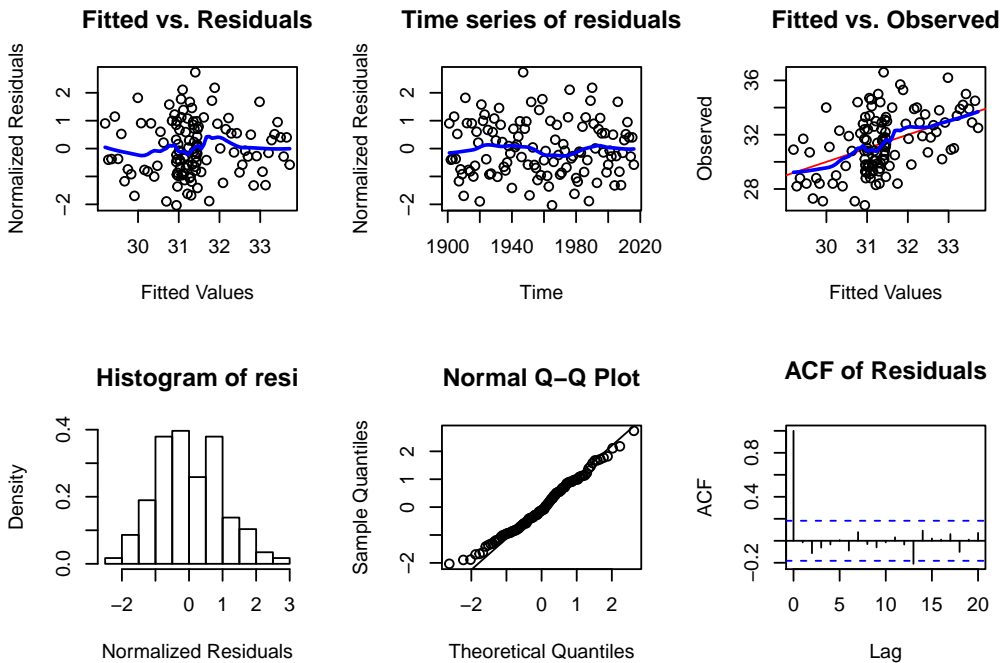


Figure C.4: Diagnostics of the chosen GAM model with Whinte Noise process on the errors, based on the residuals.

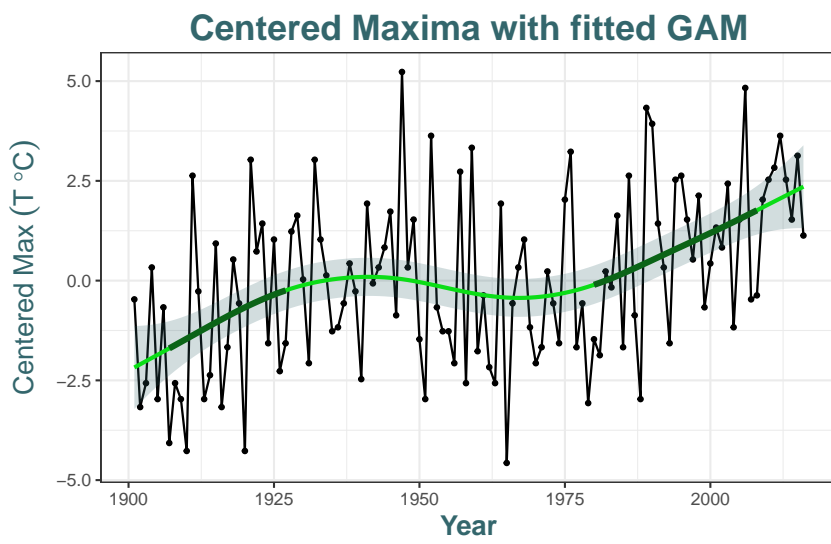


Figure C.5: Series of annual maxima together with the fitted GAM model (in green) **with MA(1) model on the residuals**. Thicker lines indicate that the increase is significant for pointwise confidence interval. Shaded area represent a "95%" interval for the predicted values which looks quite narrow.

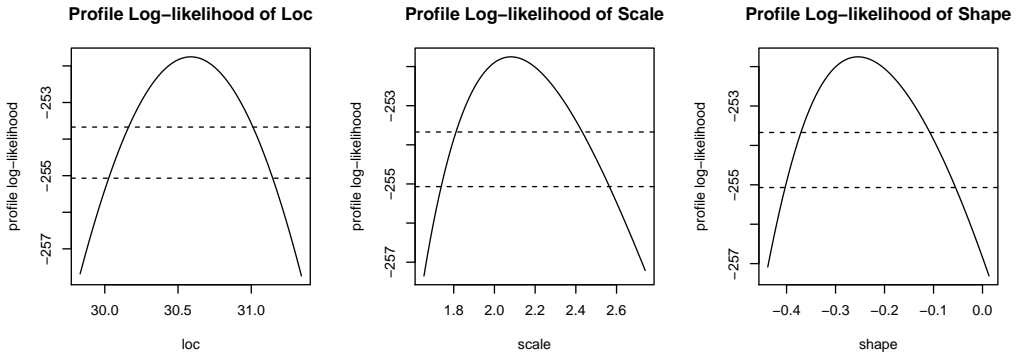


Figure C.6: Profile likelihood intervals for the stationary GEV parameters. The two horizontal dotted lines represent the 95% (above) and 99% (below) confidence intervals by taking the intersection with the horizontal axis.

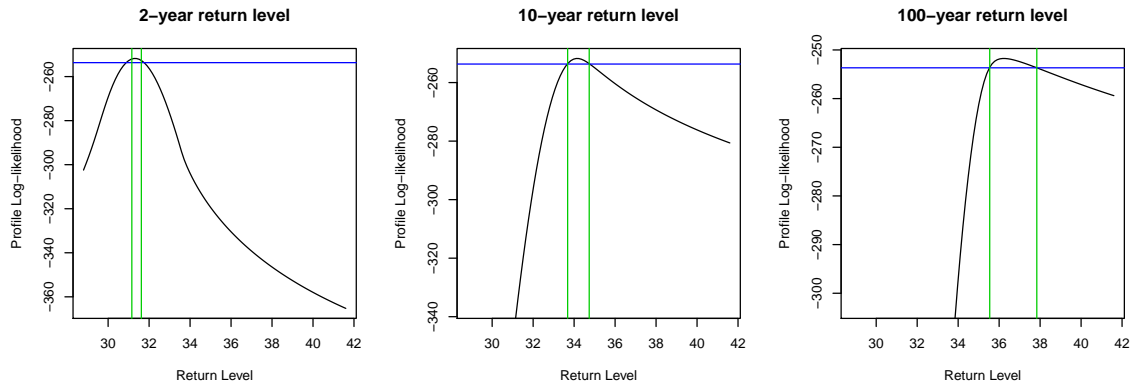


Figure C.7: 95% Profile likelihood intervals for return levels with return periods of 2, 10 and 100. We kept the same x -scales for the three plots but not the y -scales. We used the `ismev` package but we modified the function to allow for more flexibility because the default y -scale in produced ugly visualizations for high return levels. Green lines represent the intervals from Table 6.3 computed with another package from E.Gilleland, `extRemes`.

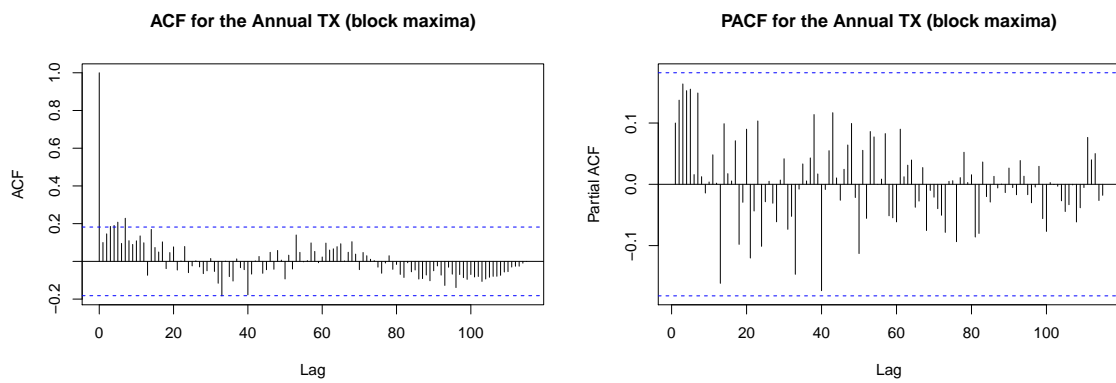


Figure C.8: ACF and PACF for the series of annual maxima.

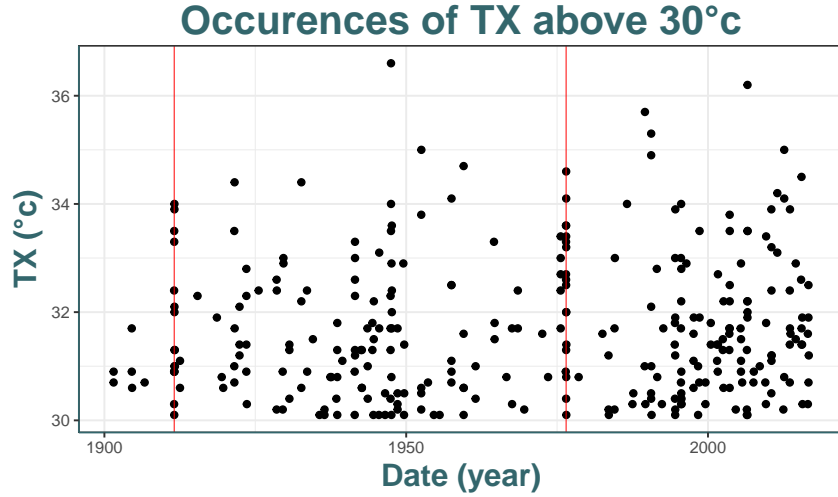


Figure C.9: Plot of all daily TX that exceeded 30°C in the period [1901,2016] in Uccle. Red lines highlights two periods of heavy heat waves during summers 1911 and 1976.

Table C.2: Estimation of the bootstrap aggregated GEV-CDN model with 2 hidden layers for $\sigma(t)$ and $\mu(t)$, and $M = 500$ resamples. In red are denoted rough estimates of the nonstationary parameters as if the model were parametric for both parameters $\sigma(t) = \exp(\alpha_0 + \alpha_1 \cdot t)$ and $\mu(t) = \beta_0 + \beta_1 \cdot t$. But this is actually not reliable since there are 2 hidden layers, and only the shape parameter can be reliably estimated.

	Location β_0	Location β_1	Scale α_0	Scale α_1	Shape ξ
Estimates	29.19	0.0242	0.686	-0.0012	-0.199

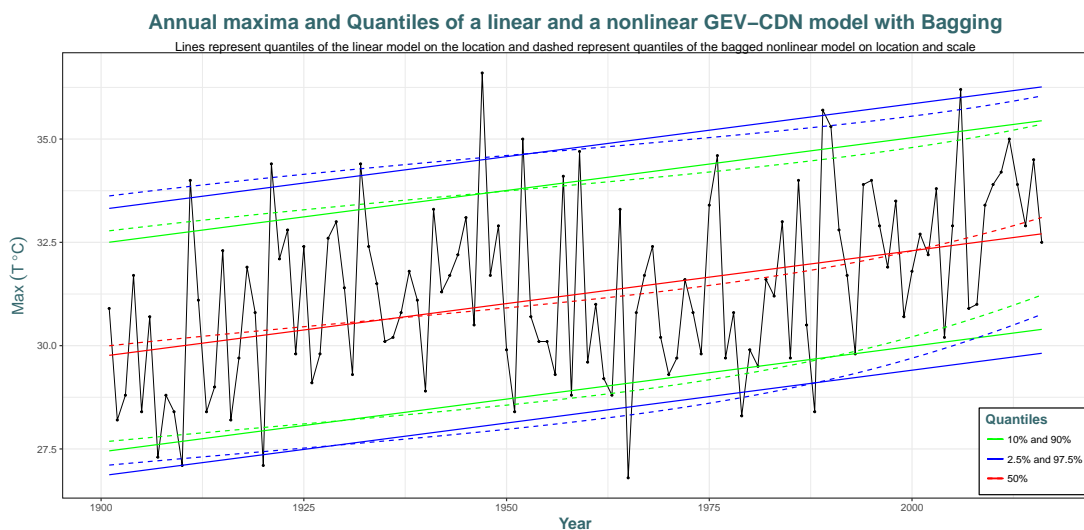


Figure C.10: This graph gathers the two plots of Figure 6.5 which could yield to a better visualization.

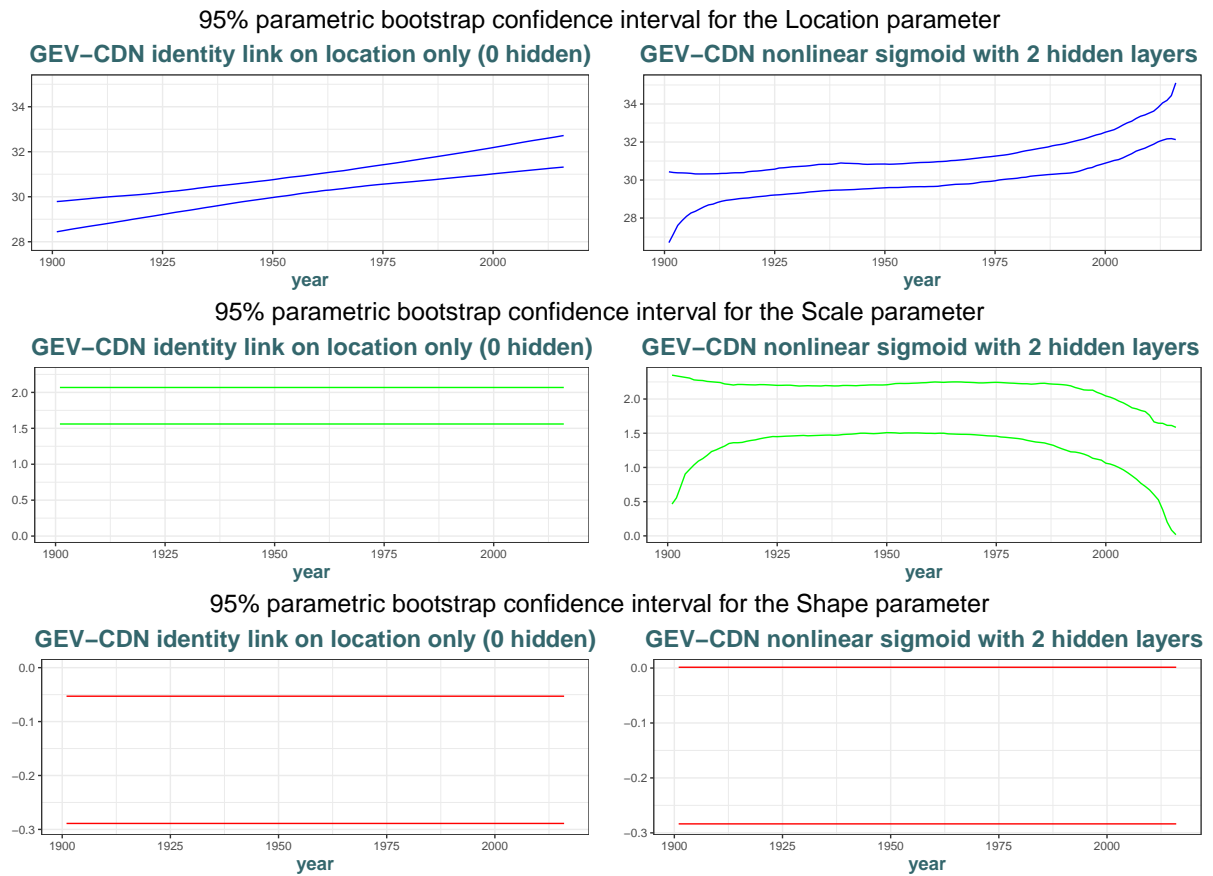


Figure C.11: Left plots show the **parametric** bootstrap 95% intervals computed with the GEV-CDN model allow a linear nonstationary location parameter only, and Right plots show these interval for the nonlinear nonstationary model in location and scale parameters with 2 hidden layers.

APPENDIX D

GITHUB REPOSITORY STRUCTURE

The Github repository build for this thesis can be found on this address :

<https://github.com/proto4426/PissoortThesis>

where the R package **PissoortThesis** is located. It has the following **structure** :

- **/R/** : contains the scripts with all the functions that are made available through the package. The functions are located in the script by "category", i.e.
 - **1UsedFunc.R** : some functions created for the introduction, the stationary analysis of yearly maxima in GEV, analysis in POT, nonstationary analysis in GEV and POT,...
 - **BayesFunc.R** : functions created for the Bayesian Analysis, e.g. the Metropolis-Hastings algorithm and Gibbs Sampler (both stationary and nonstationary).
 - **BootstrapFunc.R** (not updated)
 - **NeuralNetsFunc.R** : functions slightly refined from [Cannon \[2010\]](#) to allow for better outputs for the nonstationary analysis with NN.
 - **runExample.R** : contains the function allowing to run the Shiny applications directly through the package (put the name of the application in '' in the function to load the application).

The documentation of the functions are directly made through the package, by typing `?Function_Name`.

- **/Scripts-R/**
 - **1GEV_plots_(chap1).R** and **1GEV_ggplot_(chap1).R** : contain the plots made for the chapter 1, but only the last latter scripts contain the code to construct the final plots (made with `ggplot2`)
 - **intro_stationary.R** introduction and preprocessing + descriptive analysis, stationary analysis of yearly maxima in GEV, analysis in POT, analysis with other time scale and with minima, ...
 - **intro_trends(splines).R**
 - **intro_stationary.R**

- **1intro_stationary.R**
- **1intro_stationary.R**
- **1intro_stationary.R**
- **1intro_stationary.R**
- **1intro_stationary.R**
- **1intro_stationary.R**
- **/Shiny_app_visu/** (not updated)
- **/data/**
- **/inst/**
- **/man/**
- **/stan/**
- **/vignettes/**

Bibliography

- K. H. S. S. S. Amir AghaKouchak, David Easterling. *Extremes in a Changing Climate*, volume 65 of *Water Science and Technology Library*. Springer Netherlands, Dordrecht, 2013. ISBN 978-94-007-4478-3 978-94-007-4479-0. URL <http://link.springer.com/10.1007/978-94-007-4479-0>.
- E. Angelino, M. J. Johnson, and R. P. Adams. Patterns of Scalable Bayesian Inference. *Foundations and Trends® in Machine Learning*, 9(2-3):119–247, 2016. ISSN 1935-8237, 1935-8245. doi: 10.1561/2200000052. URL <http://www.nowpublishers.com/article/Details/MAL-052>.
- A. A. Balkema and L. d. Haan. Residual Life Time at Great Age. *The Annals of Probability*, 2(5):792–804, Oct. 1974. ISSN 0091-1798, 2168-894X. doi: 10.1214/aop/1176996548. URL <http://projecteuclid.org/euclid.aop/1176996548>.
- J. Beirlant, J. L. Teugels, and P. Vynckier. *Practical Analysis of Extreme Values*. Leuven University Press, 1996. ISBN 978-90-6186-768-5. Google-Books-ID: ylR3QgAACAAJ.
- J. Beirlant, Y. Goegebeur, J. Segers, and J. Teugels. *Statistics of Extremes: Theory and Applications*. John Wiley & Sons, Mar. 2006. ISBN 978-0-470-01237-6. Google-Books-ID: jqmRwfG6aloC.
- M. Betancourt. Diagnosing Suboptimal Cotangent Disintegrations in Hamiltonian Monte Carlo. *arXiv:1604.00695 [stat]*, Apr. 2016. URL <http://arxiv.org/abs/1604.00695>. arXiv: 1604.00695.
- M. Betancourt and M. Girolami. Hamiltonian Monte Carlo for hierarchical models. *Current trends in Bayesian methodology with applications*, 79:30, 2015.
- A. Bolívar, E. Díaz-Francés, J. Ortega, and E. Vilchis. Profile Likelihood Intervals for Quantiles in Extreme Value Distributions. *arXiv preprint arXiv:1005.3573*, 2010. URL <http://arxiv.org/abs/1005.3573>.
- L. Breiman. Random forests. *Mach. Learn.*, 45(1):5–32, Oct. 2001. ISSN 0885-6125. doi: 10.1023/A:1010933404324. URL <http://dx.doi.org/10.1023/A:1010933404324>.

- A. J. Cannon. A flexible nonlinear modelling framework for nonstationary generalized extreme value analysis in hydroclimatology. *Hydrological Processes*, 24(6):673–685, Mar. 2010. ISSN 08856087. doi: 10.1002/hyp.7506. URL <http://doi.wiley.com/10.1002/hyp.7506>.
- A. J. Cannon and I. G. McKendry. A graphical sensitivity analysis for statistical climate models: application to indian monsoon rainfall prediction by artificial neural networks and multiple linear regression models. *International Journal of Climatology*, 22(13):1687–1708, 2002. ISSN 1097-0088. doi: 10.1002/joc.811. URL <http://dx.doi.org/10.1002/joc.811>.
- M. Carney, P. Cunningham, J. Dowling, and C. Lee. Predicting probability distributions for surf height using an ensemble of mixture density networks. In *Proceedings of the 22Nd International Conference on Machine Learning*, ICML '05, pages 113–120, New York, NY, USA, 2005. ACM. ISBN 1-59593-180-5. doi: 10.1145/1102351.1102366. URL <http://doi.acm.org/10.1145/1102351.1102366>.
- M. Charras-Garrido and P. Lezaud. Extreme Value Analysis : an Introduction. *Journal de la Societe Fran  aise de Statistique*, 154(2):pp 66–97, 2013. URL <https://hal-enac.archives-ouvertes.fr/hal-00917995>.
- S. Coles. *An Introduction to Statistical Modeling of Extreme Values*. Springer Series in Statistics. Springer London, London, 2001. ISBN 978-1-84996-874-4 978-1-4471-3675-0. URL <http://link.springer.com/10.1007/978-1-4471-3675-0>.
- S. G. Coles and M. J. Dixon. Likelihood-Based Inference for Extreme Value Models. *Extremes*, 2(1):5–23, Mar. 1999. ISSN 1386-1999, 1572-915X. doi: 10.1023/A:1009905222644. URL <http://link.springer.com/article/10.1023/A:1009905222644>.
- C. Cunnane. A note on the Poisson assumption in partial duration series models - Cunnane - 1979 - Water Resources Research - Wiley Online Library, 1979. URL <http://onlinelibrary.wiley.com/doi/10.1029/WR015i002p00489/abstract>.
- A. C. Davison, S. A. Padoan, and M. Ribatet. Statistical Modeling of Spatial Extremes. *Statistical Science*, 27(2):161–186, 2012. ISSN 0883-4237. URL <http://www.jstor.org/stable/41714789>.
- L. de Haan. *On regular variation and its application to the weak convergence of sample extremes*. Matematisch Centrum, 1970. Google-Books-ID: sQ3vAAAAMAAJ.
- L. de Haan and S. Resnick. On asymptotic normality of the hill estimator. *Communications in Statistics. Stochastic Models*, 14(4):849–866, 1998. doi: 10.1080/15326349808807504. URL <http://dx.doi.org/10.1080/15326349808807504>.
- A. L. M. Dekkers and L. D. Haan. On the Estimation of the Extreme-Value Index and Large Quantile Estimation. *The Annals of Statistics*, 17(4):1795–1832, Dec. 1989. ISSN 0090-5364, 2168-8966. doi: 10.1214/aos/1176347396. URL <http://projecteuclid.org/euclid.aos/1176347396>.
- A. L. M. Dekkers, J. H. J. Einmahl, and L. D. Haan. A Moment Estimator for the Index of an Extreme-Value Distribution. *The Annals of Statistics*, 17(4):1833–1855, Dec. 1989. ISSN 0090-5364, 2168-8966. doi: 10.1214/aos/1176347397. URL <http://projecteuclid.org/euclid.aos/1176347397>.

- J. E. Dennis and R. B. Schnabel. *Numerical Methods for Unconstrained Optimization and Nonlinear Equations*. Society for Industrial and Applied Mathematics, Philadelphia, Jan. 1987. ISBN 978-0-89871-364-0.
- D. K. Dey and J. Yan. *Extreme Value Modeling and Risk Analysis: Methods and Applications*. CRC Press, Jan. 2016. ISBN 978-1-4987-0131-0. Google-Books-ID: PYhUCwAAQBAJ.
- B. Efron. Bootstrap methods: Another look at the jackknife. *Ann. Statist.*, 7(1):1–26, 01 1979. doi: 10.1214/aos/1176344552. URL <http://dx.doi.org/10.1214/aos/1176344552>.
- S. El Adlouni, T. B. M. J. Ouarda, X. Zhang, R. Roy, and B. Bobée. Generalized maximum likelihood estimators for the nonstationary generalized extreme value model. *Water Resources Research*, 43(3):W03410, Mar. 2007. ISSN 1944-7973. doi: 10.1029/2005WR004545. URL <http://onlinelibrary.wiley.com/doi/10.1029/2005WR004545/abstract>.
- P. Embrechts, C. Klüppelberg, and T. Mikosch. *Modelling Extremal Events: for Insurance and Finance*. Springer Berlin Heidelberg, Feb. 1997. ISBN 978-3-642-08242-9.
- M. Falk and F. Marohn. Von Mises Conditions Revisited. *The Annals of Probability*, 21(3):1310–1328, July 1993. ISSN 0091-1798, 2168-894X. doi: 10.1214/aop/1176989120. URL <http://projecteuclid.org/euclid.aop/1176989120>.
- C. A. T. Ferro and J. Segers. Inference for Clusters of Extreme Values. *Journal of the Royal Statistical Society. Series B (Statistical Methodology)*, 65(2):545–556, 2003. ISSN 1369-7412. URL <http://www.jstor.org/stable/3647520>.
- R. A. Fisher and L. H. C. Tippett. Limiting Forms of the Frequency Distribution of the Largest or Smallest Member of a Sample. *ResearchGate*, 24(02):180–190, Jan. 1928. ISSN 1469-8064. doi: 10.1017/S0305004100015681.
- A. Gelman, J. B. Carlin, H. S. Stern, D. B. Dunson, A. Vehtari, and D. B. Rubin. *Bayesian Data Analysis, Third Edition*. CRC Press, Nov. 2013. ISBN 978-1-4398-4095-5. Google-Books-ID: ZXL6AQAAQBAJ.
- A. Gelman, J. Hwang, and A. Vehtari. Understanding Predictive Information Criteria for Bayesian Models. *Statistics and Computing*, 24(6):997–1016, Nov. 2014. ISSN 0960-3174. doi: 10.1007/s11222-013-9416-2. URL <http://dx.doi.org/10.1007/s11222-013-9416-2>.
- E. Gilleland and R. W. Katz. **extRemes** 2.0: An Extreme Value Analysis Package in R. *Journal of Statistical Software*, 72(8), 2016. ISSN 1548-7660. doi: 10.18637/jss.v072.i08. URL <http://www.jstatsoft.org/v72/i08/>.
- B. Gnedenko. Sur La Distribution Limite Du Terme Maximum D’Une Serie Aleatoire. *Annals of Mathematics*, 44(3):423–453, 1943. ISSN 0003-486X. doi: 10.2307/1968974. URL <http://www.jstor.org/stable/1968974>.
- J. A. Greenwood, J. M. Landwehr, N. C. Matalas, and J. R. Wallis. Probability weighted moments: Definition and relation to parameters of several distributions expressable in inverse form. *Water Resources Research*, 15(5):1049–1054, Oct. 1979. ISSN 1944-7973. doi: 10.1029/WR015i005p01049. URL <http://onlinelibrary.wiley.com/doi/10.1029/WR015i005p01049/abstract>.

- S. D. Grimshaw. Computing Maximum Likelihood Estimates for the Generalized Pareto Distribution. *Technometrics*, 35(2):185, May 1993. ISSN 00401706. doi: 10.2307/1269663. URL <http://www.jstor.org/stable/1269663?origin=crossref>.
- L. d. Haan. *On regular variation and its application to the weak convergence of sample extremes*. Matematisch Centrum, 1970. Google-Books-ID: sQ3vAAAAMAAJ.
- L. d. Haan and A. Ferreira. *Extreme value theory: an introduction*. Springer series in operations research. Springer, New York ; London, 2006. ISBN 978-0-387-23946-0. OCLC: ocm70173287.
- M. Hartmann and R. Ehlers. Bayesian Inference for Generalized Extreme Value Distributions via Hamiltonian Monte Carlo. *Communications in Statistics - Simulation and Computation*, pages 0–0, Mar. 2016. ISSN 0361-0918, 1532-4141. doi: 10.1080/03610918.2016.1152365. URL <http://arxiv.org/abs/1410.4534>. arXiv: 1410.4534.
- T. Hastie and R. Tibshirani. Generalized Additive Models. *Statistical Science*, 1(3):297–310, 1986. ISSN 0883-4237. URL <http://www.jstor.org/stable/2245459>.
- W. K. Hastings. Monte Carlo sampling methods using Markov chains and their applications. *Biometrika*, 57(1):97–109, Apr. 1970. ISSN 0006-3444. URL <https://academic.oup.com/biomet/article-abstract/57/1/97/2721936/Monte-Carlo-sampling-methods-using-Markov-chains>.
- K. Hornik, M. Stinchcombe, and H. White. Multilayer feedforward networks are universal approximators. *Neural Netw.*, 2(5):359–366, July 1989. ISSN 0893-6080. doi: 10.1016/0893-6080(89)90020-8. URL [http://dx.doi.org/10.1016/0893-6080\(89\)90020-8](http://dx.doi.org/10.1016/0893-6080(89)90020-8).
- J. R. M. Hosking and J. R. Wallis. Parameter and Quantile Estimation for the Generalized Pareto Distribution. *Technometrics*, 29(3):339, Aug. 1987. ISSN 00401706. doi: 10.2307/1269343. URL <http://www.jstor.org/stable/1269343?origin=crossref>.
- J. R. M. J. R. M. Hosking and J. R. Wallis. *Regional frequency analysis : an approach based on L-moments*. Cambridge ; New York : Cambridge University Press, 1997. ISBN 0521430453 (hardbound).
- W. W. Hsieh and B. Tang. Applying neural network models to prediction and data analysis in meteorology and oceanography., Sep 1998. URL <https://open.library.ubc.ca/cIRcle/collections/52383/items/1.0041821>.
- M. N. Khaliq, T. B. M. J. Ouarda, J.-C. Ondo, P. Gachon, and B. Bobée. Frequency analysis of a sequence of dependent and/or non-stationary hydro-meteorological observations: A review. *Journal of Hydrology*, 329:534–552, Oct. 2006. doi: 10.1016/j.jhydrol.2006.03.004.
- V. V. Kharin and F. W. Zwiers. Estimating extremes in transient climate change simulations. *Journal of Climate*, 18(8):1156–1173, 2005. doi: 10.1175/JCLI3320.1. URL <https://doi.org/10.1175/JCLI3320.1>.
- A. M. G. Klein Tank and Wijngaard. Daily dataset of 20th-century surface air temperature and precipitation series for the European Climate Assessment. *International Journal of Climatology*, 22(12):1441–1453, Oct. 2002. ISSN 1097-0088. doi: 10.1002/joc.773. URL <http://onlinelibrary.wiley.com/doi/10.1002/joc.773/abstract>.

- A. N. Kolmogorov, N. Morrison, and A. T. Bharucha-Reid. *Foundations of the theory of probability*. Chelsea Publishing Company, New York, 1956. OCLC: 751236060.
- M. R. Leadbetter. On extreme values in stationary sequences. *Zeitschrift für Wahrscheinlichkeitstheorie und Verwandte Gebiete*, 28(4):289–303, Dec. 1974. ISSN 0044-3719, 1432-2064. doi: 10.1007/BF00532947. URL <http://link.springer.com/article/10.1007/BF00532947>.
- M. R. Leadbetter, G. Lindgren, and H. Rootzén. *Extremes and Related Properties of Random Sequences and Processes*. Springer Series in Statistics. Springer New York, New York, NY, 1983. ISBN 978-1-4612-5451-5 978-1-4612-5449-2. URL <http://link.springer.com/10.1007/978-1-4612-5449-2>.
- F. Leisch. Creating r packages: A tutorial. 2008. URL <https://epub.ub.uni-muenchen.de/6175/>.
- A. A. Lindsey and J. E. Newman. Use of Official Wather Data in Spring Time: Temperature Analysis of an Indiana Phenological Record. *Ecology*, 37(4):812–823, Oct. 1956. ISSN 1939-9170. doi: 10.2307/1933072. URL <http://onlinelibrary.wiley.com/doi/10.2307/1933072/abstract>.
- Y. Liu, A. Gelman, and T. Zheng. Simulation-efficient shortest probability intervals. *Statistics and Computing*, 25(4):809–819, July 2015. ISSN 0960-3174, 1573-1375. doi: 10.1007/s11222-015-9563-8. URL <http://link.springer.com/10.1007/s11222-015-9563-8>.
- D. J. C. MacKay. A practical bayesian framework for backpropagation networks. *Neural Computation*, 4(3):448–472, 1992.
- J. Maindonald and J. Braun. *Data analysis and graphics using R: an example-based approach*, volume 10. Cambridge University Press, 2006.
- G. Marra and S. N. Wood. Coverage properties of confidence intervals for generalized additive model components. *Scandinavian Journal of Statistics*, 39(1):53–74, 2012. URL <http://onlinelibrary.wiley.com/doi/10.1111/j.1467-9469.2011.00760.x/full>.
- E. S. Martins and J. R. Stedinger. Generalized maximum-likelihood generalized extreme-value quantile estimators for hydrologic data. *Water Resources Research*, 36(3):737–744, Mar. 2000. ISSN 1944-7973. doi: 10.1029/1999WR900330. URL <http://onlinelibrary.wiley.com/doi/10.1029/1999WR900330/abstract>.
- P. C. D. Milly, J. Betancourt, M. Falkenmark, R. M. Hirsch, Z. W. Kundzewicz, D. P. Lettenmaier, and R. J. Stouffer. Climate change. Stationarity is dead: whither water management? *Science (New York, N.Y.)*, 319(5863):573–574, Feb. 2008. ISSN 1095-9203. doi: 10.1126/science.1151915.
- M. Mudelsee. *Climate Time Series Analysis*, volume 51 of *Atmospheric and Oceanographic Sciences Library*. Springer International Publishing, Cham, 2014. ISBN 978-3-319-04449-1 978-3-319-04450-7. URL <http://link.springer.com/10.1007/978-3-319-04450-7>.
- R. M. Neal and others. MCMC using Hamiltonian dynamics. *Handbook of Markov Chain Monte Carlo*, 2:113–162, 2011.

- S. Ni and D. Sun. Noninformative priors and frequentist risks of bayesian estimators of vector-autoregressive models. *Journal of Econometrics*, 115(1):159–197, July 2003. ISSN 0304-4076. doi: 10.1016/S0304-4076(03)00099-X. URL <http://www.sciencedirect.com/science/article/pii/S030440760300099X>.
- P. J. Northrop and N. Attalides. Posterior propriety in Bayesian extreme value analyses using reference priors. *Statistica Sinica*, 26(2), Apr. 2016. ISSN 1017-0405. URL <http://dx.doi.org/10.5705/ss.2014.034>.
- M. C. Peel, Q. J. Wang, R. M. Vogel, and T. A. McMAHON. The utility of L-moment ratio diagrams for selecting a regional probability distribution. *Hydrological Sciences Journal*, 46(1):147–155, 2001. URL <http://www.tandfonline.com/doi/abs/10.1080/02626660109492806>.
- J. Pickands. Statistical Inference Using Extreme Order Statistics. *The Annals of Statistics*, 3(1): 119–131, Jan. 1975. ISSN 0090-5364, 2168-8966. doi: 10.1214/aos/1176343003. URL <http://projecteuclid.org/euclid-aos/1176343003>.
- E. C. Pinheiro and S. L. P. Ferrari. A comparative review of generalizations of the Gumbel extreme value distribution with an application to wind speed data. *arXiv:1502.02708 [stat]*, Feb. 2015. URL <http://arxiv.org/abs/1502.02708>. arXiv: 1502.02708.
- R.-D. Reiss and M. Thomas. *Statistical analysis of extreme values: with applications to insurance, finance, hydrology and other fields ; [includes CD-ROM]*. Birkhäuser, Basel, 3. ed edition, 2007. ISBN 978-3-7643-7230-9 978-3-7643-7399-3. OCLC: 180885018.
- S. I. Resnick. *Extreme Values, Regular Variation and Point Processes*. Springer Series in Operations Research and Financial Engineering. Springer New York, New York, NY, 1987. ISBN 978-0-387-75952-4 978-0-387-75953-1. URL <http://link.springer.com/10.1007/978-0-387-75953-1>.
- M. Ribatet. A User’s Guide to the POT Package (Version 1.4). *month*, 2006. URL <http://www.unalmed.edu.co/~ndgirald/Archivos%20Lectura/Archivos%20curso%20Riesgo%20Operativo/POT.pdf>.
- M. Ribatet, C. Dombry, and M. Oesting. Spatial Extremes and Max-Stable Processes. In *Extreme Value Modeling and Risk Analysis: Methods and Applications*, pages 179–194. Chapman and Hall/CRC, 2015.
- P. Ribereau, E. Masiello, and P. Naveau. Skew generalized extreme value distribution: Probability-weighted moments estimation and application to block maxima procedure. *Communications in Statistics - Theory and Methods*, 45(17):5037–5052, Sept. 2016. ISSN 0361-0926. doi: 10.1080/03610926.2014.935434. URL <http://dx.doi.org/10.1080/03610926.2014.935434>.
- G. O. Roberts, A. Gelman, and W. R. Gilks. Weak convergence and optimal scaling of random walk Metropolis algorithms. *The Annals of Applied Probability*, 7(1):110–120, Feb. 1997. ISSN 1050-5164, 2168-8737. doi: 10.1214/aoap/1034625254. URL <http://projecteuclid.org/euclid.aoap/1034625254>.
- G. Rosso. Extreme Value Theory for Time Series using Peak-Over-Threshold method. *arXiv preprint arXiv:1509.01051*, 2015. URL <http://arxiv.org/abs/1509.01051>.

- D. Ruppert, M. P. Wand, and R. J. Carroll. Semiparametric Regression. Cambridge Books, Cambridge University Press, 2003. URL <http://econpapers.repec.org/bookchap/cupcbooks/9780521785167.htm>.
- C. Scarrott and A. MacDonald. A review of extreme value threshold estimation and uncertainty quantification. *REVSTAT-Statistical Journal*, 10(1):33–60, 2012. URL <https://www.ine.pt/revstat/pdf/rs120102.pdf>.
- J. Segers. Generalized Pickands Estimators for the Extreme Value Index: Minimal Asymptotic Variance and Bias Reduction. 2001. URL <http://citeseerx.ist.psu.edu/viewdoc/citations;jsessionid=0C9C7CAE3938CA7A9B280DEA739EFDA9?doi=10.1.1.7.1713>.
- C. Sherlock, G. Roberts, and others. Optimal scaling of the random walk Metropolis on elliptically symmetric unimodal targets. *Bernoulli*, 15(3):774–798, 2009. URL <http://projecteuclid.org/euclid.bj/1251463281>.
- V. P. Singh and H. Guo. Parameter estimation for 3-parameter generalized pareto distribution by the principle of maximum entropy (POME). *Hydrological Sciences Journal*, 40(2):165–181, Apr. 1995. ISSN 0262-6667, 2150-3435. doi: 10.1080/0262669509491402. URL <http://www.tandfonline.com/doi/abs/10.1080/0262669509491402>.
- R. L. Smith. Maximum likelihood estimation in a class of nonregular cases. *Biometrika*, 72(1):67–90, Apr. 1985. ISSN 0006-3444. doi: 10.1093/biomet/72.1.67. URL <https://academic.oup.com/biomet/article-abstract/72/1/67/242523/Maximum-likelihood-estimation-in-a-class-of>.
- D. J. Spiegelhalter, N. G. Best, B. P. Carlin, and A. Van Der Linde. Bayesian measures of model complexity and fit. *Journal of the Royal Statistical Society: Series B (Statistical Methodology)*, 64(4):583–639, 2002. URL <http://onlinelibrary.wiley.com/doi/10.1111/1467-9868.00353/full>.
- M.-S. Suh, S.-G. Oh, D.-K. Lee, D.-H. Cha, S.-J. Choi, C.-S. Jin, and S.-Y. Hong. Development of New Ensemble Methods Based on the Performance Skills of Regional Climate Models over South Korea. *Journal of Climate*, 25(20):7067–7082, May 2012. ISSN 0894-8755. doi: 10.1175/JCLI-D-11-00457.1. URL <http://journals.ametsoc.org/doi/abs/10.1175/JCLI-D-11-00457.1>.
- A. Vehtari, A. Gelman, and J. Gabry. Practical Bayesian model evaluation using leave-one-out cross-validation and WAIC. *Statistics and Computing*, Aug. 2016. ISSN 0960-3174, 1573-1375. doi: 10.1007/s11222-016-9696-4. URL <http://arxiv.org/abs/1507.04544>. arXiv: 1507.04544.
- R. Von Mises. La distribution de la plus grande de n valeurs. *Rev. Math. Union Interbalcanique*, 1: pp.141–160, 1936.
- J. L. Wadsworth. Exploiting Structure of Maximum Likelihood Estimators for Extreme Value Threshold Selection. *Technometrics*, 58(1):116–126, Jan. 2016. ISSN 0040-1706. doi: 10.1080/00401706.2014.998345. URL <http://dx.doi.org/10.1080/00401706.2014.998345>.

- S. Watanabe. Asymptotic equivalence of Bayes cross validation and widely applicable information criterion in singular learning theory. *Journal of Machine Learning Research*, 11(Dec):3571–3594, 2010. URL <http://www.jmlr.org/papers/v11/watanabe10a.html>.
- R. Yang and J. O. Berger. *A catalog of noninformative priors*. Institute of Statistics and Decision Sciences, Duke University, 1996. URL <http://www.stats.org.uk/priors/noninformative/YangBerger1998.pdf>.
- C. Zhou. The extent of the maximum likelihood estimator for the extreme value index. *Journal of Multivariate Analysis*, 101(4):971–983, Apr. 2010. ISSN 0047-259X. doi: 10.1016/j.jmva.2009.09.013. URL <http://www.sciencedirect.com/science/article/pii/S0047259X0900178X>.